12-2022

Elucidating the Importance of Structure, Surfaces, and Interfaces in Polymer Nanoparticles and Nanocomposites

Jacob E. Fischer
University of Tennessee, Knoxville, jfisch11@vols.utk.edu

To the Graduate Council:

I am submitting herewith a dissertation written by Jacob E. Fischer entitled "Elucidating the Importance of Structure, Surfaces, and Interfaces in Polymer Nanoparticles and Nanocomposites." I have examined the final electronic copy of this dissertation for form and content and recommend that it be accepted in partial fulfillment of the requirements for the degree of Doctor of Philosophy, with a major in Chemistry.

Mark D. Dadmun, Major Professor

We have read this dissertation and recommend its acceptance:

Alexei Sokolov, Konstantinos Vogiatzis, Gila Stein

Accepted for the Council:

Dixie L. Thompson

Vice Provost and Dean of the Graduate School

(Original signatures are on file with official student records.)

Elucidating the Importance of Structure, Surfaces, and Interfaces in Polymer Nanoparticles and Nanocomposites

A Dissertation Presented for the
Doctor of Philosophy
Degree
The University of Tennessee, Knoxville

Jacob Fischer
December 2022

DEDICATION

This work is dedicated to my wife, Amber, who without her love, support, and most importantly patience this would not have been possible. I also dedicate this work to my parents, Jack and Karen, and siblings, Karianne and Ben, who have been pillars of support and inspiration throughout my life. A special dedication goes to my grandparents, Harry and Marge Fischer and Roger Warren, who were some of my biggest supporters my entire life but were unable to see all of my hard work come to fruition, I miss them dearly.

ACKNOWLEDGEMENTS

At the conclusion of my time as a graduate student, the list of people who deserve thanks is nearly endless. I am thankful for my advisor Dr. Mark Dadmun, for his scientific guidance and mentorship during this journey, and to my committee member's Dr. Alexei Sokolov, Dr. Konstantinos Vogiatzis, and Dr. Gila Stein for their commitment to my scientific career, and Dr. Tomonori Saito, Dr. Lu Han, Dr. Kevin Cable, and Dr. Antonio Faraone for their collaboration and contributions to my research. I would also like to recognize Dr. Bonita Lawrence, Dr. Lisa Reilly, Dr. Scott Brothers, Mr. Adam Fletcher, and Mr. Robert St. Clair for shaping my academic career in many ways prior to my time at Tennessee. Finally, a shoutout to the friends I have made outside of academia while in Knoxville who helped me maintain a healthy school-life balance, making Knoxville a wonderful place to be during my time in graduate school.

ABSTRACT

This dissertation details research conducted to elucidate the importance of structure, surfaces, and interfaces in both polymeric nanoparticles and polymer nanocomposites. The fundamental understanding that is garnered in these studies provides a foundation to rationally develop nanocomposites tailored for unique functionalities, performance and applications.

Soft polymeric nanoparticles, have shown to imbue non-traditional diffusive properties, the strength of which decreases with crosslinking density of the nanoparticle. The crosslinking dependent morphology of these nanoparticles is first characterized in a dilute solution of good solvent (Chapter 2). The scattering results revealed that the structure ranges from a swollen polymer in good solvent (0% XL), to a collapsed polymer in theta solvent (0.4%XL), to unequivocally particle-like ($\geq$ 0.8%XL). The transition to a particle-like morphology hinges on the clear presence of a measurable surface. To better understand the mechanisms behind their non-traditional diffusive properties, the internal dynamics of these nanoparticles were probed (Chapter 3). While globally exhibiting Zimm-like dynamics, the nanoparticles showed a heterogeneity of local internal dynamics, exhibiting significantly slowed dynamics on length scales that contained crosslinks and linear-like dynamics over length scales where crosslinks were mostly absent. The clear separation of internal dynamics magnifies the importance of the nanoparticle's core-shell structure.

The consequences of surfaces and interfaces within polymer nanocomposites is also explored. The permanency of a bound polymer layer is characterized by monitoring

the time evolution of the volume fraction profile of an adsorbed polymer layer (Chapter 4). While the total thickness of the layer remained unchanged, the composition varied indicating that individual chains are not necessarily “irreversibly” adsorbed. Additionally, the molecular weight dependence on the kinetics of chain desorption are studied, finding that desorption in the melt transitions from diffusion limited to a combination of diffusion and surface detachment limited with increasing molecular weight. Finally interfaces between a fire-retardant small molecule and polymer is compatibilized using a polymeric dispersant (Chapter 5). The average and homogeneity of particle size is improved in melt mix blends of the three components as the polymer dispersant can disrupt the *intra*molecular hydrogen bonding within the flame-retardant with intermolecular interactions.

TABLE OF CONTENTS

LIST OF TABLES

LIST OF FIGURES

INTRODUCTION

Polymer Nanocomposites

The use of, and research regarding, polymer nanocomposites has exploded in the last few decades for their ability to provide enhanced properties to materials over a wide range of applications.[1-9] Polymer nanocomposites most often consist of a solid nanoscale filler, typically less than 100nm in size, dispersed throughout a polymer matrix. The nanofillers can be comprised of clays, carbon nanotubes, graphene, inorganic nanoparticles, or organic nanoparticles and are not restricted to particle dimensionality. The inception of polymer nanocomposite research occurred in the last 1980s to mid 1990s when a research group within Toyota Motor Company described the use of a polyamide/clay nanocomposite as an improved material for use within their automobiles. The group detailed a nanocomposite, which contained roughly 5%wt clay, that showed a 300% increase in the material's modulus, and a 25% increase in its heat deflection temperature.[10] Prior to this work, fillers were primarily seen as a cost-reduction technique rather than a route to improve the mechanical, thermal, and/or chemical properties of the material.[11] The ability of a nanofiller to enhance the moduli of a material without sacrificing its mechanical strength catalyzed a decades long research trend of attempting to better understand the physics leading to this phenomenon of improved or new properties. Using fillers that fall within the nanoscale regime proved beneficial as the surface area to volume ratio of the additives is much greater than micron-size fillers, allowing for a heighted degree of interaction between the polymer matrix and the nano-scale additive. When on the nanometer length scale, particles can become thermodynamically unstable because of excess surface energies.[12] That excess surface

energy and high surface area to volume ratio can lead to a change in the crystalline structure of the nanoparticles, which is often directly connected to the unique properties that are only seen on the nano-scale.[13-15]

Polymer Nanocomposites with Inorganic Nanoparticles

A significant portion of polymer nanocomposite research pertains to systems using hard nanoparticles (NPs) as the additive. The nanoparticles utilized in these systems are generally entirely inorganic, impenetrable, and spherical in shape. The most commonly used hard nanoparticles are primarily comprised of either gold or silicon oxide. A major hurdle in incorporating these types of nanoparticles into a polymer matrix is the poor mixing between the two materials, where poor interactions between the polymer matrix and nanoparticle filler causes the nanoparticles to agglomerate.[16, 17] In most cases, a polymer nanocomposite requires good dispersion of the nanoparticles throughout the polymer matrix to achieve the enhanced properties provided by the nanoparticles. Poor dispersion can also lead to diminishing optical and mechanical properties of the nanocomposite.[3, 18-27] However, there are instances with certain types of nano-fillers, typically of the inorganic variety, where a self-assembled mesoscale structure of the nano-filler is more desirable than a complete and random dispersion throughout the polymer matrix.[28-31]

Efforts have been made to control the dispersion of nanoparticles within a polymer matrix by improving the interactions between the nanoparticles and the polymer chains. One of the more popular routes to induce improved interactions between the nanoparticles and bulk polymer is by modifying the surface of the nanoparticle by

grafting it with polymer chains that interact more favorably with the bulk polymer, often using chains that are chemically equivalent to the bulk polymer matrix.[32-36]

A consequence of using hard, inorganic nanoparticles within a polymer nanocomposite is their effect on the dynamics of the bulk polymer. The hard, impenetrable make-up of inorganic nanoparticles produces a confinement for polymer chain motion which results in an increase in the viscosity and decrease in diffusion coefficient of the polymer in the nanocomposite.[37] In systems using both "simple" and polymeric liquids, the magnitude of the change in viscosity can be expressed as a function of the particulate volume fraction within the system. Choi et. al. extensively characterized the effect of nanoparticles on the reduction of the diffusion coefficient of a polymer chain in a polymer nanocomposite.[38] It was reported that the depression in the rate of the diffusion of the polymer in a nanocomposite containing impenetrable nanoparticles collapses onto a master curve, where the magnitude of the decrease is primarily dependent on the nanoparticle's radius of gyration and interparticle spacing.

Polymer Nanocomposites with Organic Nanoparticles

Expanding upon research involving polymer nanocomposites with hard, impenetrable nanoparticles, organic all-polymer nanoparticle centric research has recently flourished.[17, 39-54] Similar to grafting chains to the surface of an inorganic nanoparticle to increase the nanoparticle's miscibility with the bulk polymer, an all-polymer nanoparticle is entirely comprised of polymer, and in many cases consists of a similar polymer to the bulk, resulting in a high miscibility of the nanoparticle and bulk polymer. These soft nanoparticles can be viewed as a structure that removed the

inorganic core entirely rather than "masking" the inorganic core with grafted polymer chains. Forming a nanoparticle without the inorganic center requires some control over it's morphology where a particle-like structure is formed via internal crosslinking of a polymer chain. One example are single-chain nanoparticles (SCNPs), formed by lightly crosslinking polymer chains to form soft nanoparticles, or synthesizing a molecule with extensive branching, like hyper-branched or dendritic-like nanoparticles. [17, 39, 40, 42, 49, 50, 55-60]

While both SCNPs and soft nanoparticles are formed via crosslinking, the methods of inducing those crosslinks differ between the two types of nanoparticles. The production of SCNPs is typically accomplished in two steps. A polymer chain precursor is first synthesized with a set content of reactive crosslinker randomly distributed throughout the chain. This first step allows for control over the crosslinking density and molecular weight of the nanoparticle. Higher crosslinking content on the precursor results in a higher crosslinked nanoparticle and is the norm in the production of SCNP. In most cases the crosslinking densities of SCNPs is in excess of 20%.[7, 40, 46, 48, 55, 56] While many SCNPs are formed using a linear precursor, there have been a number of studies where the SCNPs are developed from ring, star, and dendritic polymers where the structure of the precursor can have drastic effects on the morphology of the final SCNP.[61] Reports of single chain nanoparticles synthesized from a ring, star, and dendrimer precursor have been reported.[41, 43, 47, 54, 62-65] These studies showed that the use of a non-linear precursor afforded a higher degree of compactness/globule nature than typically achievable using a linear precursor.[43, 47] In a second step, the precursor is exposed to an external stimulus,

activating the reactive groups on the chain, inducing intramolecular crosslinking, where the end result is a globule-like particle similar to a folded protein. Depending on the reactive group used, there are many methods to induce crosslinking which can be covalent, dynamic covalent, or non-covalent.[48]

An interesting consequence of using an all-polymer nanoparticle in a polymer nanocomposite is the effect of the soft nanoparticle on the transport properties of components in the nanocomposite. While the inclusion of a hard nanoparticle typically inhibits chain motion and increases the viscosity of the system, Mackay et al first reported the opposite effect in a nanocomposite using polystyrene SCNPs.[66] In this seminal work, polystyrene SCNPs were mixed with linear polystyrene in loadings up to 10% weight, and rather than exhibiting an increase in the viscosity of the system as predicted by Einstein's theory of Brownian motion, the system exhibited a nearly 50% reduction in viscosity for all SCNP loadings.

At the time, the exact cause of the viscosity reduction was unknown by Mackay and coworkers, however later research performed by Goldansaz et al tested several of the leading theories on the mechanisms leading to the change in viscosity.[45] Goldansaz's study utilized a different type of all-polymer nanoparticle, a dendritic polyethylene, but observed the same reduction in viscosity as seen using SCNPs. This research confirmed that surface slippage, gap discrepancies, shear thinning, shear banding, reduction in entanglement density, confinement induced constraint release, and alteration of free volume are not the fundamental source of the viscosity reduction in the all-polymer nanocomposite systems. Around the same time, Chen et al. studied the dependence of the

molecular weight of the bulk polymer on the reduction of viscosity in similar nanocomposites.[57] These studies found that for nanocomposites with the same nanoparticle conditions (NP molecular weight, NP crosslinking density, and NP loading) but varying bulk polymer molecular weight, the magnitude of viscosity reduction scales with the molecular weight of the bulk linear polymer. It was suggested in this research that the inherent deformability and penetrability of the soft all-polymer nanoparticles was the source of decrease in viscosity in all polymer nanocomposites.

A second method for creating crosslinked all-polymer nanoparticles can be accomplished by forming crosslinks during polymerization. Not only is the nanoparticle formation completed in a single step, but the method of synthesis allows for a higher degree of control over the nanoparticles morphology when compared to SCNPs. First reported by Holley et al, these polystyrene nanoparticles are synthesized using a nano-emulsion polymerization where a known amount of crosslinking monomer (divinylbenzene in this case) is added to the monomer feedstock to promote crosslinking during the polymerization.[17] The end result is a spherical nanoparticle that has a well-defined crosslinked core and a fuzzy outer layer comprised of polymer chain loops and tails. Martin et al expanded upon the research done by Holley, by employing a monomer starved semi-batch nanoemulsion polymerization to control the rate of monomer addition during the polymerization and the molar fraction of divinylbenzene (crosslinking agent) to styrene (monomer).[50] This provided great control and tunability of the overall structure of the soft nanoparticles, including

independent control of crosslink density and soft nanoparticle molecular weight. Moreover, while most SCNPs have crosslinking densities in excess of 20%, well-defined structures formed using this synthetic method can attain crosslinking densities as low as 0.1%. The rigidity of the polystyrene nanoparticles was found to be directly related to their crosslinking density, where the higher the crosslinking density the more rigid the structure.[50] Similarly to SCNPs, these soft nanoparticles have also shown unexpected effects on the transport properties in polymer nanocomposites.[52, 67, 68] First reported by Miller et al, the addition of these soft polystyrene nanoparticles to a bulk polystyrene matrix resulted in an increase in the measured diffusion coefficient of the linear polystyrene matrix.[52] In these studies, a lower crosslinking density (i.e., less rigid) nanoparticle was found to have a more dramatic influence on the bulk polymer diffusion than more rigid nanoparticles.

Relationship between Polymer Conformation and Crosslinking Density

Soft polymeric nanoparticles synthesized via a monomer starved semi-batch nano-emulsion polymerization, when mixed with a linear polymer, have been shown to result in an unexpected increase in the measured diffusion coefficient of the linear polymers in the nanocomposite.[51, 52] Martin et al characterized the impact of these nanoparticles on the diffusion of the bulk polymer chain over a range of crosslinking densities from 0.81 to 10.7%.[51] This study found that the change in diffusion of the bulk polymer is dependent on two parameters, the crosslinking density of the nanoparticles and the relative size of the nanoparticle and polymer chains. When mixed with smaller chains ($R_{g(NP)} > R_{g(PS)}$), the diffusion coefficient of the bulk chains

decreases, and it is suggested that nanoparticles are acting as physical barriers which are impeding the motion of the chains. Whereas when mixed with larger chains ($R_{g(NP)} < R_{g(PS)}$), it is believed that the fuzzy interface of the soft nanoparticles enables constraint release of the polymer diffusion, increasing their diffusion rate. However, in these studies, the crosslinking density of the nanoparticles exhibits a clearly defined trend regarding the measured change in diffusion. In systems where diffusion is slowed by the inclusion of the soft nanoparticles, the impedance is more drastic as the crosslinking density of the nanoparticle increases. While in systems where diffusion is increased in the presence of the soft nanoparticles, the increase is more prominent with decreasing crosslinking density. Therefore, if one were to want to "optimize" the increase in diffusion with the inclusion of a soft nanoparticle, one would want to employ a minimally crosslinked variant, that still maintains particle-like functionality.

A standard definition of a nanoparticle is any object that ranges in characteristic size from 1-100nm, however ultra-high molecular weight polymer chains can achieve radii within this range and are not considered, and do not behave as, nanoparticles. Chremos and Douglas hypothesized upon this chain-to-particle transition in relation to polymer branching.[69] Performing molecular dynamic simulations, they investigated the influence of the functionality of star polymers on their segmental density and glass transition temperature. In star polymers with less than 5 arms, both their segmental density and glass transition temperature increases with increasing molecular weight. However, when a star polymer contains 5 or more arms, the segmental density

and glass transition temperature instead decrease with increasing molecular weight. This change in dependency at 5 arms can be attributed to a change in their molecular dynamics and a potential transition from chain-like to particle-like morphologies.

However, identifying a transition from chain-like to particle-like characteristics of a crosslinked polymer have not been examined in depth. Chapter 2 of this thesis will seek to address this shortcoming and identify the characteristics that define the transition of a polymer chain to particle-like with variation of crosslinking density. The impact of molecular weight on a polymer's particle like tendencies will also be evaluated by characterizing samples at the same crosslinking density but differing molecular weights. Additionally, the impact of polymer backbone rigidity on the transition from polymer chain to particle will also be evaluated by comparing polymers of equal crosslinking density but different backbone structure (polystyrene and poly(ethyl hexyl methacrylate)). The nanoscale structure and conformation of polymer chains or nanoparticles in dilute solution (1%wt) will be characterized using small angle neutron scattering (SANS). The polymeric nanostructures will be evaluated for their size, structure, compactness, and globular nature using a dimensionless Kratky plot, extracting the fractal dimension, and the ratio of radius of gyration to radius of hydration (R_g/R_H) from the SANS data.

Effect of Soft Nanoparticles on Dynamics of Polymer Nanocomposites

Penetrable, soft organic nanoparticles have been shown to alter the dynamics and transport properties of the matrix when added to a bulk polymer that deviates from the predictions of Einstein's theory of Brownian motion.[33, 57, 66, 70-77] First reported by

Mackay et al, where the addition of a polystyrene SCNP reduced the viscosity of the resultant nanocomposites, the investigation of non-Einstein-like behavior in transport properties has flourished over the last several decades. The inclusion an organic nanoparticle leads to a highly complex dynamic system whose mechanisms have eluded researchers since the seminal work by Mackay et al. Initially proposed as a conformational change and reduction in free volume by Mackay, much of the following research from groups attempting to understand this effect in other systems arrived at their own, different conclusions for the mechanistic source of viscosity reduction.[45, 71-75, 78-81] However, most of this research was conducted on systems slightly different than the one studied by Mackay, where many of the systems use additives that are not chemically equivalent to the bulk material. This results in further complications to the dynamics of the system and limits the universality of the conclusions. More recently, two studies by Goldansaz and Chen utilized systems where the nanoparticle and bulk material are chemically equivalent.[45, 57] Through a series of analyses, Goldansaz was able to eliminate many of the proposed mechanisms, including the reduction of free volume initially hypothesized by Mackay. Moreover, Goldansaz and Chen both arrived at the same conclusion, that the viscosity reduction effects being observed are a direct result of the softness, and penetrability, of the all-polymer nanoparticles.

The effects of soft polystyrene nanoparticles on the diffusive properties of the bulk polymer have also been well characterized. First reported by Miller et al., the inclusion of soft polystyrene nanoparticles to a bulk polystyrene matrix increases the diffusive properties of the bulk polymer.[52] These results were expanded upon by Martin

where a wider range of crosslinking densities were analyzed and a trend was observed where the lower crosslinking density nanoparticles provided the largest boost to the diffusion of the bulk polymer, when the size of the bulk chains were larger than the particle.[51] These studies attributed the observed changes in diffusion of the bulk polymer to a constraint-release mechanism provided by the fuzzy, soft nanoparticles.

The diffusion of the nanoparticles themselves have also been recently studied, first by Imel et al.[67] In systems containing an inorganic nanoparticle, the nanoparticles are approximated to being stationary, creating an impedance to chain diffusion, where the polymer motion is when required to move around the immobile nanoparticles. The observation that the inclusion of a soft, penetrable nanoparticle enhanced the diffusion of surrounding polymer chains spurred investigations into the mobility of the nanoparticles themselves. Imel found that the soft polymeric nanoparticles adhere to the slow mode theory, where diffusion is dictated by the slowest moving component in the system, and that they were in fact not stationary. The motion of these soft nanoparticles was found to be three orders of magnitude slower than a linear counterpart of comparable molecular weight. Similar to the previous studies using these soft nanoparticles, it was also determined that the crosslinking density, which dictates the softness and deformability of the nanoparticle, is a key contributor to their motion, where the higher the crosslinking density, the slower the diffusion of the nanoparticle. Shrestha et al expanded upon the findings by Imel to identify the mechanism that dominates nanoparticle diffusion in polymer melts.[68] This work identifies that the threading/dethreading of linear polymer chains through the loops and tails in the fuzzy corona of the soft nanoparticles controls

the nanoparticle diffusion. As the crosslinking density increases, the loops become tighter and the dethreading slows resulting in the slower diffusion of the nanoparticle.

While these studies offer insight into the global dynamics of the soft nanoparticle, there remains little insight into the local, segmental dynamics of the soft nanoparticle, including how the presence of the crosslinks impacts the temporal and spatial dependence of these faster modes. Results presented in Chapter 3 of this thesis seeks to address this knowledge gap, where the dynamics of the soft polystyrene nanoparticles in solution are probed using neutron spin echo (NSE) spectroscopy. NSE is a useful tool to observe relaxational motion in polymeric materials on the order of 10^{-12} to 10^{-6} s and can describe motion over a wide range of length scales from 1-600Å, the largest range of neutron techniques. This technique can identify length and time scales where the dynamics of these soft nanoparticles differ from the dynamics of a similar linear chain, thus elucidating the unique dynamic characteristics of the soft nanoparticle. In this chapter, the dynamics of four soft nanoparticles are probed to identify the impact of both crosslinking density and molecular weight on their motion. The dynamics of the nanoparticles are then compared to the dynamics of a linear chain of comparable molecular weight, and a length scale dependent diffusion coefficient, $D_{eff}(q)$, characterizes the length scales where the nanoparticle dynamics diverge from that of a linear chain. These results show that the effective diffusion coefficient of the soft polystyrene nanoparticles deviated from the behavior of a linear chain over length scales that are comparable to the size of the soft nanoparticle's core, indicating that the presence of the crosslinks is the main contributor to the variation in dynamics of the nanoparticles. This result is consistent with other

studies that monitor the center of mass diffusion of these nanoparticles, where the softness of the nanoparticle, which correlates to the extent of crosslinking, is directly related to an increase in the measured diffusion coefficient.

Permanency of Bound Layer in Polymer Nanocomposites

When creating a polymer nanocomposite, a beneficial interaction between the polymer and nanosized additive is usually required to minimize aggregation of the nanofiller.[16] While some nanocomposites may require a specific dispersion of the nanofiller to achieve the desired effects, in many cases the homogeneous dispersion of the nanofiller is targeted to ensure optimal properties. One of the more common methods to improve nanoparticle dispersion is by inducing attractive interactions between the nanoparticle and polymer matrix to inhibit aggregation of the nanoparticles.[82-84] Typically, these interactions derive from grafted polymer chains or the presence of functional groups that foster non-covalent interactions between the chain and nanoparticle. These interactions between the bulk polymeric material and the nanofiller frequently result in exceedingly suppressed mobility of bulk chains near the nanoparticle surface forming a bound polymer layer at the interface between the bulk polymer and nanofiller.[85-87] The motion of the surrounding chains becomes so slow that they are often considered to be stationary and irreversibly bound to the nanoparticle.[88-93] The presence of such a polymer bound layer results in interesting behavior. Generally, when the interactions between two components in a polymer blend/composite become stronger, the glass transition temperature is expected to increase. However, there are many reports of polymer nanocomposites where this increase in glass transition temperature is not

observed, even though strong interactions between the bulk polymer and nanoparticle exist.[90, 91, 94-98] One explanation is that the bound layer “shields” the nanoparticle from the bulk polymer, resulting in no observable change in the glass transition temperature of the polymer matrix in the nanocomposite. While chains adsorbed to the surface are typically considered to be "irreversibly” bound, the bound polymer layer as a whole is generally characterized rather than chain specific kinetics within the bound layer. Characterizing the bound polymer layer as a whole insinuates that the chains are completely immobile, whereas monitoring the individual chains that make up the bound polymer layer may reveal motion of “irreversibly” adsorbed chains.

Chapter 4 of this dissertation describes experiments that seek to gain a better understanding of the desorption behavior of a bound polymer layer. These experiments monitor the desorption of adsorbed chains on a flat substrate, which serves as a model for the bound layer in a polymer nanocomposite. An adsorbed polymer layer on a flat surface experience a significant suppression of their mobility/different dynamics from the bulk and are often considered to be irreversibly absorbed.[99] Studying the permanency of an adsorbed layer allows for simplification of the topology of the system (flat vs curved substrate) and a more direct observation of the motion of chains at the interface. Deuterating one of the components in the system provides contrast between the adsorbed and free polymer chains, where neutron reflectivity can be used to monitor the motion/desorption of the adsorbed layer. Therefore, in this chapter, neutron reflectivity is used to observe changes in the depth profile of a bilayer film that initially consists of a protonated adsorbed polystyrene layer and a deuterated free polystyrene layer. The

polystyrene in both layers have similar molecular weights, creating a system that limits the number of parameters that impacts the desorption and motion of the polymer chains. Many of the previous studies that monitor the desorption of polymer chains are solution based or drive the desorption by replacing the desorbing polymer with a more strongly adsorbed species. [86, 100-106] The current study differs from these previous works as it focuses on the desorption of polymer chains in the melt phase using chemically equivalent polymers. Monitoring the desorption and diffusion of adsorbed chains over an annealing time ranging from 2 to 24 hours and with two polystyrene chain lengths offers insight into the factors that control the desorption process. The desorption of polymer chains from a surface is rate limited by two kinetic steps, diffusion away from the surface and chain/surface detachment. In the melt these two processes are in competition with one another to be the dominating factor controlling desorption. In the solution state these processes appear to be mutually exclusive, with a very small molecular weight window where both processes contribute to the desorption. However, in our studies the melt state appears to have contributions from both processes. The characterization of the desorption of the two molecular weights show different processes dominate the desorption process. The desorption of the lower molecular weight species (20kDa) is primarily controlled by chain diffusion away from the surface, while the desorption of the larger species (62kDa) is impacted by a combination of the two processes with surface detachment exhibiting a stronger influence. The persistence of chain diffusion as a crucial process in the desorption process appears to be unique to the melt state where the mutual diffusion of desorbing chains away from the surface and adsorbing chains towards the surface is

sufficiently slow regardless of chain length. The desorption process appears to coour by fist the desorption of the loosely bound chains, where vacant adsorption site can be replaced with a newly adsorbing chain. Therefore, in the melt the total thickness of the adsorbed layer does not change despite the identity of the adsorbed chains changing with time. This indicates that while a bound polymer layer will persist for extended periods of time, specific chains are not indefinitely bound to a surface. Instead, there is an equilibrium where individual binding sites that are vacated by desorption are replaced with a newly adsorbing chains.

Non-Covalent Compatibilization of Polymer Matrix Composites

Polymer nanocomposites offer a route to imbue a bulk polymer with properties or functionality that it does not possess on its own. Similarly, polymer matrix composites are a class of materials comprised of a polymer matrix and an added filler that is usually larger than the nanoscale, which exhibit properties that exceed, or are a combination of, the bulk properties of the two components. One of the distinguishing features of a polymer matrix composite is that the components remain identifiably separate from each other when mixed.[107] In some instances, this visibly heterogeneous mixture of polymer and additive is beneficial to the system, typically when the filler's primary function is to enhance the structural properties of the bulk polymer. For instance, the addition of graphite, Kevlar, or glass fibers to a bulk polymer greatly enhances the structural strength of the polymer.[108-112] Similar to the effect of poor dispersion of nanoparticles in polymer nanocomposites, aggregation of additives in polymer composites suffer similar plights. Poor dispersion of an additive is usually a consequence of the immiscibility between the

components, poor intermolecular interactions between components, or exceedingly strong intramolecular interactions of one of the components. While grafting comparable polymer chains to a nanoparticle surface improves the dispersion of an additive in a polymer nanocomposite, that technique may not be viable in all systems using a small molecule filler. For instance, there may not exist a surface on which to graft a compatible polymer. Other techniques to increase the dispersion of additives within a bulk polymer include incorporation of covalent interactions, non-covalent interactions, or reactive compatibilization.[7, 113-124] These techniques often involve either functionalizing an existing component or introducing a third component to prompt compatibilizing interactions. Compatibilizing a polymer mixture with non-covalent interactions (i.e. hydrogen bonding) can be realized by introducing a functionalized additive without significantly altering the makeup of the bulk polymer. Polymer matrix composites containing a fire-retardant additive are one such category where this technique may be successful, where the success of compatibilizing techniques in improving the dispersion of an immiscible additive in a polymer matrix may improve the fire retardancy of the polymer.

Chapter 5 of this thesis focuses on the compatibilization of a fire-retardant polymer matrix composite to decrease the particle size and improve the dispersion of the additive throughout the bulk polymer. Melamine cyanurate is a common small molecule used as a fire-retardant additive to polymers. An adduct of melamine and cyanuric acid, melamine cyanurate (MC) benefits from a high nitrogen content as well as an extensive hydrogen bonding network making its decomposition strongly endothermic and serving

as a promising fire-retardant additive for a polymer matrix composite. However, that extensive hydrogen bonding network provides sufficiently strong intramolecular interactions that the melamine cyanurate agglomerates into large crystalline domains when mixed with most polymers. To address this poor dispersion, non-covalent compatibilization techniques are employed as a method of breaking up the crystalline MC domains. By replacing the intramolecular hydrogen bonding of melamine cyanurate with intermolecular hydrogen bonding using a polymeric dispersant, the sizes of the large crystalline MC domains decrease significantly. Additionally, coordinating the melamine cyanurate with a polymer dispersant not only reduces the overall particle size by breaking up the hydrogen bonding network, but also serves as a buffer around those particles to prevent them from aggregating further. These results show that the addition of a water-soluble polymer dispersant to promote good interactions with the melamine cyanurate creates a composite where the size of the MC domain decreases by more than 50% relative to composites with no dispersant. Not only does the dispersant decrease the average measured particle size, but it also improved the homogeneity of the measured particles as well. The addition of a polymer dispersant results in a nearly 75% increase in the homogeneity of the particle sizes. This reduction of particle size and increased homogeneity provides clear pathways to develop polymer dispersants that are instrumental in creating more uniform fire-retardant polymer matrix composites.

Summary

The introduction of soft nanoparticles to a polymer matrix can introduce non-Einstein-like effects on the transport properties of the system , and investigating these systems on a fundamental level can provide insight that will enable to rational design and production of polymer composites and nanocomposites with targeted properties. For instance, the addition of soft polystyrene nanoparticles to a bulk polystyrene matrix increases the diffusion coefficient of polymer when the size of the nanoparticles is smaller than the size of the matrix chains, where these systems have been very well characterized. However, a thorough understanding of the structure and dynamics of the nanoparticles is still lacking. The first two chapters of this dissertation concentrate on characterizing the structure and dynamics of soft polystyrene nanoparticles using neutron techniques. In Chapter __ the impact of crosslink density on the morphological identity of these nanostructures from polymer chain to nanoparticle is probed. The evolution of a surface is the distinguishing factor that delineates these nanostructures between polymer chains and nanoparticles. Chapter __ analyzes the differences in the global and local dynamics of these nanoparticles using neutron spin echo spectroscopy. The variation in behavior of these nanoparticles and that of a linear chain is elucidated based on the suppression of local dynamics caused by the presence of crosslinking within the nanoparticle. Chapter __ examines the behavior of a bound polymer layer in polymer nanocomposite analyzing the adsorption and desorption of chains whose mobility are greatly suppressed due to the presence of an adsorbing surface. The processes that control the desorption of the polymer in the melt are found to be dependent on their molecular weight, where the

importance of the detachment of bound sites quickly outpaces the chain diffusion from the surface as the molecular weight increases. Additionally, neutron reflectivity provides a unique perspective of the evolution of the bound layer during annealing, showing that some chains can completely desorb from the surface. Finally, Chapter __ concentrates on optimally dispersing small molecule additives throughout a polymer matrix via non-covalent interactions. Melamine cyanurate, a small molecule formed through an extensive hydrogen bonding network, produces smaller crystalline domains when a hydrogen bonding capable polymeric dispersant is added to the blend. Scanning electron microscopy shows that both the average size and size distribution of the crystalline melamine cyanurate domains within a polymer matrix decrease with added dispersant. Fourier transform infrared spectroscopy monitors the change in the extent of hydrogen bonding in a blend to confirm the disruption of the hydrogen bonding network of the melamine cyanurate by the polymeric dispersant.

CHAPTER 2 : WHEN DOES A SOFT NANOPARTICLE TRANSITION FROM POLYMER CHAIN TO A NANOPARTICLE?

Abstract

Frequently, the defining characteristic of a nanoparticle is simply its size, where objects that are 1-100nm in size are characterized as nanoparticles. However, macromolecules, in particular high molecular weight polymer chains, can satisfy this size requirement without providing the same phenomena as one would expect from a nanoparticle. At the same time, the recent flourish of all polymer nanocomposites has led to the synthesis of soft all-polymer nanoparticles, which emerge from internal crosslinking of a macromolecule. Moreover, soft polymer nanoparticles are important in a broad range of fields, including understanding protein folding, drug delivery, vitrimers, catalysis and nanomedicine. The performance of all-polymer nanoparticles is exquisitely dependent on its softness, which is directly correlated to its crosslinking density. Thus, there exists a transition of an internally crosslinked macromolecule from a polymer chain to a nanoparticle as the amount of internal crosslinks increases, where the polymer chain exhibits different behavior than the nanoparticle. Yet, this transition is not well understood. In this work, we seek to address this knowledge gap and determine the transition of a macromolecule from a polymer chain to a nanoparticle as internal crosslinking increases. In this work, small angle neutron scattering (SANS) offers insight into the structure of polystyrene and poly(ethyl hexyl methacrylate) (PEHMA) nanostructures in dilute solutions, where the crosslinking densities of the soft nanostructures varies from 0.1-10.7%. Analyses of the SANS data provides structural characteristics to assist in classifying a nanostructure as chain-like or particle-like and identifying a crosslinking dependent transition between the two morphologies. The

particle-like behavior of a soft polymeric nanostructure is correlated to the existence of a surface that manifests as a measurable peak height of a dimensionless Kratky plot and a fractal dimension greater than 3. It was found that for both types of polymeric nanostructures, a crosslinking density of 0.81% (~ a crosslink for every 1 in 125 monomers) or higher exhibit clear particle-like behavior. Lower crosslinking density nanostructures showed amounts of collapse similar to that of a star polymer (0.1% XL) or a random walk polymer chain (0.4% XL). Thus, the transition of an internally crosslinked macromolecule from a polymer chain to a nanoparticle occurs at very low crosslink densities and occurs via the gradual contraction of the chain with incorporated crosslinks.

Introduction

Polymer nanocomposites (PNC) are a class of materials in which a nano-sized particle is dispersed in a bulk polymer matrix. The addition of these small structures improves the bulk mechanical, thermal, or chemical properties of the polymer.[4, 5, 9, 34, 125] Often, the nanomaterial is comprised of an inorganic core with polymer grafted to the surface,[33, 35, 36] however, recent interest has focused on developing and implementing all-polymer nanocomposites, or all-PNC.[49, 61, 68, 126, 127] An all-polymer composite consists of a polymer matrix with a nanoparticle that is entirely comprised of organic material, foregoing the traditional inorganic center. This class of nanoparticles is interesting and desirable as the nanoparticle generally disperses more readily in the polymer matrix than hard impenetrable nanoparticles.[16, 39, 52] This is primarily due to more favorable interactions between the bulk polymer and polymer nanoparticle.[17] Poor interactions between nanoparticle and polymer usually leads to nanoparticle agglomeration, and inferior properties.[3, 18-27]

More broadly, soft nanoparticles have received great interest lately due to their potential use in a range of applications, including drug delivery, all polymer nanocomposites, and self-healing materials.[51, 52, 60, 68, 127, 128] These soft nanoparticles are generally formed via extensive branching and/or internal crosslinking of macromolecules to form nanoscale particle-like structures.[50, 56, 57, 126] Two classes of Polymer nanoparticles formed via internal crosslinking include a single chain nanoparticle (SCNP), or a soft polymeric nanoparticle. SCNPs are commonly formed by synthesizing a linear precursor polymer chain with a known amount of crosslinker distributed along

the polymer chain.[46, 53, 129-131] This precursor then undergoes crosslinking reactions, collapsing the chain, and forming a nanoparticle. This process is akin to protein folding and typically contains crosslinking moieties in excess of 20%.[7, 40, 46, 48, 55, 56] Because of the random distribution of the crosslinking sites along the polymer chain and during particle formation, the structure of SCNPs is typically not well defined or controlled. Alternatively, soft polymer nanoparticles are synthesized in a reaction where the monomers and crosslinking agents react simultaneously during polymerization. The structure of soft polymeric nanoparticles is very well controlled synthetically, where the molar ratio of crosslinking agent to monomer and the rate of monomer addition in the polymerization are easily varied and controlled and impact the structure of the fabricated soft nanoparticle.[17, 50] Soft polymeric nanoparticles exhibit a fuzzy sphere morphology defined by a crosslinked core, and fuzzy loops and tails on the outer shell of the particle. In general, increasing crosslinking density increases the core size and reduces the size of the fuzzy interface.[17, 50, 52, 67, 132]

One of the more interesting results regarding all polymer nanocomposites is the variation of the transport properties of all PNCs from Stokes-Einstein behavior. In the early 1900s, Einstein's study of Brownian particles suspended in a liquid led to the understanding that the viscosity of a liquid increases with the inclusion of particles, where this concept holds true for polymeric melts as well.[37, 133] Mackay et. al. were one of the first to observe a reduction in the measured viscosity of a polymeric melt with the addition of a *nanoscale* additive, an SCNP.[66] Further work by Chen et al. hypothesized that the source of this viscosity reduction is rooted in the deformability,

or softness, of the SCNPs and is related to a reduction in the friction between the nanoparticle and polymer chain.[57]

On the other hand, the addition of an impenetrable nanoparticle to a polymer matrix slows the center of mass diffusion of the polymer chain.[134-139] However, when a soft penetrable (i.e. polymeric) nanoparticle is added to a polymer matrix, the diffusion coefficient of the polymer chain may *increase.*[50-52] For instance, Martin et al. showed that the relative size of the polymer chain to that of the soft nanoparticle plays an important role in realizing this modification of polymer diffusion. This work showed that the diffusion of the polymer is enhanced when the radius of gyration of the bulk polymer is greater than that of the soft polymer nanoparticle. Moreover, nanoparticles with lower crosslink density enhance the polymer diffusion the most.[51] Following this logic, a polymer chain is the nanostructure with the lowest crosslink density (i.e. 0%), and thus should provide the optimal enhancement of the polymer diffusion in the nanocomposite. However, the addition of a linear polymer with the same molecular weight as the soft nanoparticle *slows* polymer diffusion. Thus, the 'particle-like' nature of the soft nanoparticle must be an important factor in realizing this diffusive behavior. Therefore, to maximize the polymer diffusion in an all-PNC, a polymeric nanoparticle with minimal crosslinking density that still exhibits particle-like behavior is needed. To date, the lowest crosslink density examined is 0.81%, where all structural analyses confirm particle-like structure. Given the requirement for particle like behavior, the correlation of crosslink density to particle-like behavior must be more thoroughly defined. Will a single crosslink in a long polymer chain form a

‘nanoparticle’? Is there a limiting percent of crosslinking that is needed to transition a polymer chain to a soft nanoparticle? The experiments described in the paper seek to address these questions.

From a broader perspective the definition of what makes a construct a ‘nanoparticle’ is not clearly defined. In the most general sense, nanoparticles are defined as objects with sizes ranging from 1-100nm. However, the dominance of the presence of a surface on a nanoparticle often results in unique properties that differ from those of the bulk material, a feature that makes nanoparticles an area of great research interest.[12-15, 140] Typically, the emergence of unique properties of a nanoparticle arises from the balance between the bulk properties of the particle and those of its surface. When sufficiently small, the particles may become thermodynamically unstable due to excess energy of the surface.[12] In order to stabilize the nanostructure, the nanoparticles often change their crystallographic structure, and this variation in assembly leads to many of the unique features of nanoparticles.[13-15] Thus, many of the unique properties observed in nanoparticles are governed by the presence and properties of the surface structure of the nano-object. Therefore, we posit that for a polymeric nanostructure to behave as a nanoparticle, the assembly of the crosslinked assembly must develop an external surface. To test this hypothesis, we have completed a set of small angle neutron scattering experiments to correlate the topology, morphology, and crosslink density to the presence of a surface in soft nanoparticles to identify the correlation of crosslink density to the transition of a crosslinked polymer chain to a polymeric nanoparticle.

Small angle neutron scattering (SANS) offers a method to determine the morphological characteristics of soft polymeric nanostructures including size, structure, compactness, and the globular nature of the nanostructure. Because the configurations of soft polymeric nanostructures are readily controlled synthetically by varying the crosslinking density of the sample, the impact of varying crosslink density on the chain-like or particle-like nature of the nanostructure is examined. The impact of segmental rigidity on the chain to particle transition is also investigated by synthesizing polymeric nanostructures from poly(ethyl hexyl methacrylate) (PEHMA) and polystyrene (PS). The neutron scattering curves are analyzed to elucidate particle like structure by examination of the Kratky plot, fractal dimension, and ratio of the radius of gyration to the hydrodynamic radius of the nanostructure. Careful analysis of the scattering data offers insight into the transition of the morphology of the soft polymer nanostructure from random coil chain-like to collapsed globular particle-like as a function of structure crosslink density.

Experimental

Materials

2-Ethyl hexyl Methacrylate (EHMA, TCI, >99.0%), 1,6 hexanediol dimethacrylate (HDDMA, Aldrich, ≥90%), styrene (Aldrich, 99.9%) and divinylbenzene (DVB, Aldrich, 90%, 80 para content, technical mixture) were passed through an alumina column to remove inhibitors prior to use. Dodecyl trimethylammonium bromide (DTMAB, TCI >98%), potassium persulfate (KPS, >99% Acros Organics), tetrahydrofuran (THF,

Sigma-Aldrich, >99%), methanol (Sigma-Aldrich, >99%), and deionized water (DI water, Sigma-Aldrich, HPLC Plus) were used as received.

Synthesis of soft nanostructures

The soft polymer nanostructures were synthesized via a modified semi-batch nano-emulsion polymerization previously detailed by Martin *et. al.*[50] In this procedure, a surfactant solution is first prepared by combining 20g of DTMAB, 25mg of KPS, and 50mL of DI water in a round bottom flask. The flask is then capped with a rubber septum, purged with argon, and sonicated for 30 minutes to ensure homogeneity of the solution. The surfactant flask is then placed into an oil bath at 65°C and stirred for 10 minutes to allow the solution to reach the required reaction temperature. In a separate vial, 5mL of the monomer (EHMA or styrene) is combined with the appropriate amount of crosslinker (HDDMA or DVB) to attain the targeted crosslinking density. The monomer solution is then capped and purged with argon for 10 minutes. The monomer solution is then drawn into an airtight glass syringe and added to the surfactant solution at the desired rate of addition using a syringe pump. For the polystyrene (PS) samples, the monomer rate of addition was varied from 1, 2, and 10mL/hr depending on the sample, while the poly(ethyl hexyl methacrylate) (PEHMA) samples all utilized a monomer rate of addition of 2mL/hr. The variation in the monomer rate of addition results in control of the nanoparticle molecular weight, independent of crosslinking.[50] Following the entire monomer addition, the reaction is allowed to proceed for 2hr. Once completed, 5mL of THF was added to the flask to swell the polymer, which were then precipitated in excess methanol (~300mL) in a refrigerator (~7°C) overnight. The precipitate was then plated

into a Soxhlet extractor and extracted with methanol to completely remove residual surfactant. The resulting polymer was then dried in a vacuum at 50°C (PS) and 90°C (PEHMA) for 48 hr.

Small Angle Neutron Scattering

Small angle neutron scattering (SANS) experiments were conducted using 1%wt solutions of the soft polymer nanostructures in d_8-THF at the Oak Ridge National Laboratory (ORNL) HFIR beam line CG-2 (GP-SANS). Three sample-to-detector distances were used; 18m, 2m, and 0.3m with a wavelength of 12 Å allowing for a q range of 0.0015 to 0.6 $Å^{-1}$ where $q = (4\pi/\lambda)\sin(\theta/2)$, λ is the neutron wavelength, and θ is the scattering angle. The raw data was reduced using SPICE ORNL reduction macros in Igor Pro. Samples were measured at 25°C and the data was transformed into absolute intensities by correcting for incoherent, background, solvent, and empty cell scattering, neutron beam flux, and normalized to the scattering of a known standard. The fitting of the data was performed using SASView software.[141]

Dynamic Light Scattering

Dynamic Light Scattering (DLS) was used to determine the hydrodynamic radius, R_h, of the polymeric nanoparticles. The nanoparticles were dissolved in THF (1 mg/mL) and filtered through a 0.22 μm syringe filter. DLS was performed with a home-built instrument in 90 degree geometry. The vertically polarized light was generated from a HeNe laser – Newport R-31425, 633 nm, 35 mW and focused by an F = 100 mm lens into a cylindrical vile. The light scattered at 90 degrees was passed through a similar lens

and filtered with 632.8 nm MaxLine laser clean-up filter from Semrock to suppress fluorescence and improve signal to the noise ratio. The filtered light went through an enhances + fiber optical beam splitter from ALV and was captured by Single Photon Counting Module (SPCM) light detectors from Exilitas. These detectors were connected to an ALV-7004/Fast correlator that was used in cross-correlation mode for all experiments.

SANS Analyses

The conformation of a polymeric nanostructure is determined by the analysis of its scattering curve, where different structural characteristics are elicited with various analyses. A Kratky plot, which emphasizes the rate of change in scattering intensity at higher q, provides insight on the local structure of a scattering object. Similarly, a fractal analysis offers insight to the fractal dimension of an object which can be correlated to the structure's compactness. Finally, the ratio of the radius of gyration (R_g) of an object to its hydrodynamic radius (R_H), which will be referred to as the 'radius ratio' of an object, varies with the architecture of the nanoscale object, and when considered in conjunction with the results of a Kratky and fractal analysis will further illuminate the structural conformation of the polymeric nanostructures.

Typically, SANS curves are depicted as a plot of the scattering intensity, I(q), as a function of the scattering vector, q. The variation of the scattering intensity with q provides information on the size, compactness, structure, and alignment of a polymeric nanostructure. Guinier's law is a common model used to fit scattering data to determine

the radius of gyration of the scattering object as shown in Equation 2.1, which is valid at low q where qRg << 1.

$$\ln\left(\frac{\boldsymbol{I(q)}}{\boldsymbol{I(0)}}\right) = -\frac{\boldsymbol{R_g^2}}{\boldsymbol{3}}\boldsymbol{q^2} \qquad 2.1$$

Kratky Plot

A Kratky plot, which presents the data as $I(q) \cdot q^2 \; vs \; q$, is a common analysis method used to monitor the structure of biomacromolecules such as proteins, where the analysis elucidates the random-coil nature or extent of molecular folding of a protein molecule (i.e., globular nature). Similarly, the Kratky analysis of the scattering of a polymer chain provides a measure of the deviation of the chain from an ideal Gaussian coil. The scattering intensity of an ideal Gaussian chain scales with q^{-2}, which manifests in a Kratky plot as a plateau at high q due to the coupling of the scattering intensity with q^2. Moreover, as a polymer chain deviates from ideal Gaussian behavior, a deviation from that plateau is readily apparent in the Kratky plot. Furthermore, as a polymer chain collapses and becomes more compact, its scattering intensity scales more strongly with q which leads to the emergence of a peak in the Kratky plot before the plateau.[142-146] Therefore, the Kratky plot offers evidence of the particle-like behavior of a polymer based on the existence and intensity of a peak found in the Kratky plot.

While a standard Kratky plot offers a qualitative assessment of the particle-like nature of a polymer chain, a dimensionless Kratky plot is necessary to compare the structure of different polymeric nanostructures that may differ in size (Rg) and molecular

weight. The normalization of the Kratky plot is implemented by scaling the q axis with radius of gyration of the measured polymer, where doing so normalizes the differences in size of the polymeric nanostructures. The scattering intensity, I(q), is also divided by I(0), where this normalization takes into account the polymer molecular weight and solution concentration. These normalizations are implemented in the analysis discussed below and allows the quantitative comparison between different polymer nanostructures in the determination of their particle-like behaviors.[143]

Further, the location and intensity of a peak that may occur in a dimensionless Kratky plot provides insight into the exact conformation of the polymer, where a globular compact particle will exhibit a peak at $qR_g = \sqrt{3} \approx 1.73$ and have an intensity of approximately 1.1. Deviations from this peak location and intensity in a dimensionless Kratky plot indicate that the structure is less compact than that of a completely compacted globule.[142, 147]

Fractal Dimension

Scattering in the range of wavevectors $2\pi/R < q < 2\pi/b$, where R is the radius of the polymer chain, and b is the statistical segment length, probes length scales that are below that of the polymer chain as a whole, but are larger than a statistical segment of the polymer. Analysis of the scattering over this q-range provides information on how compact the polymer segments are packed in the nanostructure, or its fractal dimension. The scattering intensity in this regime scales with q^{-D}, where D is the fractal dimension of the polymer. Therefore, analysis of the slope of a log-log plot of the scattering intensity

as a function of the scattering vector, sometimes referred to as a Porod plot, provides a quantitative measure of the fractal dimension of the polymer nanostructure.

Moreover, correlating the fractal dimension of a polymer chain to its conformation is reasonably straight forward. It is well established that the size of a polymer coil, *R*, scales with its molecular weight as $R \sim M^{\upsilon}$, where υ is the Flory exponent of the polymer. The scattering vector is defined as $q = 4\pi \sin\theta/\lambda$, where θ is the scattering angle, and λ is wavelength of the radiation source. The intensity of scattering at scattering vector q monitors the structure of the scattering object at a length scale, *d*, where $d \sim 2\pi/q$. Therefore, the fractal dimension is inversely related to the Flory exponent of a polymer, ν, as shown in Equation 2.2.

$$\boldsymbol{I(q) \propto q^{-D} = q^{-1/\upsilon}} \qquad 2.2$$

The Flory exponent for polymers in good solvents, theta solvents and in the melt are well known, where a linear polymer in a good solvent behaves like a self-avoiding walk (υ = 0.6) and a linear polymer in a theta solvent or a melt behave like a random walk (υ = 0.5). Further collapse of a polymer chain in a poor solvent will form a globular like structure ($0.3 < \upsilon < 0.5$). These translate into a swollen polymer chain in a good solvent having fractal dimensions of 1.67, the D of a polymer in a theta solvent equal to 2, and a globular like polymer has $2 < D < 3$. Therefore, as a chain collapses (and becomes more particle like), the fractal dimension increases.

Fractal dimensions below 3 correspond to a mass fractal dimension, where a value of 3 describes a collapsed, 3-dimensional solid structure. However, once a structure is fully collapsed the scattering of the surface contributes to the measured scattering and

provide a measured fractal dimension that exceeds 3. In this case, a measured fractal dimension that emerges from the analysis above ranges between 3 and 4 and is a "surface fractal dimension" that physically describes the structure of a surface, ranging from a rough surface to one that is very smooth. [146, 148, 149]

Ratio of R_g/R_h, The Radius Ratio of a Nanostructure

The ratio of a polymer's radius of gyration, found via SANS, to its hydrodynamic radius, found via dynamic light scattering, is related to the conformation and assembly of a polymer nanostructure. We designate this parameter the 'radius ratio'. The change in the value of the radius ratio of a macromolecule with variation in conformation has been well documented, where a polymer chain that obeys a self-avoiding walk (i.e. in a good solvent) exhibits a radius ratio of ~1.56, while a polymer chain that obeys a random walk (i.e., in a theta solvent) has a radius ratio of ~1.24.[150-153] Moreover, it is also well documented that a hard sphere exhibits a radius ratio of 0.78.[150] Furthermore, values of the radius ratio that are less than that of a hard sphere correlate to an object that adheres to a core-shell structure. A core shell structure shows a smaller R_g/R_h when the mass of the structure is more densely concentrated in the core but is less dense in the outer shell. This construct results in the radius of gyration of the nanostructure that is much smaller than the hydrodynamic radius, resulting in a small R_g/R_h. Thus, a decrease in R_g/R_h from above 1 to 0.78 signifies the densification of the nanostructure to a homogeneous globule, with values of R_g/R_h below 0.78 signifying heterogeneity of the radial distribution of mass within the nanostructure, i.e., a core-shell type structure.

Results and Discussion

Kratky Plot Analysis

The scattering of a linear, or 0% crosslinked, nanostructure of both polymers (i.e., a polymer chain) is measured and analyzed and serves as a baseline to compare the behavior of other nanostructures that are crosslinked. The dimensionless Kratky plots of polystyrene and poly(ethyl hexyl methacrylate) are shown in Figure 2.1 and present similar behavior. As previously stated, a polymer in a theta solvent, which obeys a random walk, is expected to exhibit a plateau in the Kratky plot at $qR_g \gtrsim 1.5$, and that the emergence of a peak in this region indicates particle-like behavior. Neither the PEHMA nor PS chains show these characteristics, but rather show a linear increase above $qR_g \gtrsim 1.5$, which indicates that the polymer does not obey random walk statistics. This lack of a plateau is consistent with the conformation of the polymer in a good solvent, i.e., a self-avoiding walk. This is not surprising, as deuterated THF is a good solvent for both polymers at the concentration and temperature of the scattering experiments. The nanostructures formed with the addition of crosslinking agents to the synthetic procedure show considerably different Kratky plots compared to that the linear samples. These results are plotted in Figures 2.2 and 2.3, where the samples with less than 0.8% crosslinking are plotted in Figure 2.2, while those with crosslinking ≥ 0.8% are plotted in Figure 2.3. In Figure 2.2, the samples with the lowest crosslinking density readily show Kratky plots that differ significantly from that of the linear polymer chain. The scattering of the 0.1%XL PS sample, the blue closed squares in Figure 2.2a, shows a short plateau in the Kratky plot from ca. $1.5 < qRg < 2.5$, followed by a monotonic

a.)

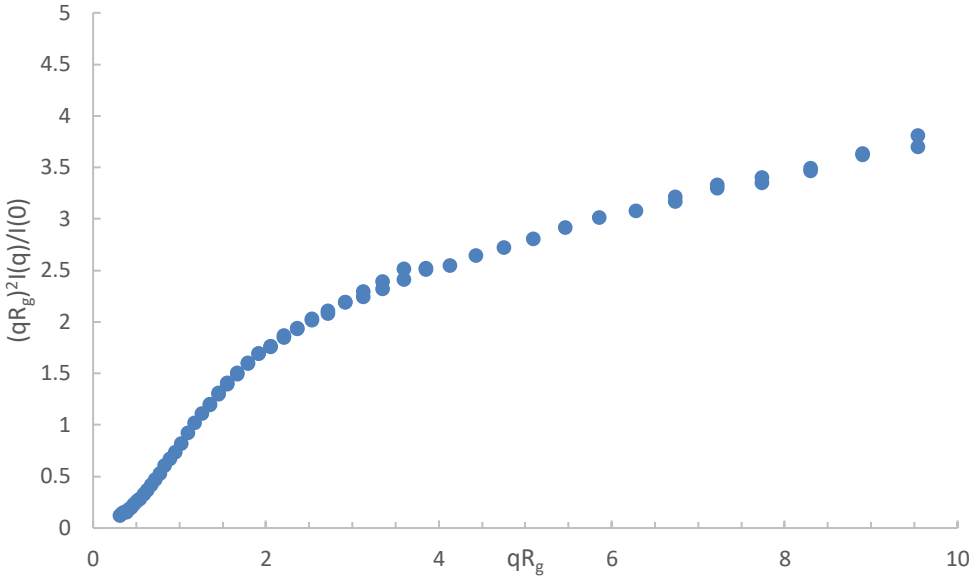

b.)

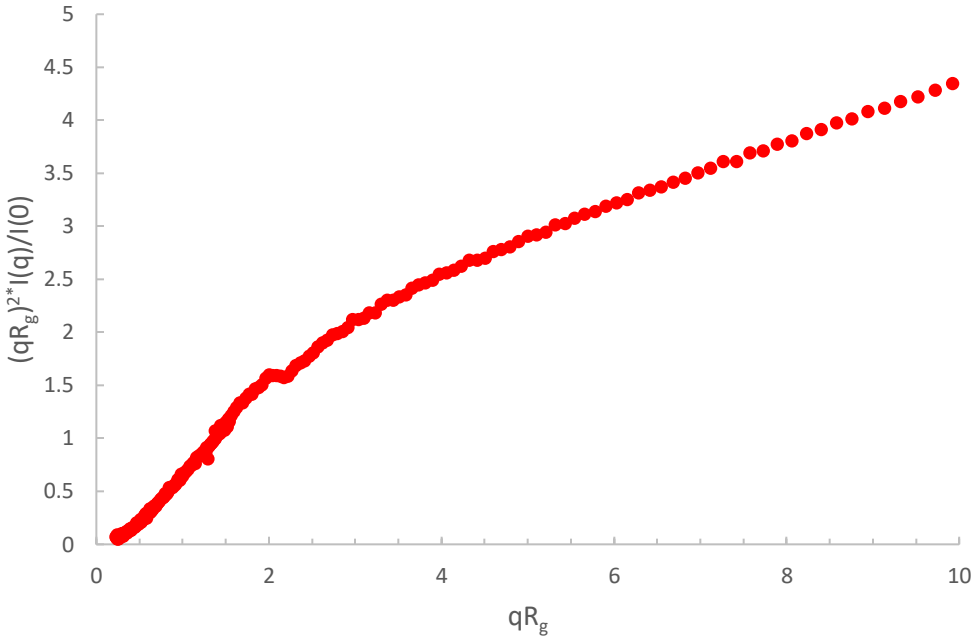

Figure 2.1 Dimensionless Kratky plot of 0% crosslinking, linear, nanostructures. a.) PS, b.) PEHMA

a.)

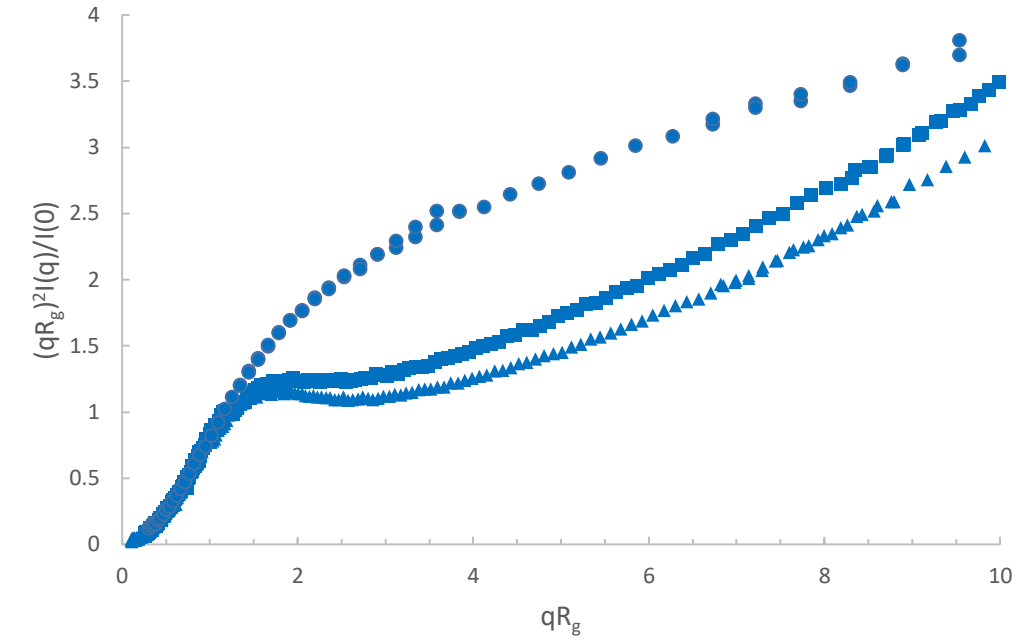

b.)

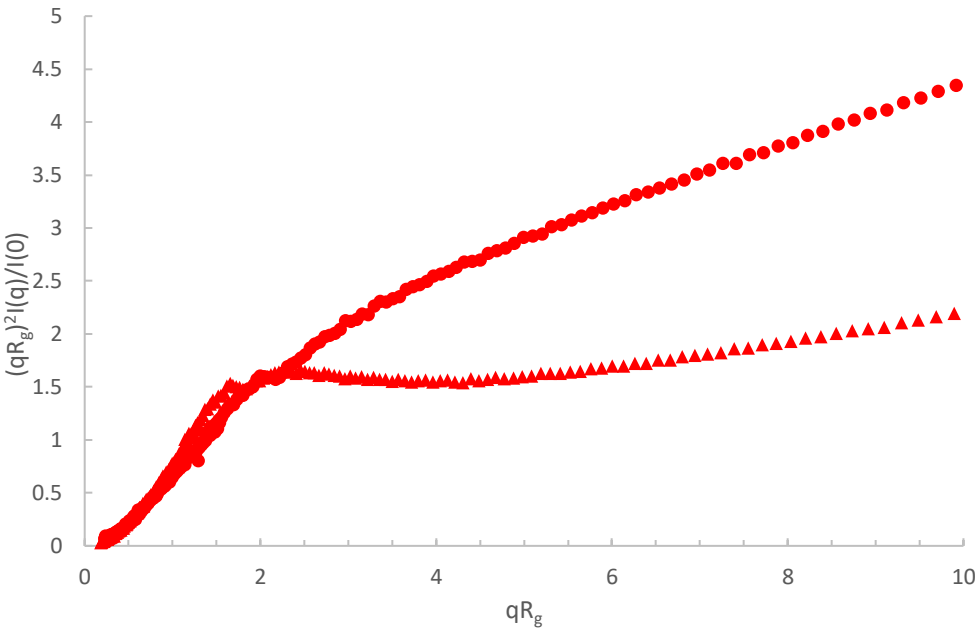

Figure 2.2 Dimensionless Kratky plot of low crosslinking nanostructures. a.) PS, b.) PEHMA; ● = 0%XL, ■ = 0.1%XL, ▲ = 0.4%XL in both plots

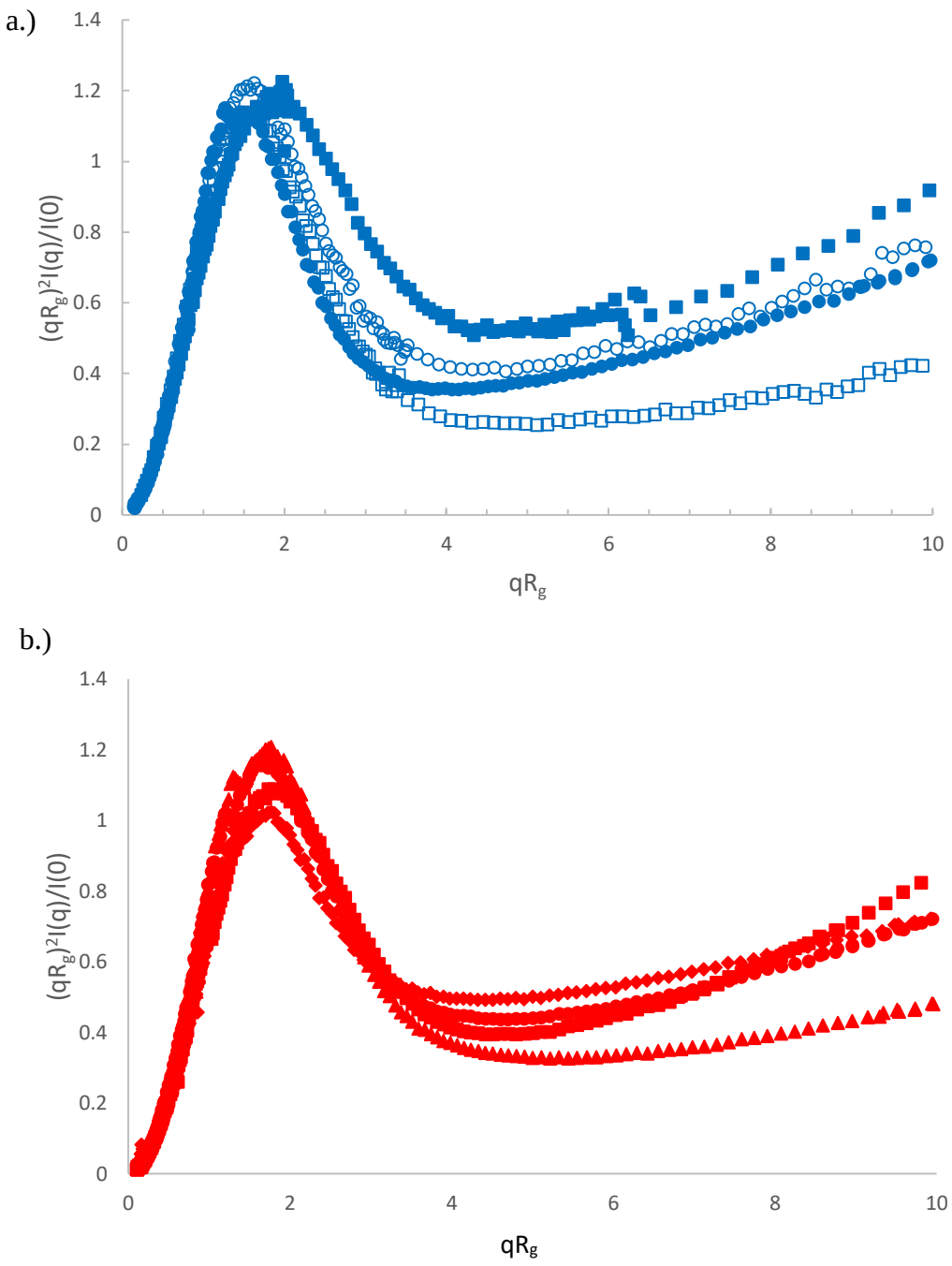

Figure 2.3 Dimensionless Kratky plot of high crosslinking density nanostructures. a.) PS, b.) PEHMA; ●=0.8%XL, ◆=1.9%XL, ▲=4.6%XL, ■=10.7%XL in both plots; Closed markers signify low MW, open markers signify high MW

increase. The emergence of this plateau, and lack of any measurable peak in this sample is consistent with a structure that resembles a polymer chain in a theta solvent, i.e., a random walk. Thus, the incorporation of only 0.1% crosslinking (*ca.* 1 in 1000 monomers is crosslinked) transforms the conformation of the polymeric nanostructure from a swollen polymer chain to a more collapsed polymer chain, but does not establish an observable surface based on the absence of a peak. Increasing the crosslinking density to 0.4%, which is plotted as the blue closed triangles in Figure 2.2a, results in a Kratky plot that exhibits similar characteristics, but a slight peak at qRg ~ 1.7 begins to emerge. At this crosslink density, the plateau begins at a similar qRg as the 0.1%XL sample and spans a similar range. Further, the increase from the plateau occurs at a similar qRg, indicating that these two nanostructures have comparable flexibility (i.e., identical Kuhn or persistence length). Thus, increasing the crosslinking by a factor of 4 (*ca.* 1 in 250 monomers is crosslinked) results in a similar collapsed polymer chain-like structure, and the beginnings of an observable surface as indicated by the peak emergence. Inspection of the scattering of the 0.4%XL PEHMA sample, plotted as the closed triangles in Figure 2.2b also displays an extended plateau with a slight peak at qRg ~ 2.4 in the Kratky plot. The deviation from the plateau occurs at a larger qRg than the polystyrene nanostructures, which is consistent with the fact that the PEHMA is more flexible (i.e., smaller Kuhn length) than the polystyrene. The shift of the peak to a larger qRg value for similar crosslink densities is also consistent with the greater flexibility of the low crosslinked PEHMA samples relative to the polystyrene structures.

All of the nanostructures with higher crosslink density (≥ 0.8%) show Kratky plots that differ significantly from those of the nanostructures with lower crosslink density, as shown in Figure 2.3. In each of these samples, a clear and well-defined peak in the Kratky plot is observed indicating that all of these samples have definable surfaces and attain a globular particle-like structure. The upturn in normalized scattering intensity at larger qR_g indicates that these particles still maintain some flexibility/deformability at local lengths scales ($qRg \gtrsim 4\text{-}5$).

More detailed analysis of these peaks provides further insight into the variation in structure of these particle-like structures with crosslink density. The peak height, position, and maximum scattering intensity of the Kratky peak at $qRg \sim 1.5\text{-}2$, are determined and listed in Table 2.1. The peak height is defined as the difference between the local maximum peak intensity and the local minima following the peak. A nanostructure akin to an ideal Gaussian chain does not exhibit a peak in the Kratky plot, and as a result will not have a measurable peak height. Recalling that the low crosslinking density nanostructures in Figure 2.2 present plateaus in their Kratky plot, this results in a minimal measurable peak height. As the crosslinking density increases and the nanostructures begin to take on more particle-like morphologies, the peak height increases. This is a particularly effective analysis to quantitatively compare the extent of the particle-like nature of the lower crosslinking nanostructures whose morphologies are somewhere between that of an ideal Gaussian chain and a fully formed particle.

Inspection of the peak height reinforces the previous qualitative observations of the Kratky plot that indicate a clear transition to particle-like behavior for nanostructures

Table 2.1 Kratky Plot Peak Parameters*

Nanoparticle	Peak Height[a]	Peak Maximum[b]	Peak Location[c] (qR_g)
0.1%XL PS	0.033 ± 0.004	1.268 ± 0.078	1.761 ± 0.053
0.4%XL PEHMA	0.123 ± 0.001	1.663 ± 0.350	2.456 ± 0.009
0.4%XL PS	0.071 ± 0.001	1.160 ± 0.018	1.737 ± 0.013
0.8%XL PEHMA	0.737 ± 0.009	1.173 ± 0.015	1.629 ± 0.011
0.8%XL PS (low MW)	0.796 ± 0.004	1.150 ± 0.003	1.270 ± 0.005
0.8%XL PS (high MW)	0.816 ± 0.001	1.220 ± 0.001	1.625 ± 0.014
1.9%XL PEHMA	0.532 ± 0.002	1.024 ± 0.004	1.767 ± 0.003
4.6%XL PEHMA	0.883 ± 0.016	1.209 ± 0.021	1.770 ± 0.016
10.7%XL PEHMA	0.694 ± 0.010	1.087 ± 0.015	1.734 ± 0.012
10.7%XL PS (low MW)	0.716 ± 0.003	1.223 ± 0.001	1.975 ± 0.046
10.7%XL PS (high MW)	0.884 ± 0.001	1.137 ± 0.001	1.494 ± 0.011

*Black and blue text denote PS and PEHMA respectively

[a]Peak height - Difference in normalized scatting intensity of local peak maxima and local minima following peak

[b]Peak maximum - Normalized scattering intensity of local peak maximum

[c]Peak qRg Location – qRg corresponding to local peaks maximum

with a crosslink density of at least 0.8%. This transition can be seen in Figure 2.4, which plots the Kratky plot peak height as a function of crosslink density. In this plot, the nanostructures fall into three distinct clusters. The 0.1%XL polystyrene is in a group of its own, there the dimensionless Kratky peak height is minimal, and is the only nanostructure categorized as behaving similarly to a random walk polymer chain. The two 0.4%XL nanostructures make up the second cluster corresponding to an intermediately collapsed polymer chain. While these nanostructures behave similar to the ultra-low crosslinking sample, indicating some chain-like behavior, they exhibit a discernible peak which is an indication of the development of a measurable surface, which is a property not associated with polymer chains. The remaining nanostructures (crosslink density ≥ 0.8%) all exhibit a distinct and measurable peak height denoting a well-defined particle like structure.

Interestingly, inspection of Table 2.1 shows that the PEHMA nanostructures behave very similar to an ideal globular particle as their normalized peak maximum and position are very similar to the theoretical values of 1.74 and 1.1, respectively. The peak position of the 0.8%XL PEHMA nanostructure is most shifted from the expected value ($qRg \sim 1.63$). This variation suggests that this lower crosslinked nanostructure maintains a higher local flexibility than its higher crosslinking counterparts, while this nanostructure still exhibits strong particle-like behavior. The PS nanostructures show a wider variation in their peak location compared to the PEHMA samples. A deviation from the theoretical qR_g value of 1.74 indicates that these nanoparticles are not fully compacted and may show some asymmetry in their surface structure, while still

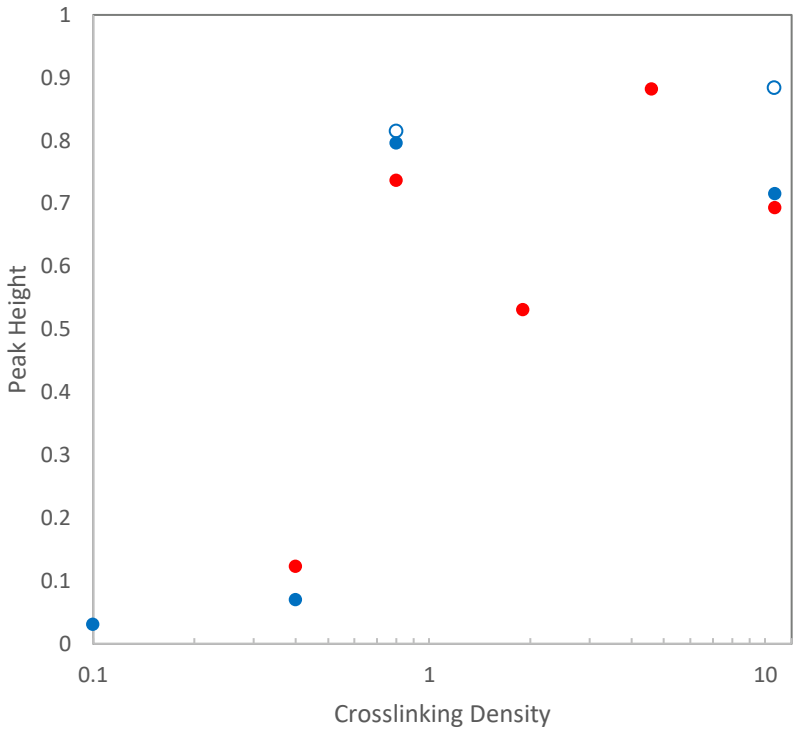

Figure 2.4: Peak height in the dimensionless Kratky Plot analysis as a function of the crosslinking density of each polymeric nanostructure. Red corresponds to PEHMA, and blue corresponds to PS. Open markers correspond to a higher molecular weight. Error bars are smaller than markers.

exhibiting very strong particle-like characteristics. This suggests that the local rigidity of the styrene segments impacts the local assembly, limits the globule like nature of the particle, and results in a less compact structure than similar PEHMA nanoparticles.

Fractal Dimension Analysis

The measured fractal dimension, *D*, of the polymeric nanostructures provides corroborating evidence of the chain-like or particle-like nature of the nanostructures to the analysis and interpretation of the dimensionless Kratky plots. The measured fractal dimensions of each nanostructure are plotted in Figure 2.5, where the blue symbols denote the polystyrene nanomaterials, while the red symbols denote the PEHMA structures. Both linear polymer chains (0% crosslinked) have fractal dimensions of approximately 1.5. This result is not surprising as it indicates that both polymeric nanostructures are slightly more swollen than a polymer in a good solvent. The fractal dimension of the crosslinked samples offers further evidence that their internal structures differ from that of the linear polymer chain. The 0.1%XL PS sample manifests as similar to random-walk polymer chain with a fractal dimension of 2.04, which is consistent with the Kratky analysis of this sample. Furthermore, the fractal dimension of the 0.4% crosslinked sample shows that the polystyrene nanostructure becomes slightly more collapsed (D = 2.21). This difference in fractal dimension illuminates a slight variation in the structures of the two low-crosslinked polystyrene samples that is not immediately evident from analysis of the Kratky plot. Interestingly, the fractal dimension of the 0.4% crosslinked PEHMA sample shows a comparable fractal dimension to the 0.1%XL PS sample despite showing a more pronounced peak in the Kratky plot. It's believed that

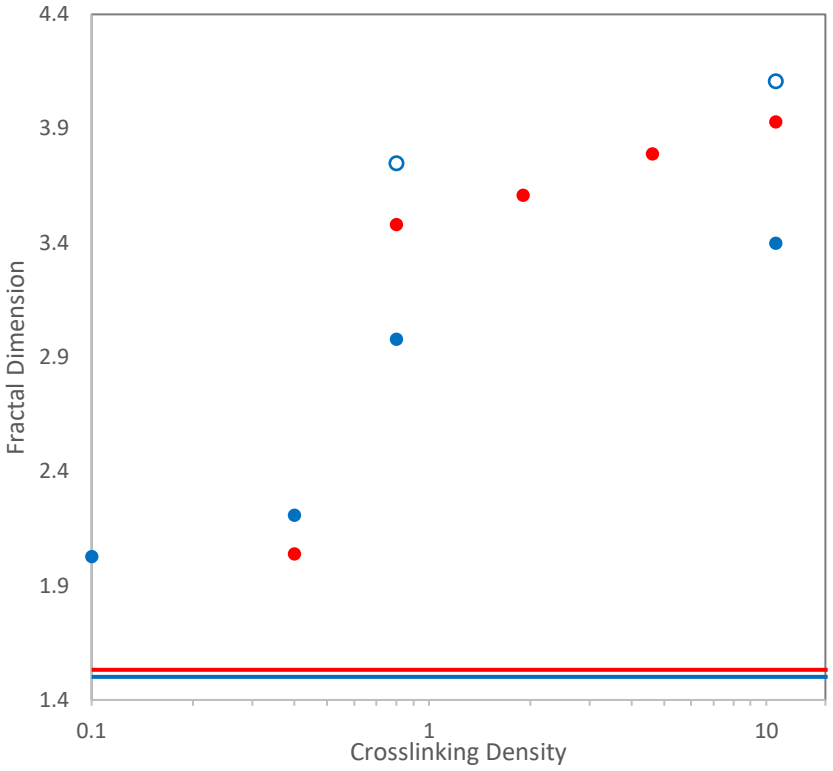

Figure 2.5: Relationship between crosslinking density of nanostructures and measured fractal dimension. Red corresponds to PEHMA, blue to PS nanostructures. Open circles denote higher MW PS. Solid lines denote fractal dimension of linear PS and PEHMA chains. Error bars are smaller than markers.

this variation is a product of the higher flexibility of the PEHMA monomer, as indicated by the much longer Kratky plot plateau than either of the low-crosslink density polystyrene nanostructures.

All nanostructures, both PEHMA and PS, with at least 0.8% crosslink density show fractal dimensions of at least 3 signifying that the cores of the nanostructures are collapsed, a surface emerges that contributes to the scattering ($D > 3$) and these nanostructures can be thought of as particles. In these samples, the fractal dimension offers further evidence that delineates these structures as particles, where progressing from a fractal dimension of 3 to 4 signifies the change in the surface of the particle from a rough surface to a smooth surface (i.e., a sharp interface). Thus, the increase in the measured fractal dimension of nanoparticles above 0.8% crosslinking shows that increasing crosslinking density correlates to the formation of smoother surfaces.

R_g/R_h - Radius Ratio Analysis

The ratio of the radius of gyration to hydrodynamic radius (R_g/R_H) of all of the polymeric nanostructures are shown in Figure 2.6. For many of the nanostructures, the radius ratio corroborates the interpretation of the Kratky plot and Fractal dimension analyses. The linear PEHMA chain possesses a radius ratio of 1.7, while the linear PS chain's radius ratio is slightly lower at 1.58. Recalling the expected radius ratio of a self-avoiding walk polymer chain (i.e. in a good solvent) as 1.56, these values indicate that both linear chains adhere to a self-avoiding walk conformation. There is some variation of the radius ratios of nanostructures with comparable crosslinking densities, which can be attributed to the variation in flexibility of the PS and PEHMA segments, where more

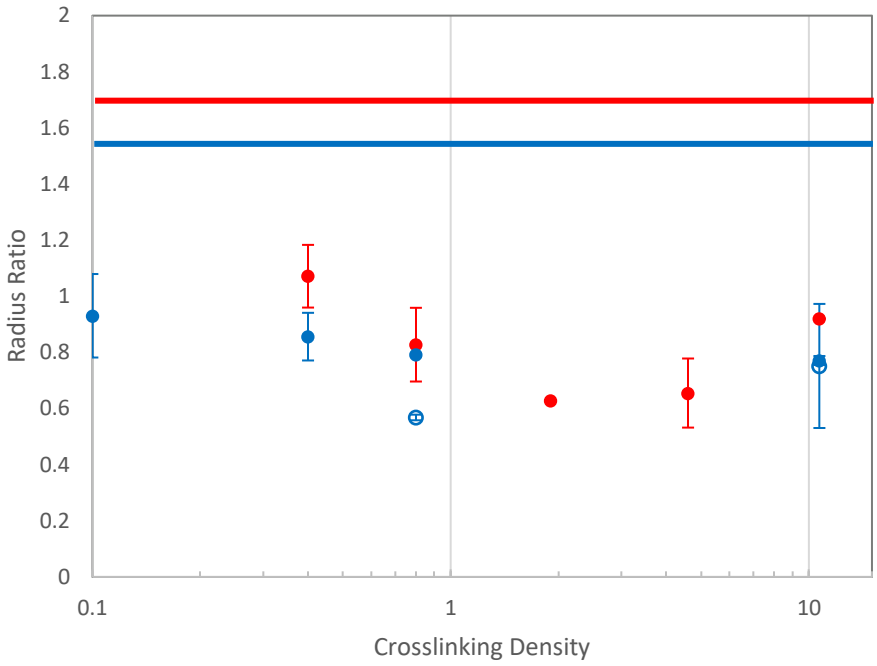

Figure 2.6: Polymeric nanostructure's radius ratio (Rg/RH) as a function of crosslinking density. Red Corresponds to PEHMA, blue corresponds to PS, open circles correspond to a higher MW. Solid lines correspond to linear chains.

flexible PEHMA chains exhibit to a larger radius ratio. Since PEHMA has a smaller Kuhn length than polystyrene, but shows a larger radius ratio, this suggests that while both linear chains adhere to a self-avoiding walk conformation, the PHEMA is slightly more soluble in THF than PS. This is an artifact that was not immediately identifiable in the previous analyses.

Interpretation of the radius ratios of the low crosslinking density samples provides additional insight that is not obvious from the Kratky or fractal dimension analyses. The 0.1% XL polystyrene sample exhibited strong signs of a random walk polymer chain in the Kratky plot and fractal dimension, but only possesses a radius ratio of 0.93, which is well below the theoretical value of a random walk polymer chain radius ratio of 1.24. This lower radius ratio is consistent with that of a star polymer in good solvent,[154, 155] suggesting that this low crosslinking density nanostructure is star-like in structure. This is consistent with previous studies which have characterized these nanostructures as a fuzzy sphere with the crosslinks concentrated at core of the structure with an outer corona of loops and tails.[44, 50, 156-158] The 0.1% crosslink density nanostructure corresponds to a crosslink between every 1 in 1000 monomers. The molecular weight of this nanostructure is below 100 kDa, therefore, on average, there is 1-2 crosslinks in these nanostructures. A nanostructure with one or two divinyl benzene crosslinks near the core will resemble a multi-armed star-like topology, as depicted in in Figure 2.7. In this figure, the chains connect near the core at a single crosslink, as designated by the red box, which results in four “arms” emerging from that crosslink. Therefore, the 0.1% XL nanostructure is better

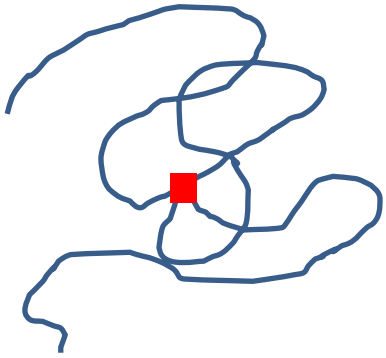

Figure 2.7: A polymer chain with a single crosslink (red square), mimicking a four armed star polymer.

described as a star like structure than a slightly collapsed, random-walk chain, as the previous analyses suggest.

Comparing the 0.4% XL polystyrene to the 0.1% XL polystyrene nanostructure, the radius ratio continues to decrease, consistent with the collapse of the structure, which is in line with the Kratky and fractal analyses. The 0.4% XL PEHMA structure exhibits a radius ratio of 1.07, which indicates the nanostructure is slightly more collapsed than a random walk polymer chain, while the 0.4% XL polystyrene nanostructure exhibits a decrease in its radius ratio compared to the 0.1% XL nanostructure indicating that it is further collapsed.

At 0.8% XL the radius ratios of the polymeric nanostructures are near that of a homogeneous globule at approximately 0.8, which indicates a near complete collapse of the chain, aligning with the particle-like characterization that arose from the other analyses. The higher molecular weight polystyrene sample has a radius ratio far below that of a hard sphere which is consistent with a core shell structure, this suggests that while the two 0.8% XL polystyrene samples have similar particle like structures, the internal morphology of the higher molecular weight is much less homogenous. The radius ratios of the PEHMA samples with crosslinking density above 0.8% also adhere to a core shell morphology. The interpretation that these nanostructures form a core-shell morphology is consistent with the structural characterization of similar polystyrene nanostructures at crosslinking densities of at least 0.8% using SANS.[51] In these studies, the scattering of the polystyrene samples are best modeled by a fuzzy-sphere Gaussian gel model that have a measurable core and a fuzzy outer shell.[50] The fit of the SANS

scattering of the PEHMA nanoparticles to the fuzzy-sphere Gaussian gel model was confirmed and is presented in the supplemental information. Furthermore, the R_g/R_H increases with increasing crosslink density in the PEHMA sample, approaching the theoretical value for a hard sphere at 10% crosslinking. Thus, the nanoparticles become more homogeneous, and less core-shell like with increased crosslink density. This interpretation also agrees well with the fractal dimension analysis where the nanostructures approach a smooth surfaced, compact particle-like structure as the crosslinking density increases

In summary, the particle like nature of crosslinked soft nanoparticles is quantified by a thorough analysis of small angle neutron scattering data using of Kratky analysis, and determination of the fractal dimension and radius ratio. The results of these analyses show that these soft polymeric nanostructures can be described as particle-like for any crosslinking density of at least 0.8%, regardless of monomer rigidity or nanostructure molecular weight. This result is especially surprising as it only requires 1 crosslink for every 125 monomers to develop a clear, measurable surface, the hallmark of nanoparticle functionality. Samples with crosslinking densities between 0.1% and 0.8% show a significant amount of collapse from a swollen polymer chain in a good solvent, such that their structure is best described as between a random walk chain and a completely collapsed particle. These transitive structures exhibit both chain-like and particle-like characteristics. A plot of the dimensionless Kratky plot peak height as a function of crosslinking density (Figure 2.4) offers a depiction of the transition among these structural morphologies. Additional fractal dimension and radius ratio analyses provide

additional insight into the extent of the particle-like structure of the crosslinked nanostructures. These additional analyses further confirm the chain-like and particle-like morphologies of nanostructures that are readily characterized by the dimensionless Kratky plot. A fractal dimension of a nanostructure offers additional detail in the appearance of a surface, and provides a measure of the relative collapse of the nanostructure's chains not easily seen in the Kratky analysis. The fractal dimension analysis also allows for a measure of the homogeneity of the surface of clear particle-like structures. The analysis of the radius ratio further enhances our understanding of the structures of the nanoparticles. The radius ratio offers insight into both star-like and core-shell like morphologies that would otherwise merely appear as varying degrees of chain collapse with the Kratky plot and fractal dimension analyses.

Conclusions

Small angle neutron scattering studies have been completed to provide insight into the transition from a polymer chain to a nanoparticle via internal crosslinking. A combination of analyses of the SANS curves, including the dimensionless Kratky plot, the fractal dimension, and the ratio of R_g/R_H, provides insight into the particle-like properties of the examined polymer constructs. These results show that the primary characteristic that delineates a polymeric chain from a nanoparticle is not its size, but the presence of a surface, which can be detected via these analyses. Using the idea that a nanostructure requires the presence of a surface to be a nanoparticle leads to the surprising conclusion that crosslinking densities as low as 0.8%, or 1 crosslink for every 125 monomers, is sufficient to realize very strong particle-like characteristics. This

indicates that even at that these extremely low crosslinking densities, a measurable surface has developed in these polymeric nanostructures.

This study therefore provides analyses and insights that enable the delineation of particle-like characteristics of a polymeric nanostructure from chain-like structures. It also establishes clear domains of chain-like and particle-like morphologies with variation in crosslink density and identifies a transitive state at the lowest crosslinking densities of the nanostructure. These results clearly show that the overarching characteristic that controls whether a polymeric nanostructure is a chain or a nanoparticle is its crosslink density, with segmental flexibility or nanostructure molecular weight as secondary effects.

Acknowledgements

This research was supported by the U.S. Department of Energy, Office of Science, Basic Energy Sciences, Materials Sciences and Engineering Division. A portion of this research was also completed at ORNL's High Flux Isotope Reactor, which was sponsored by the Scientific User Facilities Division, Office of Basic Energy Sciences, US Department of Energy. This work benefited from the use of the SasView application, originally developed under NSF award DMR-0520547. SasView contains code developed with funding from the European Union's Horizon 2020 research and innovation program under the SINE2020 project, grant agreement No 654000.

CHAPTER 3 : THE IMPACT OF INTERNAL STRUCTURE ON THE LOCAL DYNAMICS OF POLYSTYRENE SOFT NANOPARTICLES USING NEUTRON SPIN ECHO SPECTROSCOPY

Abstract

Polymeric nanoparticles often impart non-Einstein-like changes to the transport properties of components in a polymer nanocomposite. However, the mechanism that drives these changes is not well understood. Recent studies have shown that the crosslinking density of soft polystyrene nanoparticles, which are defined by a lightly crosslinked core and fuzzy outer shell, dictate their impact on the properties of polymer nanocomposites — as the crosslinking density increases, their unique behavior diminishes. To better understand the role of crosslinking density on the dynamic behavior of soft polystyrene nanoparticles, their local and global dynamics are probed using neutron spin echo spectroscopy (NSE). Surprisingly, on a global scale, the soft nanoparticles studied herein behave similarly to a linear polymer chain. However, the local dynamics of these nanoparticles deviate from linear chain behavior on length scales between the total size of the nanoparticle and the diameter of the crosslinked core. At this length scale, the crosslinks within the core play a prominent role in the suppression of local dynamics. Further, at smaller length scales below the size of the nanoparticle core, the local dynamics resume linear chain-like behavior. In this regime, the influence of crosslinks is minimal and the observed dynamics are dominated by the fuzzy outer shell. These dynamic regimes within the nanoparticle are a result of their core-shell structure, where crosslinks concentrated at the center of the nanoparticle define the important length scales where internal dynamics are suppressed. Furthermore, the measured dynamics across all observed length scales depend on crosslinking density

where motion is slowed with increased crosslinks. Therefore, the heterogeneity of the local dynamics and the crosslinking density dependent dynamic slowing are major contributors towards the unique properties observed within soft nanoparticle dynamics.

Introduction

Polymer nanocomposites are a class of materials in which a nanoscale additive is dispersed throughout a bulk polymer matrix. The addition of a nanoscale filler provides improvements in the mechanical and thermal, or chemical, properties of the bulk polymer.[1-9, 159-164] While many PNC systems utilize some form of a hard inorganic nanoparticle, such as a gold or silicon nanoparticle, a new branch has recently emerged using all-polymer nanoparticles.[17, 39-54] The use of an all-polymer nanoparticle as filler is advantageous as they will typically interact with the bulk polymer matrix better than an inorganic alternative. Improved interactions between the polymer and polymeric nanoparticle result in better dispersion of the nanoparticle and often an improved, homogeneous implementation of the enhanced properties. An unexpected result of the inclusion of soft polymeric nanoparticles is their effect on the transport properties of the bulk polymer.[33, 57, 66, 70-77] First reported by Mackay in the early 2000s, the addition of a polystyrene single chain nanoparticle (SCNP) was shown to reduce the viscosity of the bulk polymer.[66] This change in viscosity contradicts Einstein's theory of Brownian motion where the addition of particles to a solution results in an increase in the system's viscosity, a theory that is suitable for polymeric solutions as well. Additionally, recent studies of soft polymeric nanoparticles have shown they also imbue unexpected changes to the diffusive properties of a polymer in the nanocomposite. Martin et al found that when the size of the nanoparticle is smaller than the size of the bulk chains, the measured diffusion increases, a stark contrast to systems using a more traditional hard nanoparticle.[51]

The mechanistic source of these unexpected changes in transport properties when a soft nanoparticle is introduced to the system have been studied in the ensuing two decades. [45, 71-75, 78-81] Mackay first suggested that the nanoparticles induce a conformation change and increase in free volume of the bulk polymer chains, which leads to the observed reduction in viscosity. Tujeta et al. further investigated the system and detailed a set of basic requirements to observe viscosity reduction — the radius of the nanoparticle must be less than the radius of gyration of the bulk polymer, some degree of chain confinement should exists within the system, and the molecular weight of the bulk polymer should be above its entanglement molecular weight.[16, 66, 73, 165] A large majority of research regarding viscosity reduction in all polymer nanocomposites offered mechanistic interpretations that might only be relevant to their specific system. Where Mackay's system was comprised of linear polystyrene and a polystyrene SCNP, most systems examined thereafter contained chemically dissimilar nanoparticles and bulk polymer. Such Systems can lead to important interactions between the polymer and nanoparticle that complicate the dynamics of the system, leading to a variety of sources for the observed viscosity changes. As a result, many studies regarding viscosity reduction in all polymer nanocomposites have come to conclusions that may. It be universal, are influenced by secondary interactions, but do not offer a fundamental understanding of the phenomenon

Due to the complexity of the dynamics of the system, eliminating possible mechanisms may be easier than definitively identifying a correct mechanism. A recent study by Goldansaz did just that verifying that artifacts such as surface slippage and

thermally induced gap discrepancies, shear banding and thinning, change in entanglement density and free volume, constraint release, and formation of emulsions and soft inclusions are not the source of the reduction in viscosity despite many of these mechanisms being proposed in prior research.[45] Chen et al. proposed that the likely source of viscosity reduction are a consequence of the deformability, penetrability, and softness of an all-polymer nanoparticle, a conclusion with which Goldansaz also agreed.[57] Work regarding the effect of soft nanoparticles on the diffusive properties of a polymer in the nanocomposite corroborate this conclusion as well. The structure a class of soft polystyrene nanoparticles has been extensively studied as well as their impact on the diffusive properties of a bulk polymer matrix.[17, 50-52, 67, 68] These nanoparticles, which are formed via internal crosslinking have been shown to adhere to a fuzzy sphere model defined by a crosslinked core and fuzzy outer shell, and the softness, or deformability, of the nanoparticle has been shown to decrease, and become more rigid, with increasing crosslinking density. These soft polystyrene nanoparticles have been shown to significantly impact the diffusive properties of the bulk polymer chain as the crosslinking density of the nanoparticles decreases.[51, 52] Therefore as these crosslinked polystyrene nanoparticles become more rigid, their impact on the diffusion of the bulk polymer dissipates. Interestingly, the addition of a nanoparticle to a linear polymer with comparable molecular weight as the soft nanoparticle actually slows polymer diffusion.

Advances have been made in understanding the motion of the soft nanoparticles themselves as a result of their impact on the diffusion of the surrounding bulk polymer.[67, 68] A traditional inorganic nanoparticle is often considered immobile in a polymer

nanocomposite and as a result bulk chain diffusion decreases in their presence, as chains must diffuse around the stationary nanoparticles. An increase in the rate of diffusion of bulk polymer with the addition of a soft nanoparticle suggests that the nanoparticles themselves may also be mobile. First reports indicated that soft nanoparticles were indeed mobile, albeit several orders of magnitude slower than a linear chain of comparable molecular weight.[67] A mechanism describing the motion of these soft nanoparticles in a melt was elucidated by Shrestha et al, where the fuzzy outer shell of the nanoparticle participates in a threading/dethreading mechanism with surrounding linear polymer chains, which dictates the diffusion of the nanoparticle.[68] The diffusion of these nanoparticles varies with their crosslinking density, whereas the crosslinking density increases, the loops "tighten" resulting in a slowing of the dethreading process and slower nanoparticle diffusion. Imel and Shrestha's studies characterize the dynamics of the nanoparticle as a whole but understanding of the local dynamics within the nanoparticle are still lacking.

The unexpected changes in polymer diffusion in the presence of these nanoparticles are related to the softness and deformability of the nanoparticles, where the lower the crosslinking density, the more pronounced the effects. However, since a linear chain of comparable molecular weight (i.e. a 0% crosslinked 'nanoparticle') slows polymer diffusion, identifying the differences in the local dynamics between a linear chain and lightly crosslinked soft nanoparticle may assist in understanding this phenomenon. Arbe et al. examined the segmental dynamics of SCNPs and compared them to their linear precursors using neutron spin echo spectroscopy to study the

differences in dynamics between the two chain connectivities.[55] In this study, the differences in dynamics of the SCNP and linear chains were examined by monitoring the effective diffusion coefficient, $D_{eff}(q)$, a length scale dependent diffusion coefficient which provides insight into the important contributions to the segmental dynamics on different length scales. The q-dependent effective diffusion coefficients of the soft nanoparticles with varying crosslink densities are compared to those of a linear polymer chain of comparable molecular weight to identify length scale dependence of the local particle dynamics. Associating the length scales where nanoparticle dynamics differ from those of linear chains offers insight into the structural characteristic of the soft nanoparticles that correlate to their non-traditional behavior.

Experimental

Materials

Styrene (Aldrich 99.9%) and divinyl benzene (DVB, Aldrich, 90%, 80 para content, technical mixture) were passed through an alumina column to de-inhibit them prior to use. Dodecyl trimethylammonium bromide (DTMAC, TCI, >98%), potassium persulfate (KPS, >99%, Acros Organics), tetrahydrofuran (THF, BDH HPLC grade), methanol (BDH, ACS grade), deuterated tetrahydrofuran (THF-d_8), deionized water (BDH), 100k polystyrene (Polymer Source), and 535k polystyrene (Polymer Source) were used a received.

Synthesis of soft polystyrene nanoparticles

Soft polystyrene nanoparticles were synthesized via a modified, monomer starved, semi-batch nano-emulsion polymerization procedure as described by Martin *et al.*[50] First, a surfactant solution is prepared by mixing 20g of DTMAB and 125mg of KPS into 50mL of DI water into a round bottom flask. The flask is sealed with a rubber septum, purged with argon, and sonicated for 30 minutes to facilitate a homogeneous solution of the surfactant in water. The flask is then placed into an oil bath and heated to 65°C while stirring. In a separate vial 5mL of styrene is mixed with the desired amount of DVB crosslinker, where crosslinking density is defined by the molar ratio of DVB to styrene. The monomer solution is then sealed, purged with argon for 10 minutes, and drawn into an airtight glass syringe and added to the surfactant vessel at a constant rate controlled by a syringe pump. The reaction is allowed to proceed for 2 hours following once the entire monomer solution has been added to the reaction vessel. Once completed, 5mL of THF was added to the flask and the polymer is precipitated in excess methanol (~300mL) in a refrigerator (~7°C) overnight. The precipitate was then placed into a Soxhlet extractor and extracted with methanol to remove residual surfactant. The precipitated polymer was then dried under vacuum at 50°C for 48 hours. The polystyrene soft nanoparticles will be referred to as PSNP X.Y where X ≡ crosslinking density and Y ≡ monomer rate of addition. For example, PSNP2.20 is the polymer sample synthesized using a 2% crosslinking density and a 20mL/hr monomer rate of addition. Soft polystyrene nanoparticles NP1.50, NP2.20, and NP10.1 were characterized in this study.

Neutron Spin Echo (NSE) Spectroscopy

NSE experiments were performed on solutions of 1%wt soft polystyrene nanoparticles in deuterated THF at 300K using the Neutron Spin Echo Spectrometer at the Center for High Resolution Neutron Scattering (CHRNS) at the National Institute of Standards and Technology (NIST) in Gaithersburg, MD. Two wavelengths (6Å and 8Å) and Fourier times ranging from $0.1 \leq t \leq 45$ ns covering a scattering vector range of $0.1 \leq q \leq 0.21$ $Å^{-1}$ were used to analyze the nanoparticles. The data was corrected for the contribution of solvent by subtracting out the background signal measured on the solvent. All data was reduced and subsequently fit using the software package DAVE.[166]

Results and Discussion

The soft polystyrene nanoparticles used in this study where previously well characterized by Martin et al.[50] These nanoparticles were found to adhere to a fuzzy sphere-Gaussian Lorentz gel form factor which is primary defined by the structure's core radius (R_c) and the half width of the fuzzy interface (τ) as shown in Figure 3.1. Table 3.1 provides the values of those characteristics of the nanoparticles and their measured diffusion coefficient (D) and radius of gyration (R_g). First the global dynamics of the soft nanoparticles can be explored by fitting the NSE data to a modified stretched exponential given in Equation 3.1. This equation, which uses the normalized data is dependent on the Fourier time, t, characteristic relaxation time, τ_q, the stretching exponent, β, and the

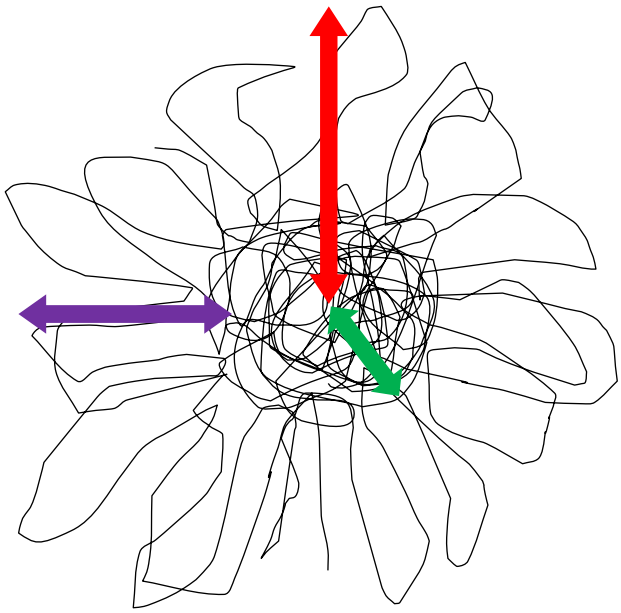

Figure 3.1 Illustration of soft polystyrene nanoparticle, where the green double arrow denotes the nanoparticle core radius, purple double arrow is the breadth of fuzzy interface, and red double arrow is the total nanoparticle radius.

Table 3.1 Structural Characteristics of Soft Nanoparticles

Nanoparticle	Mw[a] (10^6 g/mol)	R_c[b] (nm)	τ[c] (nm)	D[d] (10^{-11} m^2/s)	R_g[e] (nm)
NP1.50	0.854	3.71	5.19	4.14	11.17
NP2.20	0.692	3.40	4.77	5.49	9.64
NP10.1	0.355	2.72	3.23	11.4	7.05

[a]molecular weight calculated using the forwards scatting intensity, I(0) of the SANS data
[b]nanoparticle core radius calculated from fuzzy sphere-Gaussian Lorentz gel form factor fit
[c]width of fuzzy interfacial layer
[d]mutual diffusion coefficient
[e]radius of gyration of polymer calculated using Guinier analysis of SANS data

$$\frac{I(q,t)}{I(q,0)} = A\, exp\left[-\left(\frac{t}{\tau_q}\right)^{\beta}\right] exp[-Dq^2t] \qquad \textbf{3.1}$$

diffusion coefficient of the nanoparticle, *D*, and the scattering vector, *q*. This modified form of a standard stretched exponential function, which adds the second exponential term, is necessary to account for the motion of the nanoparticles themselves. Without this corrective term, the characteristic relaxation times of the nanoparticles are on the same time scale of the diffusion of the nanoparticles, impacting the observed dynamics.

The global dynamics of a polymer can be characterized based on the value of the stretching exponent, β, at each scattering vector. $\beta = 0.5$ is consistent with Rouse-like dynamics, while $\beta = 0.85$ is consistent with Zimm-like dynamics. The NSE data of each of the nanoparticles were first fit to Equation 3.1 with β as determined based on the fit. (Figure 3.2a, c, e). β varied from 0.75 to 0.89 in these fits with NP10.1 exhibiting the highest β value, suggesting that these nanoparticles obey Zimm-like dynamics. With this knowledge, the stretching exponent was fixed to $\beta = 0.85$ (Figure 3.2b, d, f), where the quality of the fit did not vary.

Not only does the β value provide insight on the global dynamics of the polymer, it also correlates to the stiffness of the particle, where stiffer macromolecules will present higher β values.[167] Therefore a significant increase in the stretching exponent in the 10% crosslinking sample is not surprising, as it is considerably more rigid than the other nanoparticles with lower crosslinking density. However, the adherence to Zimm-like dynamics is somewhat surprising as these nanoparticles have been shown to interact with linear polymer chains differently than linear polymer chains of comparable molecular

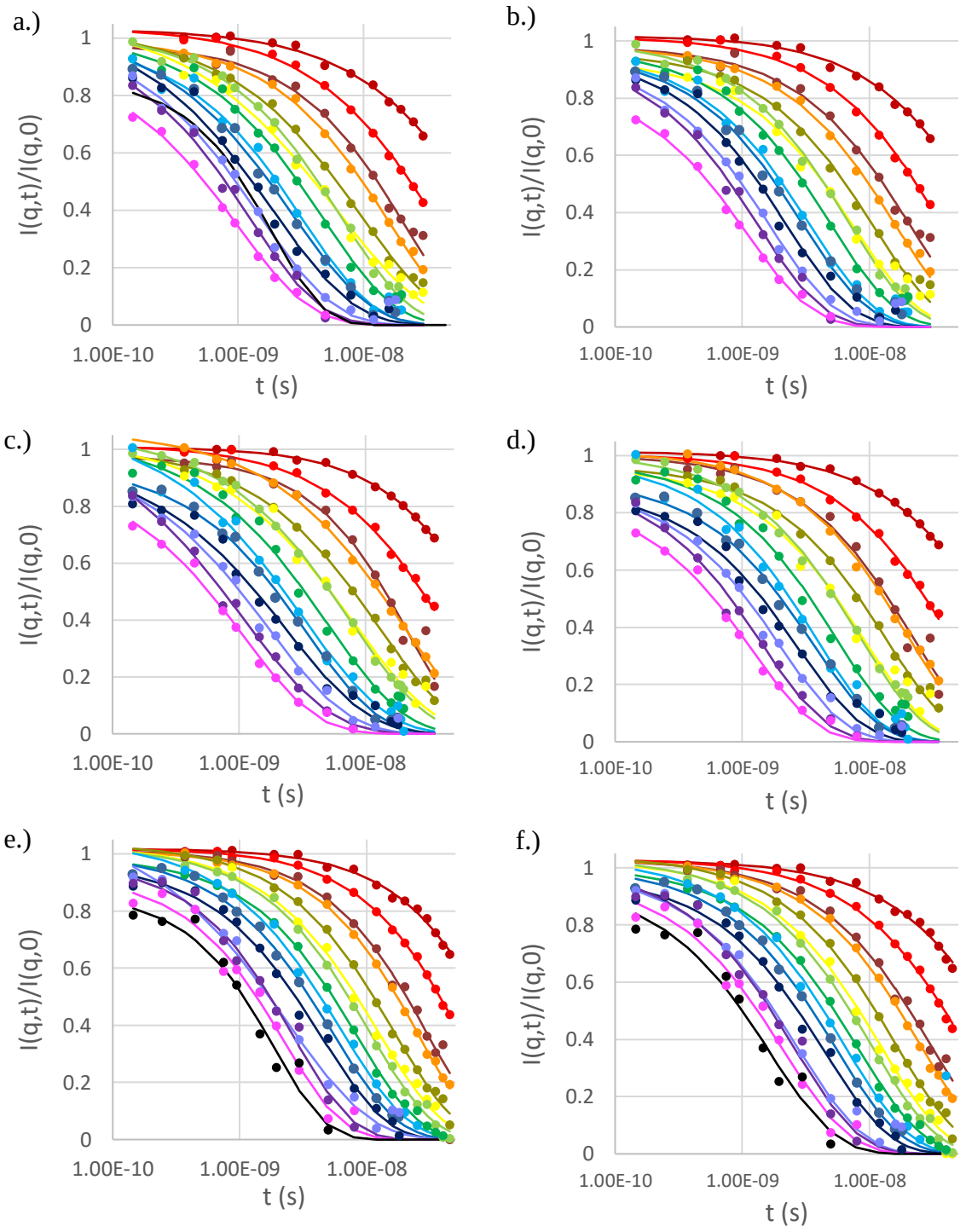

Figure 3.2 Normalized intermediate scattering of polystyrene soft nanoparticles (NP1.50 = Figure a, b; NP2.20 = Figure c, d, NP10.1 = Figure e, f) in dilute solutions of deuterated THF fit to Equation 3.1. Figures a, d, e correspond to fit where β is fit, figures b, d, f correspond to fit where β is fixed to 0.85 for ideal Zimm dynamics

weight. Therefore, the unique dynamic behavior exhibited by these soft nanoparticles may originate from the dynamics at smaller length scales within the nanoparticles.

The segmental dynamics of the nanoparticle are determined by fitting the NSE data to a an exponential function which models the normalized intermediate scattering function, *I(q,t)/I(q,0),* in terms of the *q*-dependent effective diffusion coefficient, $D_{eff}(q)$, scattering vector, *q*, and Fourier time, *t*, as shown in Equation 3.2.

$$\frac{I(q,t)}{I(q,0)} = exp\left[-D_{eff}(q)q^2t\right] \quad \textbf{3.2}$$

The analysis done using Equation 3.2 utilizes only the second term from Equation 3.1, where the global diffusion coefficient is replaced with a scattering vector dependent diffusion coefficient. This length scale dependent diffusion coefficient allows for segmental dynamics within the nanoparticle to be described independently of the global dynamics. The effective diffusion coefficient describes the dynamics of the nanoparticle as a function of q, and therefore length scale. Quantifying $D_{eff}(q)$ for the nanoparticle and comparing it to that of a linear polymer chain offers insight into the deviation of segmental dynamics between linear chains and the soft nanoparticle. Equation 3.2 is transposed into a linear form as shown in Equation 3.3, and the fits of the NSE data to Equation 3.3 are shown in Figure 3.3.

$$ln\frac{I(q,t)}{I(q,0)} = -D_{eff}(q)q^2t \quad \textbf{3.3}$$

The fits of the normalized intermediate scattering function of a linear chain polystyrene of 535kDa molecular weight to Equation 3.3 are shown in Figure 3.3a, while the fits of

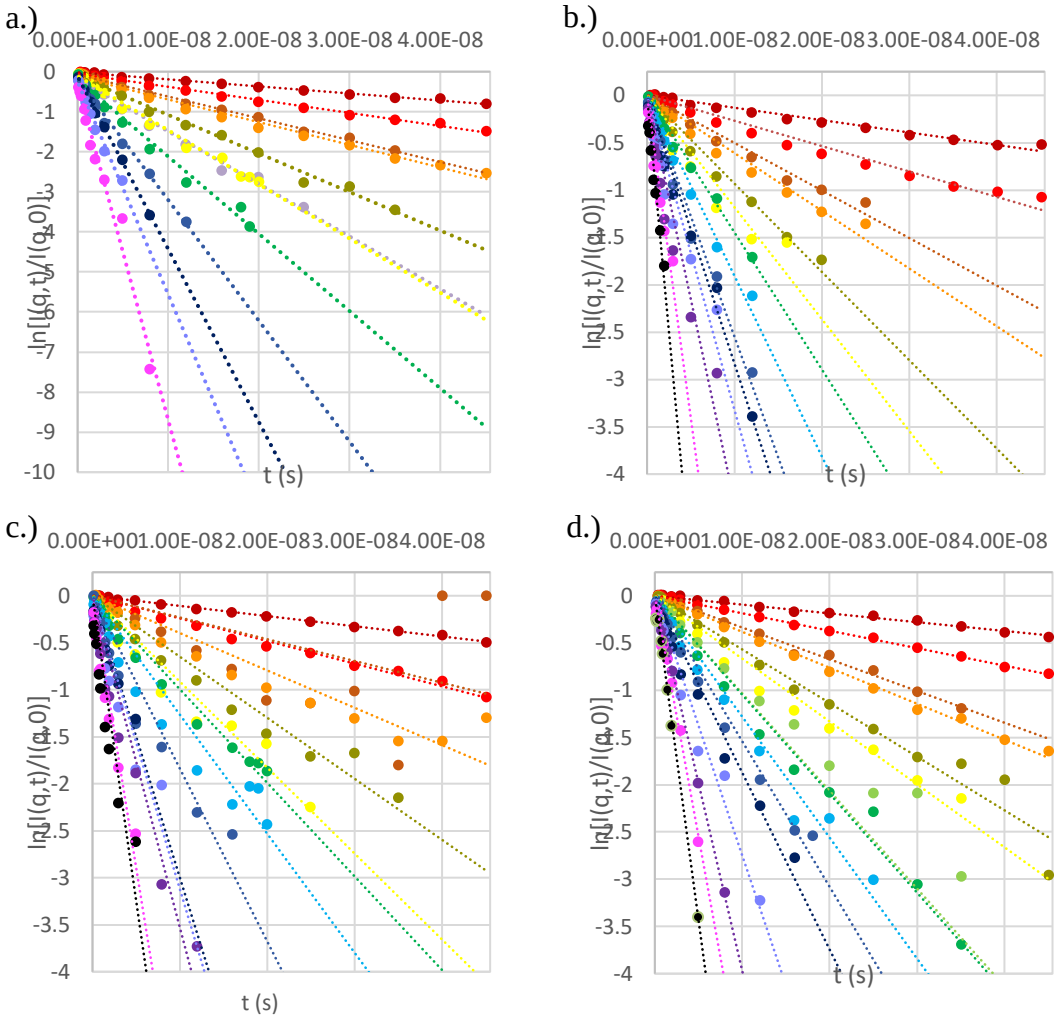

Figure 3.3 Log of the normalized intermediate scattering of a.) polystyrene and polystyrene soft nanoparticles, b.) NP1.50, c.) NP2.20, and d.) NP10.1 in dilute solutions of deuterated THF as a function of Fourier time. Dotted lines are a fit of the data to Equation 3.3

the normalized intermediate scattering function the soft nanoparticles are shown in Figures 3.3b-3.3d.

The effective diffusion coefficient of the linear polymer chain (pink asterisks) and soft nanoparticles (filled circles) as a function of scattering vector, *q* is presented in Figure 3.4. Inspection of Figure 3.4 shows that behavior of the effective diffusion coefficient of the soft nanoparticles can be broken into three distinct regimes – 1.) in the low-q regime, ranging from 0.04-0.09 $Å^{-1}$, where the D_{eff} of the nanoparticles increases with q at a rate that is comparable to the q-dependence of D_{eff} for the linear polymer. 2.) in the mid-q regime, ranging from 0.09-0.15 $Å^{-1}$, where the D_{eff} is lower than that of the linear polymer chain and nearly independent of *q*, and 3.) the high-q regime, ranging from 0.15-0.2 $Å^{-1}$, where q-dependence of D_{eff} again scales similarly to that of the linear chain. A benefit of neutron spin echo is that the q dependence of the results offers insight into the relevant length scales of the motions that are studied. Thus, the q-ranges of the three regimes illuminates the length scales of the motions studied in these regimes, where $d = 2\pi/q$. The correlation of q range and the corresponding length scales of the plateaued regions of all three nanoparticles is given in Table 3.2.

These length scales span important length scales of the nanoparticle, from about a few segments to the entire nanoparticle. Figure 3.5 depicts the correlation of the length scales examined to the structure of the nanoparticle. At low-q ($q < 0.08$ $Å^{-1}$), the scattering vector reflects length scales on the order of the entire nanoparticle, as shown in Figure 3.5a. Thus, the effective diffusion coefficients in solution of all three nanoparticles scale similarly to the linear chain in this regime, probing the global dynamics of the

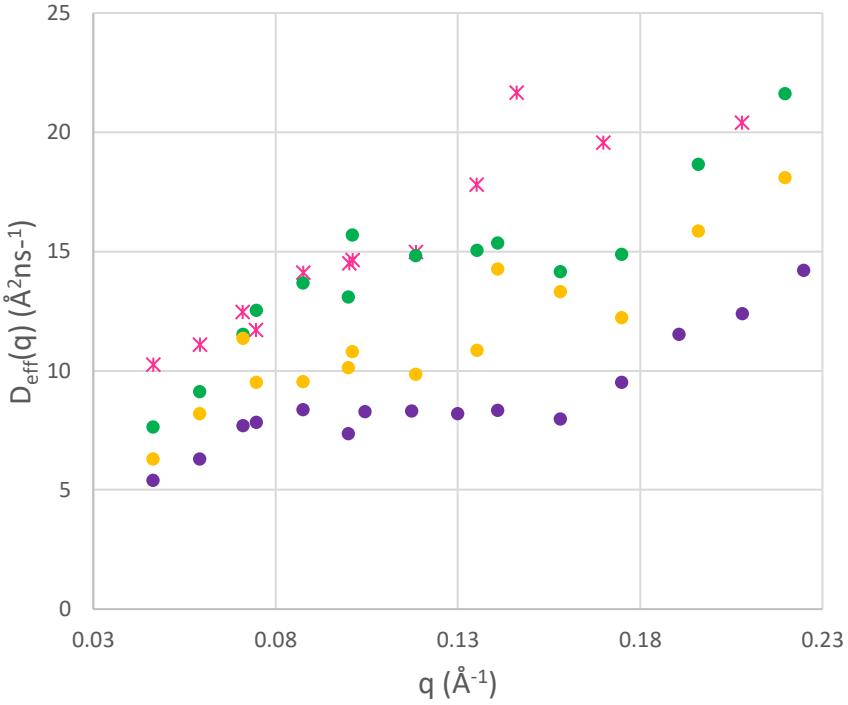

Figure 3.4 Effective diffusion coefficient, Deff, as a function of scattering vector for soft polystyrene nanoparticles, NP1.50 (green circles), NP2.20 (yellow circles), NP10.1 (purple circles), and 535kDa linear PS (pink asterisks). Error bars are smaller than markers.

Table 3.2 Plateaued Region of Effective Diffusion Coefficient of Polystyrene Nanoparticles

	Low-q		Mid-q		High-q	
Nanoparticle	q range ($Å^{-1}$)	Length Scale (nm)	q range ($Å^{-1}$)	Length Scale (nm)	q range ($Å^{-1}$)	Length Scale (nm)
NP1.50	0.041 – 0.083	7.6 – 15.2	0.083 – 0.153	4.1 – 7.6	0.153 – 0.215	2.9 – 4.1
NP2.20	0.041 – 0.070	9.0 – 15.2	0.070 – 0.130	4.8 – 9.0	0.130 – 0.215	2.9 – 4.8
NP10.1	0.041 – 0.083	7.6 – 15.2	0.083 – 0.170	3.7 – 7.6	0.170 – 0.220	2.9 – 3.7

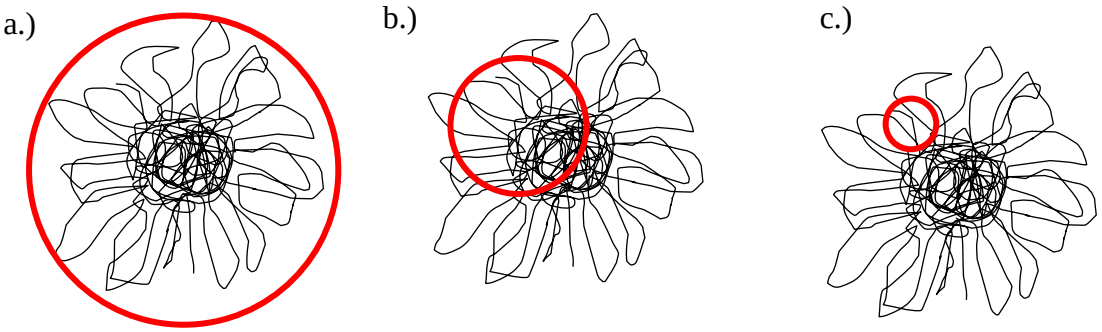

Figure 3.5 Approximate length scale of soft polystyrene nanoparticle at effective diffusion coefficient regimes of a.) low, b.) mid (plateau), and c.) high-q

nanoparticles. The commensurability of scaling of the soft nanoparticles and linear chain in this regime is consistent with the stretched exponential analysis, i.e. globally the soft nanoparticles follow Zimm dynamics in solution as linear polymer chains do. Despite there being structural differences between the soft nanoparticles and a linear chain (i.e. the presence of crosslinks), the fuzzy outer shell of the nanoparticles appears to "shield" the influence of crosslinks on the global dynamics of the soft nanoparticle, or the relatively low crosslinking density is insufficient to the global dynamics of the nanoparticle.

This low-q regime also provides quantitative data that enables the comparison of the diffusion coefficients of the nanoparticles and the linear chain. It is interesting that the absolute values of the nanoparticle diffusion coefficients are generally slower than that of the linear polymer chain. Moreover, the effective diffusion coefficients of the nanoparticles do not scale with their molecular weight where Mw (NP10.1) < Mw (linear) < Mw (NP2.20) < Mw (NP1.50). Rather, the magnitude of the effective diffusion coefficients order based on their crosslinking density where the polymers move more slowly as the crosslinking density increases. Thus, the global motion of the nanoparticles is dominated by the crosslink density more than degree of polymerization.

In the mid-q region ($0.08\ Å^{-1} < q < 0.15\ Å^{-1}$, $4.2 < d < 7.0$ nm), the D_{eff} of each nanoparticle does not vary much with q, exhibiting a plateau. This is in contrast with the behavior of a linear polymer chain, where D_{eff} increases with increasing *q* over the entire measured *q* range. At the length scales of this regime (~ 4.2 – 7.0 nm), the observable window is roughly the size of the nanoparticle core, where the diameter

ranges from 5.4-7.4 nm. Therefore, on average, the dynamics that are observed by NSE on these length scales include the interrogation of the crosslinked core of the nanoparticle, as shown in Figure 4b. Thus, when examined at this length scale, the dynamics of the nanoparticles differ from that of the linear polymer chains due to the influence of the crosslinks. Moreover, the incorporation of crosslinks slows the motion of the polymer segments, where the motions become slower as the nanoparticle becomes more highly crosslinked, D_{eff} (10.1) < D_{eff} (2.20) < D_{eff} (1.50). It is interesting that the q dependence of D_{eff} plateaus in this regime, rather than attenuates. This indicates that the motion of the segments on this length range are independent of absolute length scale, at least for this range of crosslink density. This further emphasizes the importance of the crosslinks in slowing down the segmental dynamics, but the limited length scales over which the crosslinks impact nanoparticle dynamics.

In the high-q region, ($q > 0.15$ Å^{-1} $d < 40$ nm) the nanoparticles resume a linear increase in D_{eff} with *q*, similar to the behavior of the linear polymer chain. In this regime, the "observable window" is less than ~4.0 nm, and thus focuses on smaller segmental length scales. At this length scale the observable window is less than the size of the nanoparticle core. Therefore, on average only a portion, if any at all, of the crosslinked core is interrogated. As a result, the dynamics of the outer fuzzy shell dominate the dynamics at this length scale.

The scaling of D_{eff} with *q* that is similar to a linear chain in the high-q region appears to be unique to the core-shell construct that these soft nanoparticles exhibit. For instance, Arbe. et al studied the dynamics of a SCNP in solution by neutron spin echo and

conducted a similar analysis to monitor the effective diffusion coefficient of their soft nanoparticle. Similar to the behavior of the crosslinked nanoparticles used in this study, the SCNP showed behavior similar to a linear chain at low-q followed by a plateau in the mid-q region. However their results did not show a second region of linear scaling instead the effective diffusion coefficient continued to plateau over all subsequent scattering vectors.[55]

One interpretation of the deviation of our results from those of Arbe is related to the internal structure of the nanoparticle and percent crosslinking of the different nanoparticles. The crosslink density of the Arbe's nanoparticles was 30%,[168] much higher than the nanoparticles studied here. The structures of SCNPs are typically not very well controlled due to the nature of their synthesis, and frequently resemble the globular nature of a folded protein. As a result, crosslinks are not concentrated in a central location within the nanoparticle but randomly distributed throughout the entire structure. Thus, at the relevant length scales of an NSE experiment, crosslinks between segments are generally always observable, even at very small length scales. The soft nanoparticles presently studied have a well-defined core-shell structure characterized by a lightly crosslinked core and fuzzy outer shell. The concentration of crosslinks towards the center of the nanoparticle allows for two distinct dynamic regimes to exist within the nanoparticle, those influenced by crosslinks and those that are not. Characterizing the dynamics of these nanoparticles using NSE allows for separation of the dynamics controlled by the crosslinked core from those dominated by the fuzzy outer shell. Therefore, due to the two unique dynamics present within the soft nanoparticles, the

breadth of the effective diffusion coefficient plateau is likely related to the core size of the soft nanoparticles. In the mid-q region where the plateau occurs, those length scales observe the core, and it's slowed dynamics resulting in the stagnation in the effective diffusion coefficient. Once sufficiently small length scales are examined that monitor the fuzzy interface independent of the crosslinks, the crosslinks within the core no longer dominate the dynamics and the dynamics resume a linear chain-like behavior.

Conclusions

Soft polystyrene nanoparticles have been shown to alter the diffusive properties of the linear chain in polymer nanocomposites that differs from a blend containing a comparable molecular weight linear chain. Additionally, the extent of change in diffusion behavior depends on the crosslinking density of the nanoparticle, where the deviation between a nanoparticle or polymer chain decreases with increased crosslinking. To further understand this phenomenon and the roll that crosslinking density plays, the global and local dynamics of soft polymeric nanoparticles in solution were investigated using neutron spin echo to identify the origins of variations in the dynamics of the nanoparticle from that of a linear polymer chain. Interestingly, the global dynamics of the nanoparticles adhere closely to ideal Zimm-like dynamics indicating the nanoparticles, globally, behave similarly to a linear polymer chain. The local dynamics of soft polystyrene nanoparticles, however, do vary from those of linear polymer chains, where the dynamic behavior of the soft nanoparticles examined here are dictated by its core-shell morphology. Probing local dynamics revealed a deviation from linear chain behavior on length scales between the core diameter and the total particle size, length

scales that predominantly focus on the crosslinks that fuse the nanoparticle together. Moreover, the local dynamics resume a linear chain-like behavior at length scales below the core size of the nanoparticle, or at length scales where the fuzzy outer shell is more prominent. Therefore, the localization of crosslinks within the core of the nanoparticle produces a core-shell structure that guides the dynamics of the nanoparticle as a whole.

More specifically, the breadth of the plateau of the effective diffusion coefficient of the soft nanoparticles is dependent on their crosslinking density. As the crosslinking density of the nanoparticle is increased, the breadth of the plateau increases as well. As a result, the nanoparticle exhibits slowed internal dynamics over a wider range of length scales. Further, the measured effective diffusion coefficients across all observed length scales are dependent on the crosslinking density of the nanoparticles, showing slower diffusion with higher crosslinking. Thus, the variation of the dynamic properties of these soft nanoparticles from linear polymer chains are directed by the core-shell structure that induces length scale dependent local dynamics.

Acknowledgements

This research was supported by the U.S. Department of Energy, Office of Science, Basic Energy Sciences, Materials Sciences and Engineering Division. Access to the Neutron Spin Echo Spectrometer was provided by the Center for High Resolution Neutron Scattering, a partnership between NIST and the NSF under Agreement No. DMR-2010792.

CHAPTER 4 : INSIGHT INTO THE PERMANENCY OF BOUND POLYMER LAYERS IN POLYMER NANOCOMPOSITES BY MONITORING POLYMER DESORPTION IN THE MELT

Abstract

The development of a bound polymer layer in a polymer nanocomposite due to strong interactions between the nanoparticle additive and surrounding polymer chains can drastically affect the dynamics of those chains. Once formed, the presence of a bound polymer layer is thought to be permanent – that the chains are irreversibly adsorbed to the surface. We examine this assumption, using neutron reflectivity and selective deuteration to monitor the fate of both loosely and tightly bound adsorbed chains in the melt with annealing. These results show that the total thickness of the adsorbed layer on a flat surface remains relatively constant over the observed annealing time, which many cite as evidence of the permanency of an adsorbed/bound layer. However, the composition of the layer does change over time. This change in adsorbed layer composition indicates that some chains desorb from the surface and are not "irreversibly" adsorbed as is often assumed. The kinetics of chain desorption are also studied by evaluating the time dependent change of excess (adsorbed) chains at the surface. The mechanism that dictates chain desorption transitions from primarily chain diffusion away from the surface at low molecular weights to a combination of chain diffusion *and* surface detachment mechanisms as the molecular weight increases. The continued contribution of chain diffusion to desorption kinetics at high molecular weight may be a consequence of the melt state where desorbing chains must more slowly cooperatively diffuse with surrounding chains to desorb from the surface than in a solution.

Introduction

The addition of nanoparticles to a bulk polymer can influence its mechanical properties. However optimal enhancement of the properties of these materials, referred to as polymer nanocomposites (PNCs), is dependent on achieving a homogeneous dispersion of the nanoparticle throughout the polymer matrix.[16, 75, 169, 170] Systems where the nanoparticles are poorly dispersed throughout the polymer matrix will typically exhibit diminished properties of the material. Poor dispersion of nanoparticles in the bulk polymer is usually caused by poor interactions between the two components of the system.[171, 172] However, improving the dispersion of nanoparticles in a PNC, frequently accomplished by inducing attractive interactions between the nanoparticles and the bulk polymer, results in the emergence of a bound layer of polymer on the surface of the nanoparticle.[85-87] A bound layer of polymer resides surrounding a nanoparticle in a PNC, where the dynamics of the polymer chain are significantly suppressed in this layer due to the strong interactions between the polymer chains and nanoparticle. As a result, the polymer chains are often considered to be irreversibly bound, or adsorbed, to the nanoparticle surface, hence exist as a bound polymer layer. The slowing of chain dynamics typically comes with an increase in the measured glass transition temperature, T_g, of the PNC, however minimal variation in PNC T_g has been recorded.[90, 91, 95-98] This lack of deviation in the glass transition temperature of a PNC suggests that the bound layer shields the slower bound chains near the interface preventing them from altering the thermodynamic properties of the bulk polymer.[94]

The existence of bound layers and their effects on polymer nanocomposites have been thoroughly discussed.[85, 87, 94, 98, 173-176] However due to the difficulty in parsing through all of the components of a system, monitoring the global and local dynamics of adsorbed chains within a PNC has proven to be difficult. Recently, Randazzo et al. characterized the development of the adsorbed layer and the changes exerted on the local chain dynamics by the presence of the adsorbed layer using a combination of fluorescence spectroscopy and transmission electron microscopy (TEM).[98] In many studies, the adsorption process is characterized as irreversible, however this concept of irreversibility is often assumed as the structure of the adsorbed layer does not appear to change over the course of most experientially relevant time intervals. Few have directly probed the permanency of a bound layer in a polymer nanocomposite. In addition to Randazzo's study of fluorescently marked adsorbed chains, Jimenez et al. investigated the dependance of annealing temperature on the thickness of a bound layer of poly(2-vinylpyridine) (P2VP) on the surface of silicon nanoparticles. In this study, Jimenez correlates the change in thickness of the bound polymer layer to the desorption of those chains from the nanoparticle surface and find that the desorption requires significantly high annealing temperature in order to observe a change in the bound layer thickness.[86] The structure of a bound polymer layer has been well characterized to be a combination of two distinct regions, one tightly bound and one loosely bound to the surface.[100] This study does not take into account this heterogeneity of chain attachment when describing the desorption processes, moreover, little insight into the processes that control the desorption process is provided.

Understanding polymer desorption is integrally connected to how the adsorbed layer is first formed. Polymer chains have a high propensity to adsorb to even mildly attractive surfaces due to the fact that surface interaction energies of most monomers are on the order of k_BT.[177-180] Moreover, this modest interaction energy allows for most individual monomers to equilibrate between adsorbed and free at any given time.[181-183] de Gennes predicted that the number of interactions between a random walk polymer chain and a substrate is on the order of $\sim\sqrt{N}$ where N is the degree of polymerization of the polymer chain.[184] The result is a "glue trap-like" effect where once a few monomers are adsorbed to a surface, the entire chain is considered adsorbed as it is statistically unlikely that all monomers will be free from the surface at any given time following the initial monomer adsorption.[102]

For instance, polymer chains adsorbed to a bare silicon surface form a thin layer with a structure that is a result of their adsorption mechanisms. Polymer chains adsorb to a surface monomer-wise, resulting in the adsorbed chains being comprised of trains, loops, and tails. Trains (Figure 4.1a) are sections of polymer chains where consecutive monomers are adsorbed to the surface. Loops (Figure 4.1b) are made when non-consecutive monomers adsorb leaving a section of the chain is free from, but confined near, the surface due to the adsorption of neighboring monomers. Tails (Figure 4.1c) are similar to loops but occur near the end of a polymer chain where only one end of the tail is adsorbed to the surface. O'Shaughnessy et al. proposed a mechanism of polymer chain absorption in the solution state based on simulation studies.[185] Later Simavilla et al studied polymer chain adsorption kinetics in the melt state and found similar results to

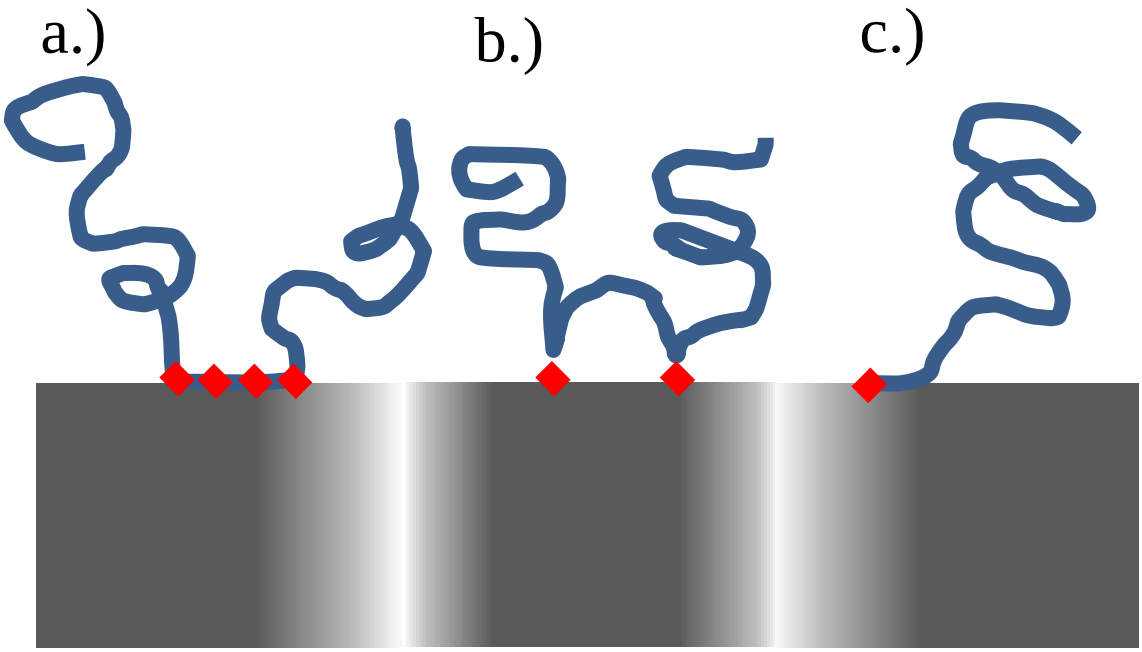

Figure 4.1 Adsorbed polymer chain conformations on substrate surface. a.) trains, b.) loops, c.) tails. The red diamonds signify the monomeric points of contact between the polymer chains and substrate.

those of O'Shaughnessy's solution state studies.[182, 186] Both of these studies show that the adsorption of polymer chains to a surface is a two-step process. Initially, at short annealing times, there is sufficient free surface area that polymer adsorption readily occurs with the adsorbed layer thickness increasing linearly with time. In this regime, no specific adsorbed chain structure (loops, tail, or trains) dominates. At longer annealing times, the growth of the adsorbed layer is slowed due to crowding at the surface and limited availability of free sites for new adsorption, where the thickness of the adsorbed layer changes to a logarithmic growth. In this regime, new chains are primarily comprised of larger loops and very few trains.[186] This results in the formation of two distinct regions within an adsorbed layer, a tightly bound region close to the surface which develops during early adsorption times, and a loosely bound region above the tightly bound one primarily comprised of loops and tails formed later in the adsorption process. This 'bilayer' type structure is illustrated Figure 4.2. These two layers can easily be observed in both neutron and x-ray reflectivity experiments because of a difference in their chain packing, and therefore scattering length density.

Polymer chains adsorb to a surface monomer-wise but desorb from the surface chain-wise, and since it is highly unlikely that all monomers will spontaneously desorb from the surface at the same time polymer chain adsorption is often considered irreversible.[181] From a spontaneous desorption standpoint polymer chain adsorption is irreversible, however chain desorption can be induced with an external stimulus. Polymer desorption from a surface is often studied in solution where adsorbed polymer chains are exposed to either a pure solvent or polymer solution, and the desorption of the

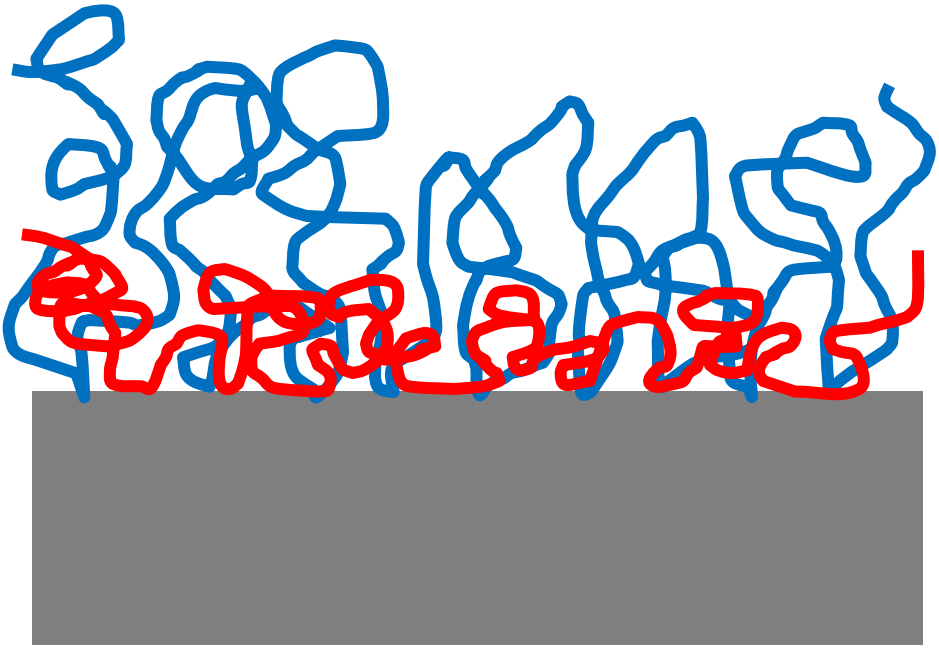

Figure 4.2 Illustration of differences between two components of adsorbed layer. Red corresponds to tightly bound dense layer comprised primarily of trains and loops. Blue corresponds to loosely bound layer comprised primarily of loops and tails.

adsorbed chains is monitored.[86, 100-106] However in systems where only a pure solvent drives desorption, the process is extremely slow, and typically does not result in complete desorption. For example, Gin et al. reported that a surface with adsorbed polystyrene in pure chloroform did not achieve full desorption after four months of solvent soaking.[100] In systems where a neighboring polymer solution drives desorption, a stronger adsorbing polymer is typically utilized which compels the initially adsorbed polymer to desorb from the surface.[101, 187] In this case, the desorption of the chains is influenced by other components in the system and this complicates the analysis of the desorption process. Thermal annealing of the adsorbed sample at sufficiently high temperature can also drive polymer chain desorption. Elevating the temperature of the system may overcome the enthalpic attraction between polymer and surface, promoting the desorption of the bound polymer chains.[99] However, the temperature required to counter the enthalpic contributions to desorption is often above the degradation temperature of the polymers, therefore thermal desorption is inaccessible under most conditions. For example, Monnier et al. monitored the adsorption and thermal desorption of poly(4-tert-butylstyrene) (PtBS) using fast scanning calorimetry where the temperature of the system is changed at a rate of 10^4 K s^{-1}. Accessing suitably high temperature to allow desorption in a short amount of time allowed for complete desorption to take place before the polymer chains thermally degraded.[99] Little research has been done that provide insight into the processes of polymer chain desorption in the melt as the temperatures needed to achieve full desorption is often above the polymer's degradation temperature, effectively making desorption inaccessible. However, the desorption of a single polymer chain in the

melt state can be monitored by exposing an adsorbed polymer layer to film of chemically equivalent free chains, creating a bilayer of adsorbed and free chains. Annealing of this 'bilayer' allows the interchange of adsorbed polymer, where adsorbing segments of previously free polymer can replace the desorption of adsorbed segments. The repetitive occurrence of this exchange will result in the desorption of the originally adsorbed chain. Monitoring the dynamics of this equilibrium exchange process can provide insight into the desorption of adsorbed polymer chains in the melt. This system differs from most solution-based studies where a stronger adsorbing polymer displaces the adsorbed polymer chain, where using a chemically equivalent species to displace the bound polymer minimizes the impact of secondary effects on the desorption process.

It has been shown that the desorption of adsorbed chains from a solid substrate is a first-order process, and has been investigated in both the solution and melt state.[99, 101] Douglas et al. examined the desorption of adsorbed chains in solution by replacing them with a stronger adsorbing polymer.[101] In that research program, it was found that the desorption of chains can be rate limited by two different processes, diffusion of the chain away from the surface or the detachment of the chain from the surface. Douglas found that the primary mechanism of desorption transitions from primarily diffusion away from the surface to chain-surface detachments with increasing temperature.[101] While this research focused on desorption that occurs in a solution, it is an interesting question if the desorption of a polymer chain in the melt will be governed by the same processes. There have been few studies that monitor the desorption of chains in a melt due to thermal decomposition limitations. Similarly, designing an experiment that can differentiate

between the adsorption and desorption processes of chemically equivalent polymers is not trivial. Moreover, examining the adsorption and desorption behavior of a polymer chain on a flat substrate can offer insight into the desorption of strongly bound chains, including the behavior of the bound layer in PNCs as in both systems the polymer chain is bound to the surface by strong interactions that significantly reduces polymer mobility. While surface topology does play a factor in the adsorption/desorption behavior of polymer chains, it has been shown that when the size of a spherical adsorbing surface is on the order of magnitude of, or larger than, the radius of gyration of the polymer chain, the system behavior is comparable to one with a flat surface topology.[188]

Thus, we report the results of an experiment that monitors the desorption of linear polystyrene from a flat silicon surface in the melt using neutron reflectivity. In this study, protonated linear polystyrene chains are adsorbed to a flat silicon substrate and a second layer of deuterated linear polystyrene is deposited on top of the adsorbed protonated layer to provide contrast between the free and adsorbed chains. Annealing the bilayer sample above polystyrene's glass transition temperature for extended periods of time allows interdiffusion of the protonated and deuterated chains and induce desorption from the surface. Similar to other adsorption/desorption studies, the change in the amount of surface excess of adsorbed chains is determined as a function of annealing time from the reflectivity data to monitor the desorption process and interpretated to provide insight into the fundamental processes that control the desorption of a polymer chain from the melt.

Experimental

Materials

Protonated and deuterated polystyrene was purchased form Polymer Source and used as received, where the molecular weights and polydispersities as reported by the manufacturer are listed in Table 4.1. Toluene (>99%, Fisher Scientific), Sulfuric acid (95-98% ACS, Sigma Aldrich), and hydrogen peroxide (30%, Fisher Scientific) were used as received.

Formation of Adsorbed Layer

Silicon wafers are first washed in a piranha solution (3:1 sulfuric acid to 30% hydrogen peroxide) for 15 minutes, then placed under a Novascan PSD-UV Benchtop UV-Ozone Cleaner for 15 minutes to ensure a clean, oxidized surface. A 1% weight solution of protonated polystyrene in toluene is passed through a 1.0μm PFTE filter to remove any large particulate contaminants and deposited onto a clean silicon wafer loaded on the spin coater. A thin polymer film is then formed by spinning the wafer at 1500 RPM for 120 seconds using a spin speed ramp of 1000 RPM/s. The silicon wafers were then placed in an oven under vacuum and annealed at 150°C for 18 hours to facilitate the adsorption of the polymer to the substrate. The wafers were then removed from the oven and quenched on a 0°C metal block to cease chain adsorption. Non-adsorbed chains were removed by soaking the wafer in a solution of toluene for 30 or 60 minutes.

Table 4.1 Polystyrene molecular weights and polydispersities

	Molecular Weight (M_w x 10^{-3})	Polydispersity
Protonated	22	1.10
	61.5	1.45
Deuterated	22	1.10
	61.5	1.45

Bilayer sample preparation

A 1% weight solution of deuterated polystyrene in toluene is spin casted at 1500 RPM for 120 second at a spin speed ramp of 1000 RPM/s onto a silicon wafer with an adsorbed protonated polystyrene thin film. The bilayer samples are annealed at 150°C for a given amount of time to promote the desorption of the adsorbed protonated polystyrene layer.

Neutron Reflectivity

Neutron reflectivity experiments were conducted at the NG7 horizontal neutron reflectometer at the National Institute of Standards and Technology (NIST) Center for Neutron Research (NCNR) and the BL-4B liquid reflectometer at Oak Ridge National Lab (ORNL) Spallation Neutron Source (SNS). All measurements were taken at room temperature over a q range of 0.008 – 0.2 $Å^{-1}$. The reflectivity was measured of the adsorbed protonated polystyrene layer, the as cast bilayer of adsorbed protonated polystyrene and free deuterated polystyrene bilayer, and the protonated/deuterated bilayer after annealing at 150 °C. The time intervals of annealing at 150 °C were 2 hours for the 22k Da samples and 6 for the 61k Da samples. These data sets provide the foundation needed to monitor the structure of the polymer layers at all points in the sample preparation process. All reflectivity data was then reduced and fit using the analysis package Motofit within the data analysis software IGOR Pro. A mass balance check was performed for each reflectivity profile by integrating the area under the scattering length density profiles for the as cast and annealed samples to ensure total composition variation did not exceed 5%.

Results and Discussion

Structure of Adsorbed PS Film

The scattering length density (SLD) profile of PS adsorbed layers emerge from fitting the reflectivity data of the adsorbed protonated PS film to two layers, one that models the densely packed layer near the surface, and the other that models the loosely packed polymers of the adsorbed layer. A fitted reflectivity curve and example SLD profile of an adsorbed polystyrene layer is shown in Figure 4.3. From this SLD profile, the two regions of the adsorbed layer are easily identifiable and mimic the profile predicted by O'Shaughnessy and Simavilla.[185, 186] The densely packed region of the adsorbed layer spans from ~ 0-70 Å from the Si wafer with an initial SLD of 2.2×10^{-6} $Å^{-2}$, nearly double that of bulk protonated polystyrene. The second, "loosely" packed adsorbed layer region, spans from 70-120Å from the Si wafer with an initial SLD of 1.4×10^{-6} $Å^{-2}$. When considering the two adsorbed regions, the densely packed layer is consistent with model predictions, where a large portion of chains confined close to the surface form trains and small loops. These conformations raise the scattering length density of the polymer in this region. Similarly, the loosely packed layer is consistent with the formation of adsorbed chains with larger loops and tails, and a lower SLD. This general structure of an adsorbed film comprised of a dense tightly bound region near the surface with a loose loops and tails region is consistent throughout all measured protonated PS adsorbed films, regardless of molecular weight or layer preparation. The-structural characteristics of the adsorbed film analyzed in Figure 4.3 are shown in Table 4.2. The roughness characterizes the breadth of the interface between layers, where a small

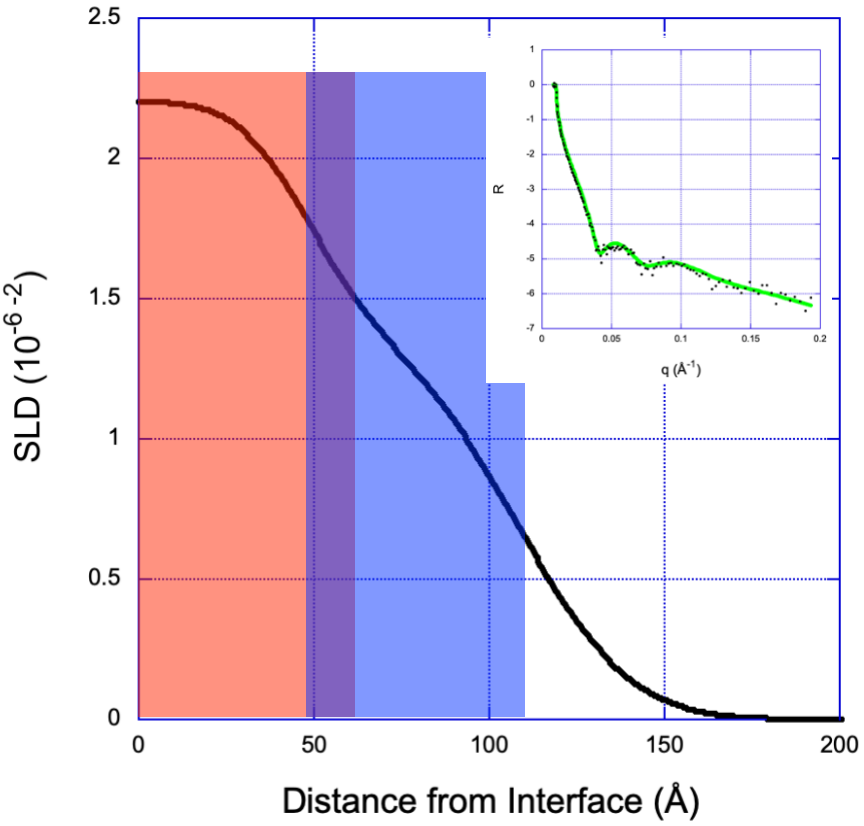

Figure 4.3 Scattering length density profile of adsorbed layer of 20kDa protonated polystyrene. In the inset, the reflectivity profile (black dots) and fit (green line) that produced the shown SLD profile. The regions of the bilayer are shaded as blue (loose) and red (dense).

Table 4.2 Fitting parameters for adsorbed layer of 20kDa protonated polystyrene

Layer	Thickness (Å)	SLD (10^{-6} Å^{-2})	Roughness (Å)
Loosely Bound Region (Red)	60.1 ± 0.9	1.40 ± .0.15	25.1 ± 2.3
Densely Bound Region (Blue)	67.3 ± 3.2	2.20 ± 0.02	15.5 ± 2.4

roughness indicates a sharp interface and a large roughness indicates significant intermixing between the two layers.

After annealing the spin cast PS films for 18hr at 150°C, the solutions were washed in toluene, for either 30 minutes or 60 minutes. Regardless of molecular weight and solvent washing time, the adsorbed layers show a moderately wide interface between the tightly bound and loose loops/tails regions. This is a result of both the tightly bound region containing loops, tails, and trains forming a very rough interface as well as the penetration of the upper layer to adsorb to the surface. Similarly, the roughness of the loose region (i.e., polymer/air interface) is larger than what one would expect from a thin polymer film cast from dilute solution. This shows the impact of removing non-adsorbed chains from the film, resulting in large fluctuations in the surface topology. The careful evaluation of the SLD profile of the initial adsorbed layer offers the foundation needed to monitor the SLD of the dPS/PS bilayer as the samples are annealed in order to accurately monitor the polymer chain interdiffusion and desorption processes.

Structural Evolution of PS/dPS Bilayer Films

The bilayer films are constructed by spin coating a second layer of deuterated polystyrene (SLD ≈ 6.0) of the same molecular weight on top of the characterized protonated adsorbed PS film. Using the previously determined adsorbed PS film structure as a reference point, the scattering length density profile of the as cast bilayer is determined by analyzing its reflectivity. To characterize the structure of this bilayer

sample, the SLD profiles that are produced as a result of the reflectivity fitting procedure are transformed into a volume fraction profile using Equation 4.1. In Equation 4.1, $\phi_{hPS}(z)$ is the volume fraction of protonated polystyrene at a distance of *z* from the

$$\phi_{hPS}(z) = \frac{SLD_{dPS} - SLD(z)}{SLD_{dPS} - \overline{SLD_{hPS}}} \qquad \textbf{4.1}$$

substrate, SLD_{dPS} is the fit SLD of the deuterated layer measured in the as-cast sample, $\overline{SLD_{hPS}}$ is the average SLD of the adsorbed layer in the as-cast sample, and *SLD(z)* is the fitted SLD of the film a distance, *z*, from the interface. Transforming the SLD profile into a volume fraction profile provides a visualization of the movement of the initially adsorbed (protonated polystyrene) chains with annealing time. Analysis of the as-cast samples show no significant movement in the adsorbed layer. The thickness and roughness of the loose and densely packed layers within the adsorbed film remain relatively unchanged, however there is a small increase in the SLD of the loose loops/tails region. This increase in the SLD is attributed to the high roughness of the loose loops/tails region allowing a small amount of penetration by the added deuterated PS into this layer. The volume fraction profiles of the 20k Da PS/dPS bilayer sample that was solvent washed for 30 minutes as a function of annealing time at 150 °C are shown in Figure 4.4.

A brief inspection of the volume fraction profiles in Figure 4.4 would suggest that there is no region of pure protonated polymer. However, this is not the case, but is an artifact of averaging the SLDs of the two layers of the adsorbed PS film in the calculation

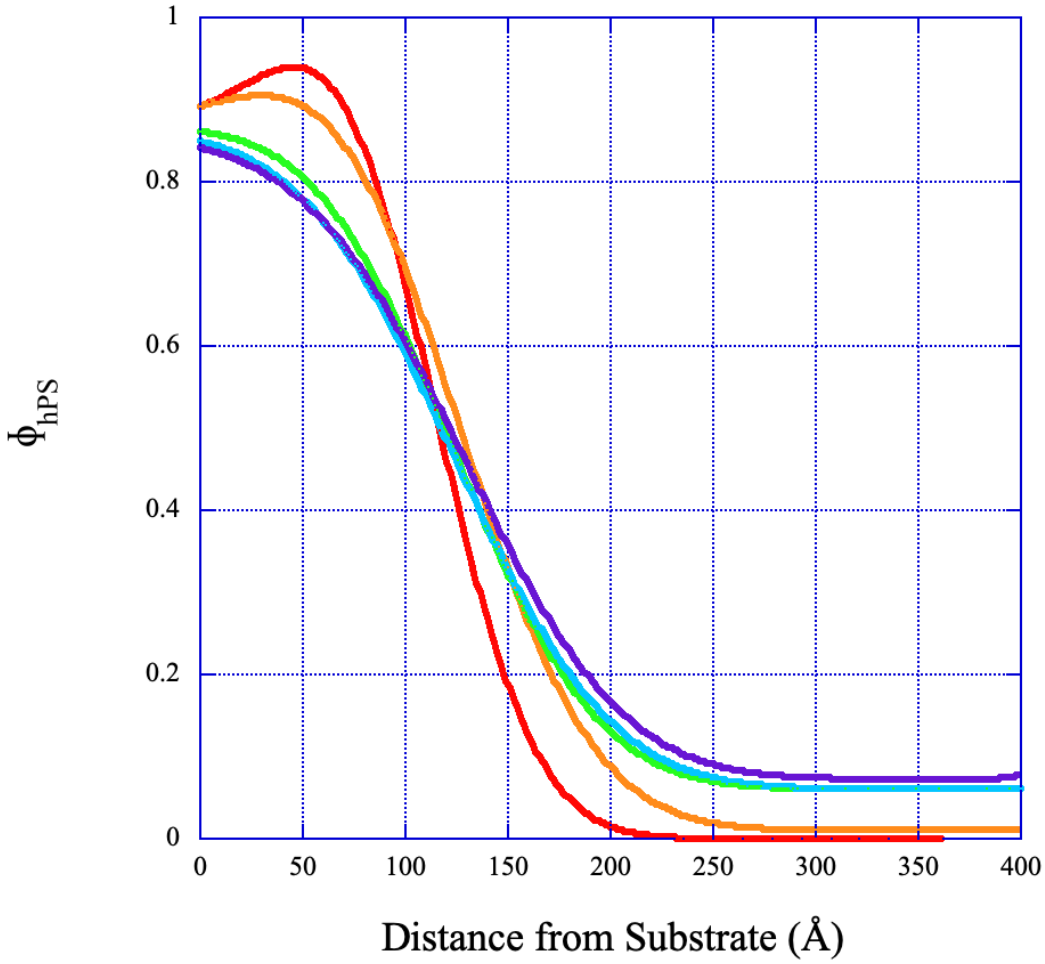

Figure 4.4 Volume fraction profiles of 20k Da PS bilayer sample annealed at 180°C where the adsorbed layer was solvent washed for 60 minutes. Red - As Cast, Orange - 2hr, Green - 4hr, Blue - 6hr, Purple - 8hr

of the volume fraction profile. Despite showing a maximum of ~95% hPS in the as cast sample (Figure 4.4 red) the region of 0-100 angstroms from the interface is indeed pure increase in the volume fraction of protonated material above ~ 250Å from the surface are of interest. For example, in the as cast sample (Figure 4.4 red) the baseline volume fraction of hPS above ~ 250 Å is ~0%, and over the course of 8 hours (Figure 4.4 purple) of annealing this value approaches ~8%.

Examination of the changes in the volume fraction profiles with annealing shows that interdiffusion of the PS and dPS chains occurs. The outer loose loops/tails region of the adsorbed film becomes less distinct. This is a result of interdiffusion between the loose loops/tails region of the adsorbed layer and the free deuterated layer. The peak in volume fraction profile of the as cast sample disappears, signifying the penetration of the deuterated polymer into the adsorbed layers. Additionally, the slope of volume fraction profile decreases further suggesting a broadening of the interface between the loosely adsorbed region and the free deuterated chains. At the same time, some initially adsorbed protonated chains have diffused into the bulk film as indicated by the increase in the volume fraction of protonated material above ~ 250Å from the surface. In the first two hours of annealing, the data suggests that some of the weakly adsorbed chains have desorbed, but it is not evident if any deuterated chains have adsorbed in their place as the volume fraction of protonated chains directly at the surface does not change over the first two hours of annealing.

Examination of the sample after 4 hours of annealing (Figure 4.4 green) shows a significant change in the volume fraction profile of the film. The volume fraction of

protonated material at the surface has decreased ~3% from the as cast film. Assuming that the surface is initially saturated with adsorbed protonated chains, this suggests that deuterated chains have now diffused through the densely adsorbed region and adsorbed at the surface. Similar to the structural evolution from as cast to 2 hour annealing, the structural evolution over the 2-4 hour annealing span continues to show a broadening of the PS/dPS interface indicating further mixing of the adsorbed layers with the free deuterated material. Additionally, the concentration of protonated material above 250 Å has increased from ~1% to ~6%. This increase corroborates the diffusion of PS away from the surface and dPS towards the surface and is consistent with the desorption of protonated chains from the surface.

When annealing the sample longer than 4 hours, there are small changes to the volume fraction profile at both the 6-hour (Figure 4.4 blue) and 8-hour (Figure 4.4 purple) annealing times, but the overall trends remain the same. There is very little change in the volume fraction of protonated chains at the surface, with each subsequent annealing time showing an additional ~1% decrease. Such small changes in the amount of protonated chains at the surface, could indicate a pseudo equilibrium. The changes in the volume fraction profile over this range of annealing times suggests that the loosely bound layer is more readily desorbed, while the more tightly bound layer requires longer times. The large drop in protonated chain content directly at the surface at the 4-hour annealing mark reveals that a significant amount of deuterated free chains have migrated to the surface and begun to adsorb. Since surfaces typically become saturated with adsorbed chains, preventing the attachment of new chains, this drop in protonated

(adsorbed) material at the surface is indicative of protonated chain desorption. For longer annealing times, there is minimal change in the protonated content at the surface, however it continues to slowly decline. This suggests that individual adsorbing sites of the tightly bound chains interchange with the free deuterated chains and become free. Over an extended period of time, this process leads to the desorption of the tightly bound chains, broadening the PS/dPS interface and an increase in the concentration of protonated chains throughout the film. The limited increase in protonated chain content throughout the film following the 4 hour annealing mark indicates that the desorption of loosely bound chains has stabilized and further changes in the structure of the adsorbed layer are likely the result of the desorption of tightly bound chains.

Quantifying the Kinetics of Desorption

To describe the kinetics of the desorption of the adsorbed chains, the excess chains at the surface is monitored. The surface excess at a given annealing time, denoted as Z*(t), is calculated as described in Equation 4.2.[189] At any given annealing time, there

$$Z^*(t) = \int_0^{z_{hPS}} [\phi_{hPS}(z,t) - \phi_{hPS}(dPS,t)]\, dz \qquad \textbf{4.2}$$

is a baseline volume fraction of protonated chains present throughout the entire film, and the surface excess is the amount of material segregated to the layer that is above this baseline concentration. The baseline concentration at a given annealing time is defined as $\phi_{hPS}(dPS,t)$, which denotes the volume fraction of protonated material found in the region primarily comprised of free chains, sufficiently far away from the surface that it is not influenced by surface environment. Surface excess chains are those considered to be

present between the substrate surface and the absorbed layer thickness, z_{hPS}, of the as-cast sample.

The surface excess is calculated for a sample for each annealing time, where an example of the area that is integrated to determine the surface excess is shown in Figure 4.5. For this system, the boundary values are $z_{hPS} = 130$Å, and $\phi_{hPS}(dPS, 8hr) = 0.072$, and Z*(8hr) = 83.66. The desorption of adsorbed polymer chains is monitored by observing the change in the measured surface excess as a function of annealing time.

Analysis of the change in surface excess with annealing time offers insight into the mechanisms that drive polymer desorption. Douglas et al. described two mechanisms that control the desorption of polymer chains in solution. While this study explores a system that is slightly different from the one at hand, the proposed processes that regulate desorption seem to endure the variations. Douglas indicates that the normalized surface excess can be described as a stretched exponential decay with respect to desorption time, or in the case of the this sytem the annealing time. This relationship is described in Equation 4.3.

$$\frac{Z^*(t)}{Z^*(0)} \sim exp\left[-\left({}^{t}/_{\tau_{off}}\right)^{\beta}\right] \qquad \textbf{4.3}$$

Here, Z*(0) is the surface excess of the as cast sample, *t* is the annealing time in hours, τ_{off} is the desorption time constant, and β is the stretched exponent. The stretched exponent of the exponential decay varies with the kinetics of polymer chain desorption, and by isolating that term can provide insight towards the processes that control desorption. When the decay of the surface excess can be described as a single exponential

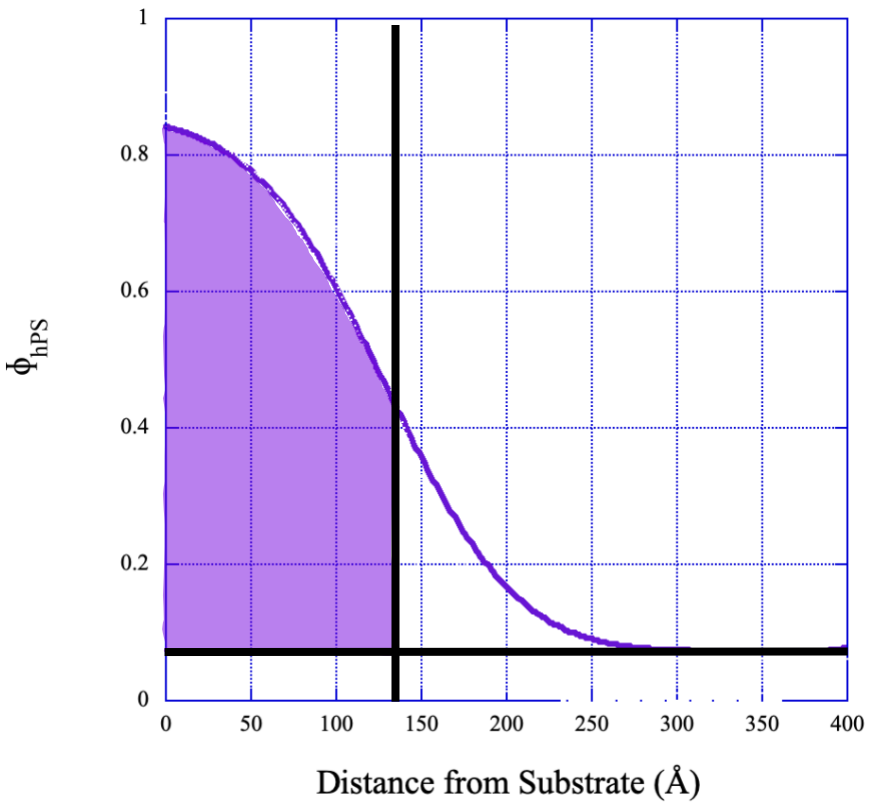

Figure 4.5 Surface excess profile of 20k Da polystyrene and annealed for 8 hours. The shaded region is the calculated Z* value for this annealing time.

decay, $\beta = 1$, the desorption is rate-limited by chains detaching from the surface, or individual monomer desorption. When $\beta < 1$, and in the ideal case $\beta = 0.5$, the desorption is rate-limited by the diffusion of chains away from the adsorbing surface.[101] Equation 4.3 can be transformed into a linear equation with respect to β by taking the natural log of both sides as shown in Equation 4.4 allowing for isolation of the stretching exponent

$$-ln\left[-ln\left(\frac{Z^*(t)}{Z^*(0)}\right)\right] = -\beta\left[\ln(t) - \ln\left(\tau_{off}\right)\right] \quad \textbf{4.4}$$

from the time evolution of the surface excess. The transformed surface excess as a function of the natural log of annealing time is shown in Figure 4.6 to determine β in our studies.

The desorption was monitored for four systems, varying molecular weight and solvent washing time. The samples studied were comprised of either 22k Da or 62k Da molecular weight polystyrene, with either 30 or 60 minutes washing time during adsorbed layer formation. The surface excess of the adsorbed layer for each annealing time were determined using Equation 4.2, then transformed into a linear form using Equation 4.4. All five of the systems measured showed reasonably good linear dependence when transformed using Equation 4.4. Those data sets were then fit to a line, and the resulting slope is the stretching exponent and are reported in Figure 4.7. Inspection of Figure 4.7 shows that the exponential decay stretching exponents can easily be grouped together by molecular weight with little impact of the solvent wash time during the adsorbed on the kinetics of chain desorption. An average stretching exponent of ~0.30-0.40 was found for the lower molecular weight (22,000 Da) sample, while the stretching

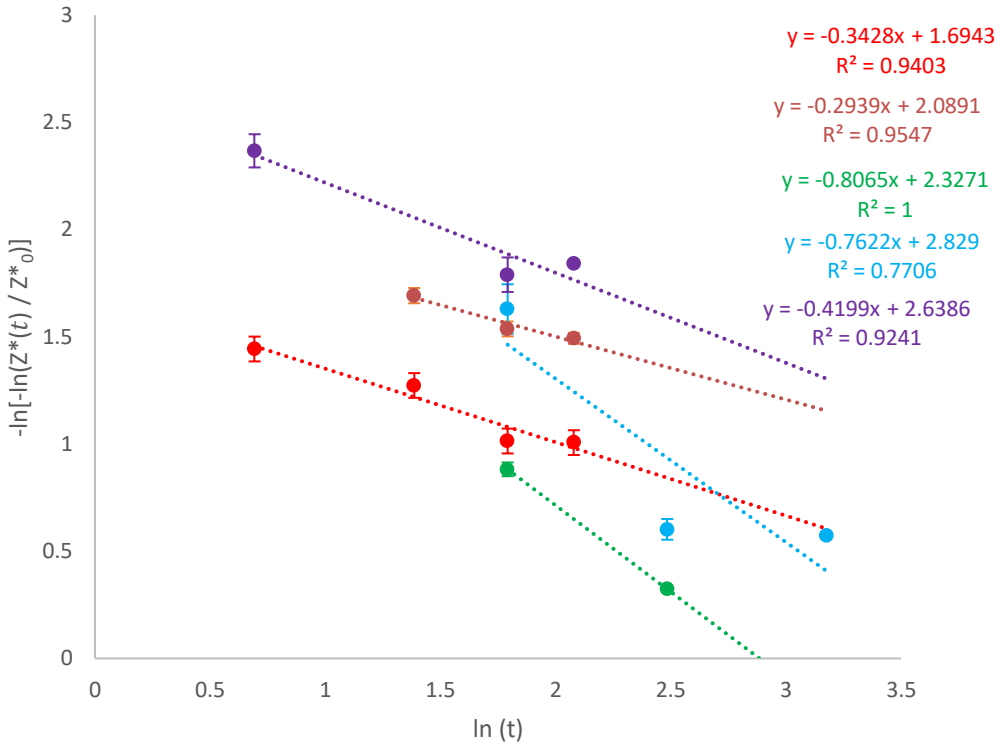

Figure 4.6 Double negative log of normalized surface excess versus log annealing time. Red - 20k Da 30 minute wash, Orange - 20k Da 60 minute wash, Green - 60k Da 30 minute wash, Blue - 60k Da 60 minute wash, Purple - 20k Da 30 minute wash

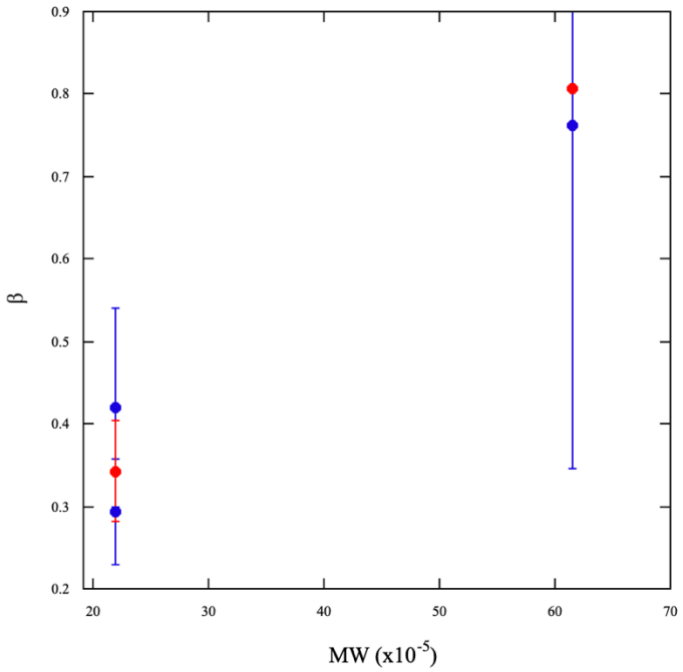

Figure 4.7 Exponential decay stretching exponent, β, dependence on molecular weight of the desorbing polymer. Blue markers signify a 30 minute solvent wash during adsorbed layer formation, red markers signify a 60 minute solvent wash.

exponent increases significantly to 0.75-0.80 for the longer PS polymers (62,000 Da) sample. The 30-minute solvent wash of the 60k Da sample shows a remarkably high error in the value of the stretching exponent, a result of the normalized surface excess exhibiting poor linear behavior with time (Figure 4.6 blue). Proceeding from 12 to 24 hours of annealing time, minimal change is observed in the volume fraction profile of the 60k Da 30-minute sample. Suggesting that an equilibrium may have been reached in this system around the 12 hour mark and characterizing the system further may skew the interpretation of the surface excess data.

Interpreting these values in terms of Douglas' model indicates that the desorption of the lower molecular weight PS is limited by the chain diffusion of the desorbed polymer from the surface, while both chain diffusion and chain detachment impact the rate of polymer desorption for the longer polymer chains. A stretching exponent of approximately 1 indicates that the rate limiting mechanism of chain desorption is the detachment of bound sites from the surface. A smaller stretching exponent (~ 0.6 – 1.0) suggests that both chain diffusion of the polymer away from the surface and surface detachment impact the desorption process, where chain diffusion becomes more prominent as the stretching exponent becomes smaller. Figure 4.7 shows the change in β with molecular weight in our experiments, where a transition from primarily chain diffusion to primarily surface detachment occurs with a decrease in molecular weight.

The transition away from chain diffusion limited desorption with increasing molecular weight may be surprising, since diffusion slows significantly with an increase in molecular weight ($D \sim M^{-2}$). The competition between chain diffusion and surface

detachment with increasing molecular weight can be qualitatively discussed by comparing the molecular weight dependencies of the probability of chain desorption and the diffusion coefficient of a polymer chain. Napolitano suggests that individual monomers of an adsorbed polymer chain can fluctuate between bound and free at any given time due to the fact that the surface/monomer interactions are on the order of k_BT at temperatures where desorption may occur. Moreover, for a chain to desorb all monomers must be simultaneously free of the surface.[181] Recall that de Gennes predicts that the number of bound sites between an adsorbed random walk chain and a substrate is on the order of $\sim\sqrt{N}$.[184] Therefore, assuming that the monomers are independent of each another, the probability of chain desorption, P_{chain}, is equal to the probability of all bound monomers desorbing, $P_{monomer}$, simultaneously which is expressed in Equation 4.5.

$$P_{chain} = P_{monomer}^{\sqrt{N}} \quad \textbf{4.5}$$

The value of $P_{monomer}$ is reliant on the strength of the interaction between the polymer and the adsorbing surface. Following Napolitano, the probability of a monomer desorbing can be approximated to 0.5. In reality, this is probably a reasonable upper bound for this probability where more strongly bound chains have a lower probability (i.e $P_{monomer} < 0.5$). Meanwhile, the dependence of polymer chain diffusion on molecular weight is well documented and described in Equation 4.6.

$$D \sim M_n^{-2} \sim N^{-2} \quad \textbf{4.6}$$

Using $P_{monomer} = 0.5$, the probability that the 20k Da PS chain will desorb is nearly 1,400x greater than the probability that the 62k Da chain will desorb. If $P_{monomer} < 0.5$, the

probability that the 20k chain will desorb is *even greater* than 1,400x than the probability that the 62k Da chain will desorb. However, the diffusion of the 20k Da PS chain is only 10x faster than the diffusion of the 62k Da PS chain. Thus, surface detachment scales much more strongly with molecular weight than diffusion does. With such strong dependence on molecular weight, it is not surprising that surface detachment dominates the kinetics of desorption as the polymer molecular weight increases.

However, surface detachment is not the only process impacting the rate of desorption in our studies, as the calculated stretching exponent is less than 1 for all systems. A stretching exponent of ~ 0.8 for the 62k Da sample suggests that the diffusion of the polymer from the surface continues to impact the desorption process. The continued influence of chain diffusion with surface detachment on desorption kinetics as the molecular weight increases may be a consequence of the process taking place in the melt. In a dilute solution system similar to the one studied by Douglas, the concentration of polymer is overlap concentration such that the polymer chain motion is independent of other polymer chain. Therefore, when a high molecular weight polymer chain desorbs from a surface in a dilute solution, there is essentially no interaction with nearby chains and the influence of chain diffusion is limited. In the melt however, polymer chain movement occurs by reptation where a single polymer chain must diffuse through other nearby chains. This reptative process is slower than diffusion in solution, and scales with molecular weight more strongly than diffusion in a solvent. Thus, as the chain length increases in our studies, the relative importance of the chain diffusion away from the surface remains at moderate molecular weights (i.e., 62k Da) because it is sufficiently slow to compete with chain

detachment. Thus, even though surface detachment mechanisms are strongly favored at high molecular weights, the reptative motion of a polymer chain in the melt results in chain diffusion impacting desorption kinetics at moderate molecular weights.

Conclusion

Adsorbed polymer chains are often thought to be 'irreversibly' attached to the surface. This study critically evaluates this assumption and seeks to provide insight into the processes that drive the desorption of polymer chains in the melt. Using neutron reflectivity, the evolution of the depth profile of an adsorbed polymer layer in the melt is monitored as a function of annealing time above the polymer's glass transition temperature. Neutron reflectivity and selective deuteration offer unique insight into the adsorption, desorption and diffusion of both loosely and tightly bound chains within an adsorbed layer. The results of this study show that despite the total thickness of the adsorbed layer remaining unchanged throughout annealing, a change in the depth profile of the protonated (adsorbed) material indicates that individual chains desorb and are replaced by new chains. Additionally, this study offers insight into the mechanisms that drive chain desorption in the melt and their dependency on molecular weight. At low molecular weights, chain diffusion appears to primarily control the rate of desorption. However, as the molecular weight of the desorbing species increases, a transition to a process that is dominated by surface detachment emerges. Over the molecular weight range evaluated here, chain diffusion continues to influence desorption kinetics at higher molecular weights. This combination of processes is believed to be a consequence of the

desorption occurring in the melt. Further studies to examine the desorption of higher molecular weight adsorbed chains are needed to more fully elucidate the molecular weight dependence of the competition between chain detachment and chain diffusion in polymer chain desorption in the melt.

Acknowledgements

This research was supported by the U.S. Department of Energy, Office of Science, Basic Energy Sciences, Materials Sciences and Engineering Division. A portion of this research was also completed at ORNL's Spallation Neutron Source (SNS), which was sponsored by the Scientific User Facilities Division, Office of Basic Energy Sciences, US Department of Energy. The authors acknowledge the support of the National Institute of Standards and Technology, U.S. Department of Commerce, in providing the neutron reflectivity facilities used in this work, where these facilities are supported in part by the National Science Foundation under Agreement No. DMR-0944772.

CHAPTER 5 : IDENTIFYING OPTIMAL DISPERSANT AIDS FOR FLAME RETARDANT ADDITIVES IN TETRAMETHYL CYCLOBUTANEDIOL (TMCD)-BASED COPOLYESTERS

Disclosure Statement: The following chapter, “Identifying Optimal Dispersant Aids for Flame Retardant Additives in Tetramethyl Cyclobutanediol (TMCD)-Based Copolyesters” is a direct write up of a publication of the same title by the author, Dr. Mark Dadmun, and Dr. Kevin Cable, first published by Wiley in the Journal of Applied Polymer Science in July 2022. This article can be found by the following URL : https://doi.org/10.1002/app.52811

Abstract

Proper dispersion of an additive throughout a polymer matrix is essential to achieving the complete desired effects of the additive. Typically, this dispersion can prove to be difficult due to poor interactions between the polymer and additive, leading to poorly performing polymer composites. In the case of melamine cyanurate, an extensive hydrogen bonding network between the principal components of the compound results in large crystalline domains and prevent it from achieving sufficient integration within many polymer matrices. While mechanical routes can reduce the domain sizes by physically shearing domains, addressing the hydrogen bonding at an atomic level can lead to smaller sized melamine cyanurate domains. Adding a hydrogen bonding capable polymer that can replace the intramolecular hydrogen bonding with the intermolecular variety will lead to an overall reduction in crystalline particle size. The disruption of the hydrogen bonding network was monitored using attenuated total reflection Fourier transform infrared spectroscopy (ATR-FTIR) by comparing the relative intensities of hydrogen bonding related peaks, while crystalline domain size was calculated via processing scanning electron microscopy (SEM) images. Water-soluble polymers were identified as an ideal category of dispersing aids for their hydrogen bonding ability and expected compatibility with melamine cyanurate. Disrupting the hydrogen bonding network on an atomic level with a water-soluble polymer dispersant led to at least a 50% reduction in measured particle size, as well as in increase in the domain size's homogeneity, as indicated by a 75% reduction in the polydispersity of particle sizes in melt mix samples.

Introduction

Enhanced properties of polymers are often achieved through the addition of small molecules or particles, typically functionalized nanoparticles, where the added material is able to provide additional thermal, chemical, or mechanical properties to the bulk polymer.[3, 18-22] However, achieving a high level of dispersion of nanoparticles within a polymer melt is difficult due to the incompatibilities between the two materials, leading to agglomeration of the nanoparticles within the polymer matrix, which then results in diminished optical, thermal, electrical, or mechanical properties of the nanocomposite.[16] There are numerous routes to improve the dispersion of nanoparticles within a polymer matrix, two of the more common methods for enhancing nanoparticle dispersion are incorporating noncovalent interactions between the polymer and nanoparticle, or covalently grafting a polymer to the nanoparticle surface that is miscible with the bulk polymer.[23-27, 34, 124] The principles behind good nanoparticle dispersion can also be applied to other types of additives to polymer systems, where poor interaction between the polymer and additive, or exceedingly strong interactions within the additive itself, can lead to the agglomeration of the additive in the system.

The addition of flame retardant (FR) small molecules to a polymer matrix is often done to suppress, or impede, the thermal decomposition of the bulk polymer. Early FRs were often halogenated or antimony-based molecules, however the use of these types of FRs have been impeded due to their inherent toxicity[190, 191]. As a result, small molecules or polymers rich in phosphorus and/or nitrogen have been found to be a suitable environmentally friendly alternative to their halogenated and heavy metal-based

predecessors.[190] Melamine cyanurate (MC) is a water soluble, nitrogen containing compound frequently used as an additive in polymeric systems for its fire-retardant properties.[192-195] The MC complex is formed via self-assembly of the two principal components in a polar solvent forming a robust network of hydrogen bonding between individual melamine and cyanuric acid molecules, as depicted in Figure 5.1. The hydrogen bonding network leads to a planar complex where any individual melamine and cyanurate acid molecule can have up to six possible hydrogen bonding sites, and because the self-assembly does not control for size of the clusters it can lead to a wide range of particle sizes, from very small to extraordinarily large. [196, 197]

The hydrogen bonding network leads to the compound having a highly endothermic decomposition temperature in excess of 320°C. When the MC is exposed to a flame, the hydrogen bonds between melamine and cyanuric acid are disrupted, vaporizing the two compounds into nitrogen containing gases which dilutes the oxygen rich fuel environment of a fire[193, 198]. Homogeneously dispersing MC into a polymer matrix can prove difficult due to the nature of its extensive hydrogen bonding network and poor interaction with most nonpolar polymers.[199] This causes the MC to agglomerate into large domains within the polymer. Moreover, it is well known that the poor dispersion of nanoparticles in a polymer matrix usually leads to decreased efficacy of the additive material and decreased tensile and optical properties of the resultant nanocomposite.[16, 199]

The incorporation of MC into a bulk polymer is accomplished in a variety of methods such as mechanical processing in the melt state, solution-based mixing, or in-situ during polymerization.[195, 197, 199-201] In situ and solution-based incorporation of MC is

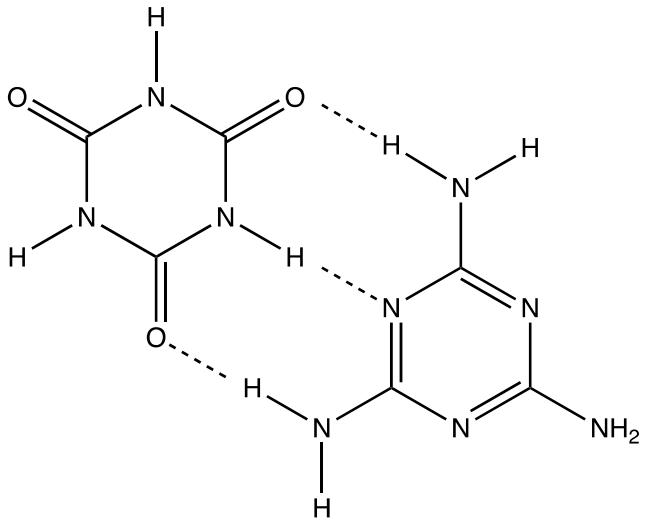

Figure 5.1 : Structure of melamine cyanurate (MC) showing hydrogen bonding between cyanuric acis (left) and melamine (right)

advantageous as it drastically decreases the average MC particle size and improves the dispersion of the crystalline particles in the polymer matrix. However, this method is limited to polymers with compatible synthetic processes or chemical properties. For instance, Huang et al. describe the process of highly dispersing MC in an epoxy resin matrix. In this process, the MC is dispersed into the epoxy resin pre-polymer solution that is subsequently polymerized[199]. This resulted in an epoxy resin solution with MC particles that are nearly an order of magnitude smaller than particles that are formed from mechanical mixing. Similarly, Mehra et al. report the incorporation of MC with poly vinyl alcohol in the solution phase to produce uniformly dispersed MC, however in this case all components (polymer, melamine, and cyanuric acid) are soluble in water.[200] For non-water soluble polymers, incorporating MC after the synthesis of the polymer typically requires melt mixing, as long as the melting temperature of the polymer is below the 350°C decomposition temperature of MC. Unfortunately, melt mixing MC with a polymer matrix typically provides less favorable dispersion than the previously mentioned methods. This is because in melt mixing, the disruption of the MC network is reliant on the mechanical shearing and pulverizing of the intramolecular hydrogen bonds during processing.[199]

Much of the research regarding MC, and FRs in general, in polymers focuses on the efficacy of the additive as a flame retardant.[197, 202-204] However, very little research has been conducted to develop methods to control the size of MC particulate domains within a polymer during melt mixing. MC particulate size is a result of its exceedingly robust hydrogen bonding network, and chemically disrupting the hydrogen bonding network should promote the formation of smaller particles. A potential solution is therefore to

introduce a third component to the blend, a polymeric dispersant, that has the ability to interrupt the melamine-cyanuric acid hydrogen bonding network creating smaller MC particle sizes and improving its dispersion. Properly designed, such a dispersant will interrupt the *intra*molecular hydrogen bonding network of MC by forming its own *inter*molecular hydrogen bonds.

The introduction of a third component to a multicomponent polymer system to improve dispersion has been studied for polymer blends, composites and nanocomposites. Polymer compatibilization is an area of polymer research in which a polymeric interfacial modifier is added to a blend of two immiscible polymers to promote a stronger, more homogeneous, interface between the two components of the blend. Typically, this is accomplished via a block copolymer comprised of the two components of the blend. A blocky compatibilizer acts as a zipper between the two domains with the blocks segregating to their preferred side of the interface producing a more mechanically robust interface.[113-117] Previous studies have also shown that the control of non-covalent interactions between components of the mixture can improve dispersion.[7, 118-124] This process generally introduces preferred *intermolecular* non-covalent interactions between mixture components that improve dispersion. We therefore seek to build off this foundation to develop an understanding of how preferred *intermolecular* interactions can be introduced to mixtures of MC and polymers to create composites with controlled dispersion of the MC, particularly for melt mixed composites.

Because MC is water soluble and contains an extensive hydrogen bonding network, we hypothesize that polymers that can form competitive hydrogen bonds with the MC will

serve as suitable dispersants of MC in blends with tetramethyl cyclobutanediol (TMCD) polyesters. Recently, Kadanyo et al. used polyethylene oxide (PEO) as a compatibilizing agent for a blend of polysulfone/poly(ethylene-co-vinyl alcohol) where the primary function of the PEO was to form intermolecular hydrogen bonds between the two blended polymers.[205] Meanwhile Ferrarezi et al. utilized PEO as a compatibilizer for a blend of poly(lactic acid) and thermoplastic starch where the PEO's ability to hydrogen bond with the blend components was credited towards its success as a compatibilizer.[206] Thus, PEO is a good candiate to form competitive *intermolecular* hydrogen bonds with MC, and improve the dispersion of MC in the TMCD polyester Tritan. A second dispersant is also examined, AQ series sulfopolyester's provided by Eastman chemical company as they are water soluble, able to form hydrogen bonds, and the polyester backbone of the polymer should promote a heightened miscibility with Tritan. Thus, the ability of these two polymer dispersants to disrupt the extensive hydrogen bonding network of MC and improve its dispersion in a polymer matrix will be evaluated via microscopic image analysis, while the extent of hydrogen bonding among MC molecules is monitored by Fourier transform infrared spectroscopy. These results will therefore provide important fundamental information on the ability of hydrogen bonding capable polymer dispersants to improve and control the dispersion of MCs in solution formed or melt mixed polymer composites. Moreover, this insight will also provide information that will also be relevant to controlling the dispersion of other functional additives in polymer matrices.

Experimental Methods

Materials

Melamine cyanurate, AQ series sulfopolyesters (AQ55S and AQ65S), and Tritan copolyester (TX1001) were provided by Eastman Chemical Company. The AQ series polymer follow the general structure shown in Figure 5.2, but with varying monomer block ratios. Two molecular weights of poly(ethylene oxide) (PEO) were used, where the 10,000 Dalton polymer was purchased from Sigma Aldrich and the 100,000 Dalton polymer was purchased from Acros. Chloroform (>99%) was purchased from Fisher Scientific. All chemicals were used as received.

Solvent Cast Thin Films

Solvent cast thin films were made by first dissolving a mixture of MC and polymer dispersant at a 5%/95% weight ratio in chloroform at a concentration of 2% weight/volume. A pure MC solution was made using the same weight concentration in chloroform as the binary mixtures. The solutions were allowed to mix overnight to ensure complete dissolution of the polymer. Prior to deposition on a substrate, the solutions are vortexed to ensure optimal homogeneity of the solution. The solutions were deposited via a syringe onto either a glass microscope slide for microscopy analysis or a potassium bromide (KBr) window for FTIR hydrogen bonding analysis. The substrates were then sealed inside a desiccator to promote the slow evaporation of solvent, which ensured the formation of bubble free films. The films were kept in the desiccator overnight at room temperature to allow for the full evaporation of the solvent from the film.

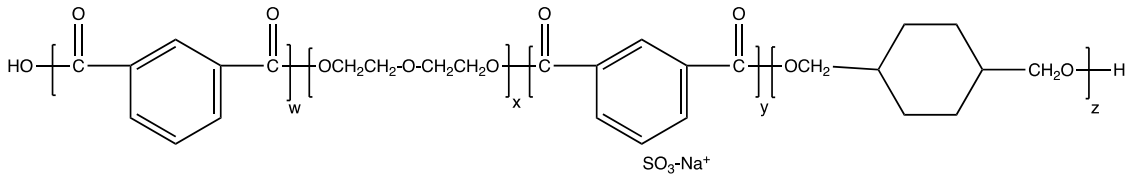

Figure 5.2 General structure of Eastman AQ series sulfopolyesters. AQ55S and AQ65S contain different ratios of the four monomeric blocks.

Optical Microscopy

The dispersion of MC in the solvent cast films were monitored by optical microscopy using an Olympus BH2 microscope equipped with a 10x magnification objective lens, and 10x magnification eyepiece. A micrometer calibration slide provided by American Scope was used to verify the observable length scales at the chosen magnification. Images were taken in bright-field, phase contrast, and under polarized optics.

Extruded Filaments

Mixtures of MC, Tritan, and a polymer dispersant are weighed into a container so that all components could be mixed by hand. Blend films containing either 4% or 8% wt MC, 0%, 0.5%, 1%, or 2%wt polymer dispersant, with the remaining 90% to 96%wt Tritan were examined. These mixtures were then fed into the hopper of a Thermo-Haake Mini Lab II conical twin screw extruder. The ternary blend is mechanically mixed at 260°C to form a filament.

Fourier Transform Infrared Spectroscopy

Fourier transform infrared spectroscopy (FTIR) was performed using a Thermo Scientific Nicolet iS50 FT-IR in the attenuated total reflection (ATR) mode. Each sample was analyzed by formed via solvent casting onto a KBr window scanned 32 times over a wavenumber range of 4000-400cm^{-1} with spectral resolution of 8cm^{-1}. FTIR is performed to provide relative concentrations of the hydrogen bound and free amine groups found within MC.

Scanning Electron Microscopy

The micron level structure of the blends were determined with scanning electron microscopy (SEM) on a ThermoFisher FEI Quanta 450F at the Eastman Chemical Company Microscopy Center. The extruded filaments were first cut to fit the sample stage holders. Each filament's cross section was then microtomed to achieve a smooth, flat surface for imaging. Each filament sample was then sputter coated with platinum to limit charge build up during imaging. Samples were imaged at 150x, 500x, 1500x, and 2500x magnification to observe the filament cross section as a whole at low magnifications, and particle size and distribution at higher magnifications. Images were taken using an Everhart-Thornley detector.

Results and Discussion

Solvent Cast Thin Films

Particle Size Analysis – Optical Microscopy

The particle size of solvent cast thin films containing only MC and the dispersant were first analyzed via optical microscopy. Images were captured using a 10x magnification lens which allowed for a 650µm x 480µm area within the film for particle analysis. At this magnification, very small MC crystalline domains are observed within the film, and their sizes are measured via the imaging processing software ImageJ. The effectiveness of the polymer dispersant is quantified with two metrics: the average measured particle size and the total number of observable particles per unit area. The dark regions within the films, as seen in Figure 5.3, were identified to be MC. In the control film, Figure

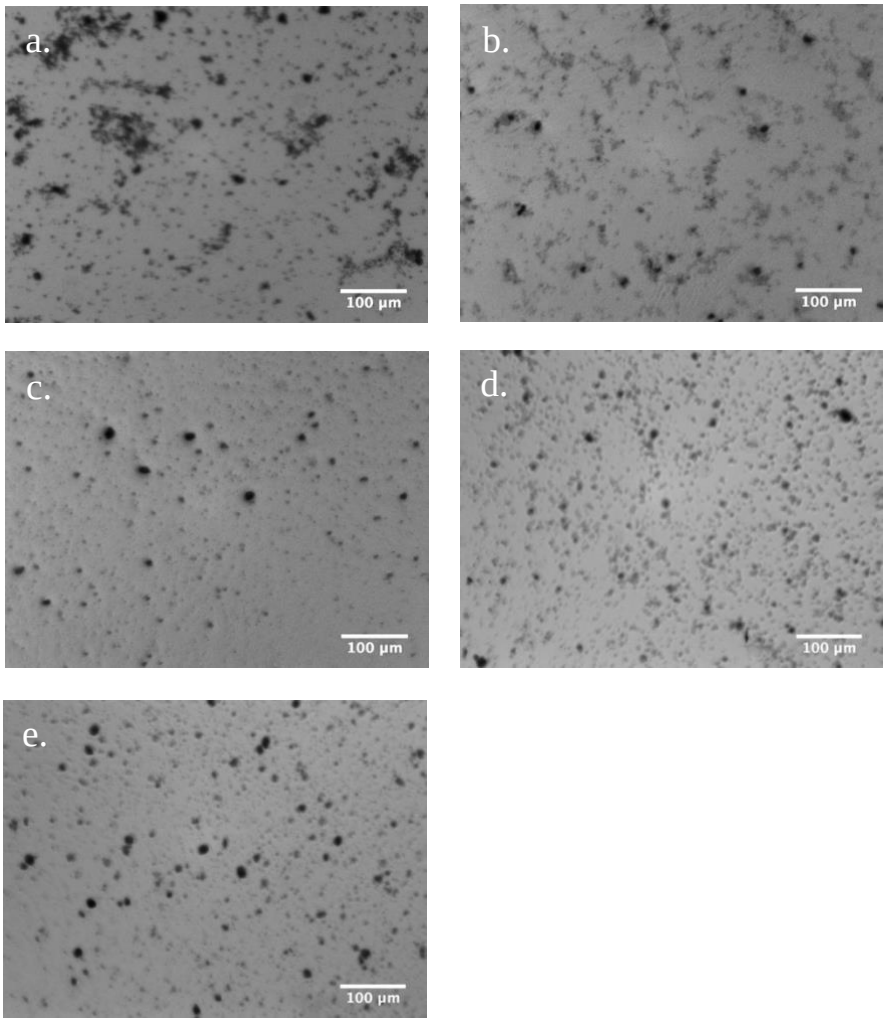

Figure 5.3: Optical microscopy images of solvent cast thin films at 10x magnification. a.) MC, b.) 10k PEO-MC, c.) 100k PEO-MC, d.) AQ55S-MC, e.) AQ65S-MC

5.3a, where no dispersant was used an average particle size of 76.7μm^2 and a total of 357 particles were observed, whereas the average particle size in films containing a polymer dispersant did not exceed 41.4 μm^2. The average particle size and number of particles observed in each film is shown in Table 5.1. These results show that the error in particle size is larger than the average area of the particles themselves. This is a result of the presence of a bimodal distribution pf particle sizes within the film with a dominance of very small particles with fewer very large particles. This can be interpreted to indicate that the primary role of the polymer dispersant is to break up the largest particles to form a relatively uniform distribution of smaller particles. Moreover, these results show that the inclusion of just 5%wt polymer dispersant is sufficient to reduce the average measured particle size by nearly 50% while the error of the mean is also greatly reduced. This reduction in error suggests that not only are the polymer additives reducing the MC crystalline size, but they are also promoting a more homogeneous size and dispersion throughout the films, which can qualitatively be seen in Figure 5.3. In the pure MC film, Figure 5.3a, there are numerous very large domains where it appears that several of the well-defined crystalline areas have agglomerated together. Where in Figures 5.3b-e, or those containing a polymer dispersant, those larger, nebulous domains are not observed. Instead, small clearly defined and separated MC sites are observed. If the polymer dispersant were successful in breaking up MC, one would expect for the average particle size to decrease, while the number of observed

Table 5.1: Average particle area from optical microscopy images of solvent cast thin films

Thin Film Blend	Average Particle Area (μm^2)	Number of Observed Particles
10k PEO – MC	32.4 ± 72.7	215
100k PEO – MC	33.4 ± 56.6	149
AQ55S – MC	32.5 ± 54.0	296
AQ65S – MC	41.4 ± 77.1	469
Melamine Cyanurate (MC)	76.7 ± 272	357

particles increases. However, that is not the case with these blends as the number of observed particles decreases for most of the films. It is believed this is because the polymer additive is breaking up the MC to form smaller domains that are below the resolution of the optical microscope. Figures 5.3b-e contain very small MC domains, which are more common than those found in the bulk MC film. However, these particles approach the optical microscope's resolution and are difficult to individually identify via optical microscopy particle size analysis. Imaging the films at a higher magnification provides an opportunity to test this prediction. As such, these films were analyzed at significantly higher magnifications via scanning election microscopy (SEM). Energy dispersive X-ray spectroscopy (EDS) of the SEM image also facilitates the determination of the presence of MC throughout the film to assess its distribution at all length scales.

Particle Size Analysis – Scanning electron microscopy

A qualitative analysis of the dispersion of the MC in the blends of interest at high magnification showed the existence of extraordinarily small domains in the blend films that are not observed in the bulk MC sample, providing credence to the theory that the polymer dispersants are creating MC domains beyond what was observable via optical microscopy. At the same time, following the presence of nitrogen by EDS maps the position of MC in the blend films, as the MC is the only nitrogen containing compound. EDS analysis of the blend films at 3000x magnification shows that the MC only exists in the blend where it is visible as a crystalline domain. Figure 5.4 shows the EDS results of a scan that contains a visible particle (orange), and part of the film that does not visually contain a particle (red).

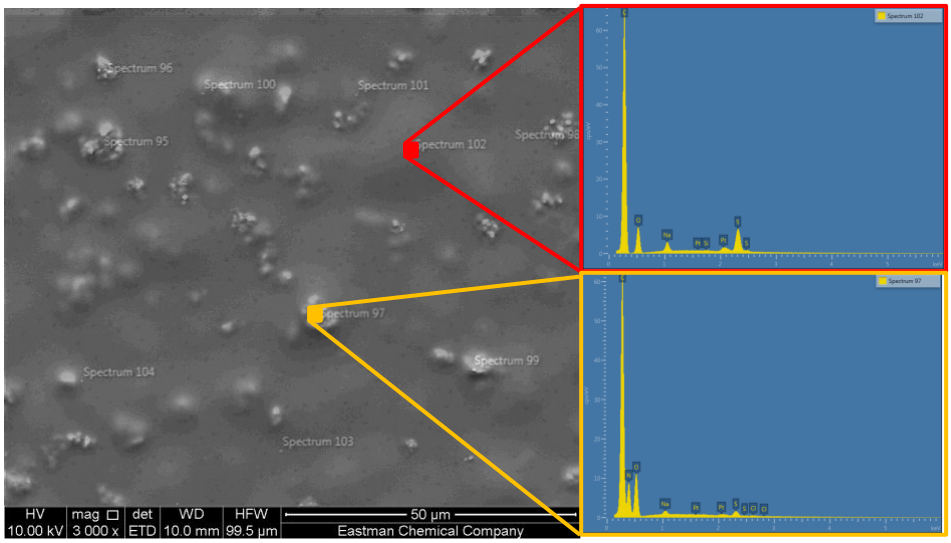

Figure 5.4: SEM-EDS scans of an AQ55S-MC films. The lack of a nitrogen peak in the red scan signifies the absence of MC outside of the clearly identifiable crystalline domains (orange scan)

A nitrogen peak in the EDS spectrum at a given spot defines where the MC is present throughout the thin film. This analysis in Figure 5.4 shows that the MC is only present in the film where a visible particle exists, and not below the resolution of the SEM. This also verifies that the polymer dispersant is disrupting large domains of MC, but those dispersants

are not entirely breaking up the complex into molecular melamine and cyanuric acid. This is an important result, as a significant dissolution of the melamine and cyanurate complex would negatively impact its flame retardant abilities, as a full dissolution of the hydrogen bonding network would greatly impact the endothermic decomposition of the hydrogen bound complex.[198]

Hydrogen Bonding Analysis

To verify the role of intermolecular hydrogen bonding between the polymer additive and the MC in improving its dispersion, Fourier transform infrared (FTIR) spectroscopy was used to monitor the intermolecular interactions that exist in the blend. MC is a complex of melamine and cyanuric acid that is held together by strong intermolecular hydrogen bonds as shown in Figure 5.1. Thus, monitoring changes in the extent of hydrogen bonds between the melamine and cyanuric acid provides a direct measure of the ability of the dispersant to interrupt these intermolecular interactions. As shown in Figure 5.5, extensive hydrogen bonding occurs between the amine groups found in melamine and amide groups on the cyanuric acid molecules. Given this structure, the infrared peaks at 3350-3450 cm^{-1}, which monitors free amines, and the infrared peaks at 3200-3250 cm^{-1} that monitor the presence of hydrogen bound amines are analyzed.[207, 208] More precisely, the extent of

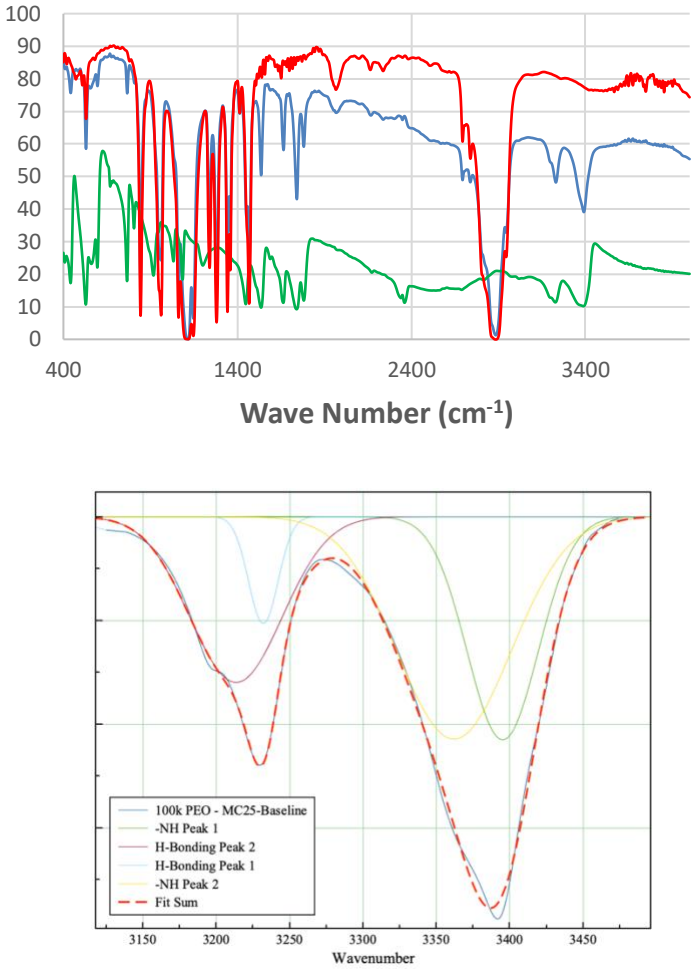

Figure 5.5: Top: FTIR spectra of 100k PEO (red), melamine cyanurate (green), 100k PEO-melamine cyanurate blend (blue). Bottom: Fitting of 100k PEO-melamine cyanurate amine peaks where the peak at 3200cm-1 corresponds to hydrogen bound amines and the peak at 3400cm

hydrogen bonding is quantified as the ratio of the area of hydrogen bound amine peaks (3200-3250 cm^{-1}) to the sum of the areas of the free and hydrogen bound amine peaks in MC as defined in Equation 5.1.

$$\%\, Hydrogen\ Bonding = \frac{A_H}{A_H + A_N} \qquad 5.1$$

In Equation 5.1, A_H is the area of the hydrogen bonded nitrogen and A_N is the area of the free (non-hydrogen bonded) nitrogen. This metric for the extent of hydrogen bonding in the binary films is presented in Table 5.2. Since there are no characteristic peaks of PEO or either of the AQ series polymers that overlap with these amine peaks, they serve as a clear representation of the extent of hydrogen bonding found within the films.

The extent of hydrogen bonding in the MC decreases in the presence of all polymer dispersants by approximately 6-8% relative to that found in the bulk MC film. This is consistent with the replacement of the *intra*molecular hydrogen bonding found within the MC by *inter*molecular hydrogen bonding between the MC and the polymer dispersant. Thus, the presence of the polymer dispersant disrupts the triple hydrogen bonding between the melamine and cyanuric acid molecules and instead replaces it with the single hydrogen bonding capable polymer dispersant. Moreover, the presence of the interacting polymer chain inhibits the formation of hydrogen bonds to neighboring amine/amide groups, aiding in the dispersion of the MC.

Combining the particle size and hydrogen bonding analyses of the solvent cast thin films demonstrates the effectiveness of both PEO and the AQ series polymers as dispersant aids in disrupting the MC hydrogen bonding network. While PEO and the AQ series polymer perform equally well when measuring MC particle size, the AQ series polymer

Table 5.2: Extent of hydrogen bonding of each binary blend thin film

Thin Film Blend	Extent of Hydrogen Bonding
10k PEO – MC	30%
100k PEO – MC	31%
AQ55S – MC	28%
AQ65S – MC	29%
MC	37%

outperforms PEO in disrupting the hydrogen bonding network of the MC. This may be because the AQ series polymer's hydrogen bonding sites are the same carbonyl functional group found in cyanuric acid, which may make them slightly more competitive with MC hydrogen bonds relative to the ether hydrogen bonding groups of PEO.[209] Because of the promising performance of the AQ series, their effectiveness in dispersing the MC in polyester matrices are also examined in melt mixed constructs.

Melt Mixed Extruded Structures

Particle Size Analysis – Scanning Electron Microscopy

The analysis of solvent cast thin films provides a measure of the ability of the polymer dispersants to disperse the MC. Further studies were completed to test the ability of these interactions to disperse MC in a polyester during melt mixing in a twin-screw extruder. The samples examined in this set of experiments consist of Tritan, MC, and the AQ series polymer as polymer dispersants. Particle analysis of SEM images of extruded filaments monitors the change in MC dispersion as a function of MC loading and dispersant concentration in the ternary mixture.

Image analysis of the MC domain size in the SEM images was completed on the extruded filaments, where three separate regions of the filament were imaged and analyzed to monitor the dispersion of the MC over the entirety of the extruded filament. This not only allows for the confirmation that the polymer dispersant is successful within an individual area, but that it is also not agglomerating within a small portion of the extrusion and is instead present throughout the entirety of the filament. The dispersion of MC in neat Tritan is the baseline to evaluate the impact of the inclusion of the polymer

dispersants on MC dispersion. The polydispersity of the particle size provides an additional parameter to quantify the effectiveness of the polymer dispersants to improve the dispersion of the MC. The particle polydispersity, calculated via Equation 5.2, quantifies the homogeneity of domain size by computing the ratio of the size average domain size and number average domain size where the lower the number, the more homogeneous distribution of domain size.

$$\boldsymbol{Particle\ Polydispersity}\ [\boldsymbol{PDI}] = \frac{\boldsymbol{A_s}}{\boldsymbol{A_n}} = \frac{\frac{\sum \boldsymbol{N_i A_i}^{\boldsymbol{2}}}{\sum \boldsymbol{N_i A_i}}}{\frac{\sum \boldsymbol{N_i A_i}}{\sum \boldsymbol{N_i}}} \qquad 5.2$$

Table 5.3 presents the average particle size and blend PDI for all examined blend compositions. These particle sizes are much lower than the measured sizes in the solution cast thin films, which is a result of both the particle dispersant and the mechanical shearing that the MC experiences during the melt mixing process. This data shows that the addition of a polymer dispersant additive greatly reduces the average particle size of the MC in all blend compositions when compared to neat Tritan/MC mixtures. Quantitatively, the average particle size is reduced by 40-67%, depending on blend composition and the type of AQ series polymer used. This data shows that the inclusion of a polymer dispersant additive also greatly reduces the polydispersity of all blends imaged. A high polydispersity in the neat blend indicates that it contains a significant number of very small particles with a few very large particles. This can be seen in Figure 5.6, which shows the dispersion of the 4% MC samples with and without 1% AQ55S. In the sample without dispersant, there is a particle with area larger than 2000μm^2, whereas

Table 5.3 Average particle size, total polydispersity for AQ55S and AQ65S blends containing 4% and 8% melamine cyanurate

	4% MC		8% MC	
Filament Blend	Total Blend Average particle size (μm^2)	Total Blend PDI	Total Blend Average particle size (μm^2)	Total Blend PDI
0% AQ	3.13	433.1	3.06	95.69
0.5%	1.38	10.66	1.56	21.85
AQ55S				
1% AQ55S	0.98	23.97	1.18	18.43
2% AQ55S	1.56	29.99	1.28	15.59
0.5%	0.88	13.98	0.61	9.32
AQ65S				
1% AQ65S	0.93	20.12	1.82	247.81
2% AQ65S	0.91	9.78	1.37	100.31

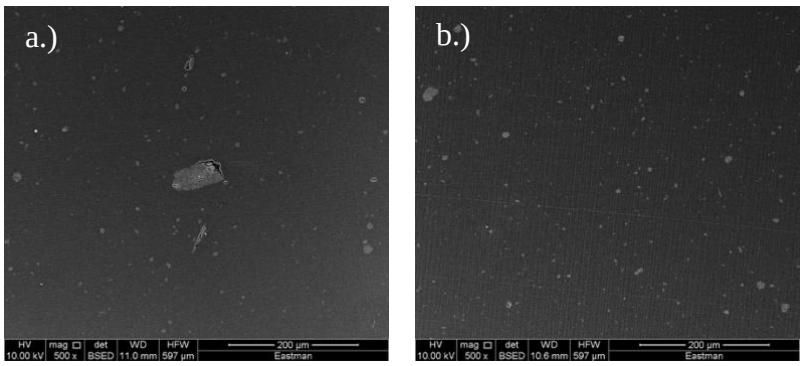

Figure 5.6: SEM images of a.) 0% AQ55S – 4% MC and b.) 1% AQ55S – 4% MC at 500x magnification.

the largest observed MC particle in any area of the other blends was 160μm^2 in a 2% AQ55S blend image. This manifestation is observed for other films as well, indicating that not only is the additive decreasing the average particle size by breaking up the large crystalline domains, but is also promoting a more uniform distribution of the MC throughout the entire filament. Further inspection of Figure 5.6 shows that in the neat blend, there exist extraordinarily large MC crystals distributed through the micrograph. These large crystals exist with very small domains, where the MC is poorly distributed over the entire observed area. Contrast these observations to the structure in Figure 5b, the 4% MC sample with 1% AQ55S. In this sample, the very large crystals are eliminated, and the remaining domains are more uniform in size and well distributed throughout the whole image.

Conclusion

The inclusion of a polymer dispersant improves the dispersion of MC domains in a polymer matrix. This occurs by the disruption of *intramolecular* hydrogen bonding between melamine and cyanurate and replacing it with *intermolecular* hydrogen bonding between the polymer dispersant and the melamine or cyanurate. Optical and scanning electron microscopy documents the effectiveness of PEO and the AQ series polymers to reduce the particle size of the MC relative to pure MC films, showing a reduction in average particle size of at least 46% in films containing a polymer dispersant. SEM-EDS results verify that while the dispersants reduce the average particle size, they did not completely disassociate the melamine from the cyanuric acid on the molecular level. FTIR quantifies a 6-10% decrease in hydrogen bonding *between* the melamine and

cyanurate with addition of the polymeric dispersants, which we ascribe as the molecular level driving force for the partitioning of the MC. Further studies validate the efficacy of the AQ series polymers to homogeneously disperse the MC in a Tritan matrix when melt mixed in a twin-screw extruder. SEM shows that the particle size of MC in extruded Tritan decreases by nearly 60% with a half weight percent of the AQ series polymer as dispersant. Notably, this work provides a foundation for compatibilizing other nanofiller additives, flame retardants or otherwise, with a bulk polymer matrix by controlling the *intermolecular and intramolecular* non-covalent interactions in the mixture by the addition of third polymer to the system.

Acknowledgements

The authors gratefully acknowledge the financial support provided by Eastman Chemical Company. The authors also thank Thomas Smart for his assistance in scanning electron microscopy imaging.

CONCLUSION AND FUTURE WORK

Conclusions

The structure of polymeric nanoparticles, and the presence of surfaces and interfaces within polymer nanocomposites can greatly affect their properties, the consequences of which were studied using neutron scattering, reflectivity, and spectroscopy as the primary means of analysis. Neutron scattering offers insight into the structure and morphology of soft polymeric nanoparticles and highlights the importance of the presence of surfaces when classifying polymeric nanostructures. Neutron reflectivity and selective deuteration provides the composition of adsorbed polymeric thin films, providing information that can elicit the importance of polymer-surface interactions within a polymer nanocomposite. Neutron spin echo spectroscopy was used to investigate and elucidate the global and local dynamics of soft polymeric nanoparticles, which highlight the importance of the structure of the nanoparticle on its local dynamics. Finally, interfaces within blends containing non-polymeric small molecules are compatibilized by inducing intermolecular non-covalent interactions thorugh the introduction of a polymeric dispersant. The average size and homogeneity of small molecule particles is characterized via image analysis of scanning electron microscopy images.

Morphological Characterization of Soft Polymeric Nanostructures

The inclusion of soft polystyrene nanoparticles to a bulk polystyrene matrix may improve the diffusion of the linear polymer in the nanocomposite when the nanoparticle is smaller than the radius of gyration of the linear chains. Additionally, nanoparticles with lower crosslink density were found to enhance the diffusion of the bulk polymer the most. However, the presence of a linear chain, or one with no crosslinks, of comparable

molecular weight to the nanoparticles will slow polymer diffusion. Thus, the changes to the nanocomposite's diffusion must be tied to the particle-like nature of the additive and identifying a transition from chain-like to particle-like behavior is needed. Small angle neutron scattering offers a pathway to characterize the morphology of these soft polymeric nanostructures as a function of crosslinking density and monomer rigidity.

The results reported in this dissertation emphasize that the presence of a measurable surface delineates a polymer chain from a nanoparticle. The presence of a surface is documented in the analyses by a fractal dimension of the nanostructure that is greater than 3 and the presence of a peak in its dimensionless Kratky plot. The nanostructures tested showed strong correlation between crosslinking density and structural morphology, where monomeric rigidity did not significantly affect the structure of the polymers. Both polystyrene and poly(ethylhexylmethacrylate) (PEHMA) showed strong particle-like behavior in all nanostructures with crosslinking densities greater than 0.8%. This leads to the surprising conclusion that 1 crosslink for every 125 monomers is sufficient to realize very strong particle-like characteristics. Polymeric nanostructures with crosslinking densities below the 0.8% particle-like threshold exhibit conformations similar to chains in solvents of varying quality, ranging from a swollen chain in a good solvent to a collapsed chain in a poor solvent with increasing crosslinking density.

Characterization of Local Dynamics of Soft Polystyrene Nanoparticles

In the soft nanoparticles studied, a higher crosslinking density results in a larger core and less prominent fuzzy interface. Moreover, these nanoparticles exhibit crosslinking dependent diffusion where both the diffusion of the nanoparticle and the

diffusion of a linear chain in the presence of the nanoparticle depends on the nanoparticle crosslink density. Neutron spin echo spectroscopy monitors the global and local dynamics of these soft nanoparticles in solution to elucidate the deviation of the nanoparticle dynamics from that of a linear chain. These results show that the examined nanoparticles behave dynamically similar to a linear chain on a global scale by adhering to Zimm-like dynamics. The local dynamics, however, vary from that of a linear chain over a finite range of length scales that range from the diameter of the crosslinked core to the size of the nanoparticle, before resuming linear-like behaviors at length scales below the nanoparticle's core size. This heterogeneity of local dynamics is a product of the core-shell structure of the soft nanoparticles where crosslinks are concentrated at the center of the nanoparticle. Additionally, the dynamics of the nanoparticles showed strong crosslinking dependency relative to each other with the effective diffusion coefficients showing a decrease with crosslinking density across all observed length scales. The heterogeneity of the soft nanoparticle's local dynamics and crosslinking dependent effective diffusion coefficients are thus likely key contributors for the presence of unexpected diffusive properties of soft nanoparticle containing polymer nanocomposites.

Permanency of Chains in a Bound Polymer Layer

Often the introduction of attractive interactions between nanoparticles and bulk polymer chains in a polymer nanocomposite can lead to confinement of polymer chains near the nanoparticle surface where its dynamics are significantly suppressed. The motion of chains in this bounded layer becomes so slow, that they are often considered irreversibly bound to the nanoparticle surface. To probe the permanency of these chains

in a polymer nanocomposite, the evolution of an adsorbed polymer layer annealed above the polymer's glass transition temperature was monitored via neutron reflectivity. To approximate a polymer nanocomposite system, the adsorption and desorption processes were observed in the melt by depositing a layer of free polymer of equivalent molecular weight and chemical structure onto a film of adsorbed chains. Neutron reflectivity studies show that the total thickness of the adsorbed layer does not vary with annealing, but the deuteration of the layer changes indicating that some chains desorb and are replaced by newly adsorbed chains. This verifies that the chains are not irreversibly adsorbed. Additionally, the molecular weight dependence of the kinetics of desorption shows that at lower molecular weights, chain diffusion away from the surface dominates desorption. However, with increasing molecular weight, surface detachment more prominently dictates the desorption, however polymer chain diffusion remains relevant to the desorption process.

Optimizing Dispersion of Small Molecule Flame Retardant in Polymer Melt

Poor dispersion of additives is a common difficulty when developing polymer composites due to poor interactions between the polymer and additive, or exceedingly strong interactions within the additive, as it can lead to diminished mechanical, chemical, and thermal capabilities of the blend. One such example is melamine cyanurate (MC), a small molecule flame retardant that is comprised of an extensive hydrogen bonding network. When mixed with a tetramethyl cyclobutanediol based (TMCB) copolyester, micro-sized agglomerations are observed in the blend. The poor interactions between the MC and polymer were improved through the introduction of a polymer dispersant which

disrupted the intramolecular hydrogen bonding within the melamine cyanurate with intermolecular hydrogen bonding between itself the flame retardant. The variation in hydrogen bonding is confirmed via Fourier transform infrared spectroscopy. Additionally, scanning electron microscopy showed significant reduction of the average melamine cyanurate particle size in an extruded filament of co-polyester with introduction of the polymer dispersant. The polymer dispersant also improved the polydispersity, or homogeneity, of the particulates with just a half weight percent loading of polymer dispersant indicating the formation of a more uniform filament compared to an uncompatibilized blend. This compatibilization demonstrates the utility of modifying the interface between a polymer and small molecule additive by controlling non-covalent interactions within the system.

Future Work

Morphological Characterization of Soft Polymeric Nanoparticles

Our understanding of the crosslinking densities where nanostructures exhibited both chain-like and particle-like characteristics is not very well fleshed out and expanding our understanding in this region could provide a clearer picture of what defines a polymer as a particle. The two major synthetic controls over soft polymeric nanoparticles via monomer starved semi-bath emulsion polymerization are the crosslinking density, determined by the ratio of monomer to crosslinking agent, and the rate of monomer addition. Nanostructures with a 0.4% crosslinking density were found to behave most similarly to a collapsed linear chain in poor solvent, while doubling the crosslinking

density to 0.8% shows extremely strong particle-like behavior. Examining the structure of nanoparticles with smaller variation of crosslink density may provide more distinct transitions between chain-like, particle-like, and transitional structures. All nanostructures examined in this thesis were synthesized with a monomer rate of addition of 2mL/hr, while nanostructures have been synthesized using rates of addition ranging from 1-50mL/hr. The primary result of increasing the monomer rate of addition is an variation in the molecular weight. Thus, the impact of molecular weight on the transition from polymer chain to nanoparticle may be more thoroughly examined in future studies.

Effect of Ultra Low Crosslinking Density on Internal Dynamics of Soft Nanoparticles

Neutron spin echo spectroscopy revealed that the soft polystyrene nanoparticles show a heterogeneity of internal dynamics dictated by the presence of crosslinks. The nanoparticles characterized where NP1.50, NP2.20, and NP10.1, showing a variety of both crosslinking densities and monomer rates of addition. The SANS study revealed that nanostructures with crosslinking densities less than 0.8% exhibited more chain-like rather than particle-like characteristics. Characterizing the internal dynamics of these ultra-low crosslinking density nanostructures for the extent of heterogeneity of their internal dynamics would be a useful endeavor to more completely understand the relationship between crosslinking density and the unique diffusive properties exhibited by soft nanoparticle containing polymer nanocomposites.

Molecular Weight Dependence of Desorption Kinetics

The neutron reflectivity study of chain desorption showed a dependence of the dominant process that controls the desorption process on the desorbing species molecular weight. Increasing the molecular weight from 20k Da to 60k Das showed a transition from nearly exclusively chain diffusion limited kinetics to a combination of chain diffusion and surface detachment. Despite showing a surface detachment showing significantly stronger scaling with molecular weight, chain diffusion continued to influence the kinetics of desorption. The continued dependence of chain desorption was attributed to the process occurring in the melt state where motion is dictated by chain reptation requiring a chain to diffuse around nearby free chains to become free of the surface. To confirm that chain diffusion does continue to impart an influence on desorption kinetics, the investigation of chain desorption of higher molecular weight species should be conducted. Alternatively, the measured kinetics of the 60k Da species may be a transitional molecular weight where both kinetic processes are present and the desorption of a higher molecular weight species may reveal exclusively surface detachment limited kinetics.

Optimizing Dispersion of Small Molecule Flame Retardant in Polymer Melt

Improving the interface between a polymer and flame retardant small molecule via the introduction of a polymer dispersant to disrupt the intramolecular hydrogen bonding network of the small molecule showed promising results. Not only did the average flame retardant particle size in extruded filament blends show significant reduction, but their size homogeneity improved and the overall dispersion of the small

molecule throughout the filament was improved as well. While ultimately the goal of the research was to improve the dispersion of melamine cyanurate in a blend with TMCB copolyester, the fruits of that compatibilization are not quantified. Improving the dispersion of a small molecule should results in an improvement of the functionality the additive brings to the blend. Therefore, a follow up study should be completed to probe the changes in strength and flame-retardant capabilities between a non-compatibilized blend and those that have been compatibilized with the polymeric dispersant. Since the endothermic decomposition of the hydrogen bonding network of melamine cyanurate is a major component of its flame retardant functionality, there may be a balance between its optimal dispersion in a blend and its effectiveness as a flame retardant.

REFERENCES

1. Feldman, D., Polymer Nanocomposites in Building, Construction. *Journal of Macromolecular Science: Pure & Applied Chemistry* **2014,** *51* (3), 203-209.

2. Gangopadhyay, R.; De, A., Conducting Polymer Nanocomposites: A Brief Overview. *Chemistry of Materials* **2000,** *12* (3), 608-622.

3. Jordan, J.; Jacob, K. I.; Tannenbaum, R.; Sharaf, M. A.; Jasiuk, I., Experimental trends in polymer nanocomposites—a review. *Materials Science and Engineering: A* **2005,** *393* (1), 1-11.

4. Kim, D. J.; Jo, M. J.; Nam, S. Y., A review of polymer–nanocomposite electrolyte membranes for fuel cell application. *Journal of Industrial and Engineering Chemistry* **2015,** *21*, 36-52.

5. Kumar, S. K.; Benicewicz, B. C.; Vaia, R. A.; Winey, K. I., 50th Anniversary Perspective: Are Polymer Nanocomposites Practical for Applications? *Macromolecules* **2017,** *50* (3), 714-731.

6. Rahman, M. T.; Asadul Hoque, M.; Rahman, G. T.; Gafur, M. A.; Khan, R. A.; Hossain, M. K., Study on the mechanical, electrical and optical properties of metal-oxide nanoparticles dispersed unsaturated polyester resin nanocomposites. *Results in Physics* **2019,** *13*, 102264.

7. Rasheed, A.; Chae, H. G.; Kumar, S.; Dadmun, M. D., Polymer nanotube nanocomposites: Correlating intermolecular interaction to ultimate properties. *Polymer* **2006,** *47* (13), 4734-4741.

8. Rupp, H.; Döhler, D.; Hilgeroth, P.; Mahmood, N.; Beiner, M.; Binder, W. H., 3D Printing of Supramolecular Polymers: Impact of Nanoparticles and Phase Separation on Printability. *Macromolecular Rapid Communications* **2019,** *40* (24), 1900467.

9. Zhang, W.; Camino, G.; Yang, R., Polymer/polyhedral oligomeric silsesquioxane (POSS) nanocomposites: An overview of fire retardance. *Progress in Polymer Science* **2017,** *67*, 77-125.

10. Kojima, Y.; Usuki, A.; Kawasumi, M.; Okada, A.; Fukushima, Y.; Kurauchi, T.; Kamigaito, O., Mechanical properties of nylon 6-clay hybrid. *Journal of Materials Research* **1993,** *8* (5), 1185-1189.

11. Anadão, P., Polymer/Clay Nanocomposites: Concepts, Researches, Applications and Trends for the Future. In *Nanocomposites : New Trends and Developments*, Ebrahimi, F., Ed. 2012.

12. Jolivet, J.-P.; Froidefond, C.; Pottier, A.; Chanéac, C.; Cassaignon, S.; Tronc, E.; Euzen, P., Size tailoring of oxide nanoparticles by precipitation in aqueous medium. A semi-quantitative modelling. *Journal of Materials Chemistry* **2004,** *14* (21), 3281-3288.

13. Lamber, R.; Wetjen, S.; Jaeger, N. I., Size dependence of the lattice parameter of small palladium particles. *Physical Review B* **1995,** *51* (16), 10968-10971.

14. Ayyub, P.; Palkar, V. R.; Chattopadhyay, S.; Multani, M., Effect of crystal size reduction on lattice symmetry and cooperative properties. *Physical Review B* **1995,** *51* (9), 6135-6138.

15. Brice-Profeta, S.; Arrio, M. A.; Tronc, E.; Menguy, N.; Letard, I.; Cartier dit Moulin, C.; Noguès, M.; Chanéac, C.; Jolivet, J. P.; Sainctavit, P., Magnetic order in γ-Fe2O3 nanoparticles: a XMCD study. *Journal of Magnetism and Magnetic Materials* **2005,** *288*, 354-365.

16. Mackay, M. E.; Tuteja, A.; Duxbury, P. M.; Hawker, C. J.; Van Horn, B.; Guan, Z.; Chen, G.; Krishnan, R. S., General Strategies for Nanoparticle Dispersion. *Science* **2006,** *311* (5768), 1740-1743.

17. Holley, D. W.; Ruppel, M.; Mays, J. W.; Urban, V. S.; Baskaran, D., Polystyrene nanoparticles with tunable interfaces and softness. *Polymer* **2014,** *55* (1), 58-65.

18. Ciprari, D.; Jacob, K.; Tannenbaum, R., Characterization of Polymer Nanocomposite Interphase and Its Impact on Mechanical Properties. *Macromolecules* **2006,** *39* (19), 6565-6573.

19. Khan, U.; Ryan, K.; Blau, W. J.; Coleman, J. N., The effect of solvent choice on the mechanical properties of carbon nanotube–polymer composites. *Composites Science and Technology* **2007,** *67* (15), 3158-3167.

20. Banerjee, P.; Conklin, D.; Nanayakkara, S.; Park, T.-H.; Therien, M. J.; Bonnell, D. A., Plasmon-Induced Electrical Conduction in Molecular Devices. *ACS Nano* **2010,** *4* (2), 1019-1025.

21. Mattevi, C.; Eda, G.; Agnoli, S.; Miller, S.; Mkhoyan, K. A.; Celik, O.; Mastrogiovanni, D.; Granozzi, G.; Garfunkel, E.; Chhowalla, M., Evolution of Electrical, Chemical, and Structural Properties of Transparent and Conducting

Chemically Derived Graphene Thin Films. *Advanced Functional Materials* **2009,** *19* (16), 2577-2583.

22. Puosi, F.; Leporini, D., Scaling between Relaxation, Transport, and Caged Dynamics in Polymers: From Cage Restructuring to Diffusion. *The Journal of Physical Chemistry B* **2011,** *115* (48), 14046-14051.

23. Ying, Y.; Saini, R. K.; Liang, F.; Sadana, A. K.; Billups, W. E., Functionalization of Carbon Nanotubes by Free Radicals. *Organic Letters* **2003,** *5* (9), 1471-1473.

24. Bahr, J. L.; Tour, J. M., Covalent chemistry of single-wall carbon nanotubes. *Journal of Materials Chemistry* **2002,** *12* (7), 1952-1958.

25. Huang, J.-E.; Li, X.-H.; Xu, J.-C.; Li, H.-L., Well-dispersed single-walled carbon nanotube/polyaniline composite films. *Carbon* **2003,** *41* (14), 2731-2736.

26. Chen, J.; Liu, H.; Weimer, W. A.; Halls, M. D.; Waldeck, D. H.; Walker, G. C., Noncovalent Engineering of Carbon Nanotube Surfaces by Rigid, Functional Conjugated Polymers. *Journal of the American Chemical Society* **2002,** *124* (31), 9034-9035.

27. Baskaran, D.; Mays, J. W.; Bratcher, M. S., Noncovalent and Nonspecific Molecular Interactions of Polymers with Multiwalled Carbon Nanotubes. *Chemistry of Materials* **2005,** *17* (13), 3389-3397.

28. Izquierdo-Lorenzo, I.; Kubackova, J.; Manchon, D.; Mosset, A.; Cottancin, E.; Sanchez-Cortes, S., Linking Ag Nanoparticles by Aliphatic α,ω-Dithiols: A Study of the Aggregation and Formation of Interparticle Hot Spots. *The Journal of Physical Chemistry C* **2013,** *117* (31), 16203-16212.

29. Saeki, S.; Kuwahara, N.; Nakata, M.; Kaneko, M., Upper and lower critical solution temperatures in poly (ethylene glycol) solutions. *Polymer* **1976,** *17* (8), 685-689.

30. Babayan, D.; Chassenieux, C.; Lafuma, F.; Ventelon, L.; Hernandez, J., Formation of Rodlike Silica Aggregates Directed by Adsorbed Thermoresponsive Polymer Chains. *Langmuir* **2010,** *26* (4), 2279-2287.

31. Genix, A.-C.; Oberdisse, J., Nanoparticle self-assembly: from interactions in suspension to polymer nanocomposites. *Soft Matter* **2018,** *14* (25), 5161-5179.

32. Corbierre, M. K.; Cameron, N. S.; Sutton, M.; Laaziri, K.; Lennox, R. B., Gold Nanoparticle/Polymer Nanocomposites: Dispersion of Nanoparticles as a Function of Capping Agent Molecular Weight and Grafting Density. *Langmuir* **2005,** *21* (13), 6063-6072.

33. Eriksson, M.; Hamers, J.; Peijs, T.; Goossens, H., The Influence of Graft Length and Density on Dispersion, Crystallisation and Rheology of Poly(ε-caprolactone)/Silica Nanocomposites. *Molecules* **2019,** *24* (11).

34. Kumar, S. K.; Jouault, N.; Benicewicz, B.; Neely, T., Nanocomposites with Polymer Grafted Nanoparticles. *Macromolecules* **2013,** *46* (9), 3199-3214.

35. Medidhi, K. R.; Padmanabhan, V., Diffusion of polymer-grafted nanoparticles in a homopolymer matrix. *The Journal of Chemical Physics* **2019,** *150* (4), 044905.

36. Shen, J.; Li, X.; Shen, X.; Liu, J., Insight into the Dispersion Mechanism of Polymer-Grafted Nanorods in Polymer Nanocomposites: A Molecular Dynamics Simulation Study. *Macromolecules* **2017,** *50* (2), 687-699.

37. Einstein, A., On the theory of Brownian movement. *Ann. Phys. (Leipz.)* **1906,** *19*, 371-381.

38. Choi, J.; Hore, M. J. A.; Meth, J. S.; Clarke, N.; Winey, K. I.; Composto, R. J., Universal Scaling of Polymer Diffusion in Nanocomposites. *ACS Macro Letters* **2013,** *2* (6), 485-490.

39. Chen, T.; Qian, H.-J.; Zhu, Y.-L.; Lu, Z.-Y., Structure and Dynamics Properties at Interphase Region in the Composite of Polystyrene and Cross-Linked Polystyrene Soft Nanoparticle. *Macromolecules* **2015,** *48* (8), 2751-2760.

40. De-La-Cuesta, J.; González, E.; Moreno, A. J.; Arbe, A.; Colmenero, J.; Pomposo, J. A., Size of Elastic Single-Chain Nanoparticles in Solution and on Surfaces. *Macromolecules* **2017,** *50* (16), 6323-6331.

41. Ding, L.; Wang, C.; Jiang, R.; Wang, L.; Song, W., Preparation of small and photoresponsive polymer nanoparticles by intramolecular crosslinking of reactive star azo-polymers. *Reactive and Functional Polymers* **2016,** *109*, 56-63.

42. Formanek, M.; Moreno, A. J., Single-Chain Nanoparticles under Homogeneous Shear Flow. *Macromolecules* **2019,** *52* (4), 1821-1831.

43. Formanek, M.; Moreno, A. J., Effects of precursor topology and synthesis under crowding conditions on the structure of single-chain polymer nanoparticles. *Soft Matter* **2017,** *13* (37), 6430-6438.

44. Galbis, E.; de-Paz, M. V.; Iglesias, N.; Lacroix, B.; Alcudia, A.; Galbis, J. A., Core cross-linked nanoparticles from self-assembling polyfma-based micelles. Encapsulation of lipophilic molecules. *European Polymer Journal* **2017,** *89*, 406-418.

45. Goldansaz, H.; Goharpey, F.; Afshar-Taromi, F.; Kim, I.; Stadler, F. J.; van Ruymbeke, E.; Karimkhani, V., Anomalous Rheological Behavior of Dendritic Nanoparticle/Linear Polymer Nanocomposites. *Macromolecules* **2015,** *48* (10), 3368-3375.

46. Hanlon, A. M.; Lyon, C. K.; Berda, E. B., What Is Next in Single-Chain Nanoparticles? *Macromolecules* **2016,** *49* (1), 2-14.

47. Lemcoff, N. G.; Spurlin, T. A.; Gewirth, A. A.; Zimmerman, S. C.; Beil, J. B.; Elmer, S. L.; Vandeveer, H. G., Organic Nanoparticles Whose Size and Rigidity Are Finely Tuned by Cross-Linking the End Groups of Dendrimers. *Journal of the American Chemical Society* **2004,** *126* (37), 11420-11421.

48. Lyon, C. K.; Prasher, A.; Hanlon, A. M.; Tuten, B. T.; Tooley, C. A.; Frank, P. G.; Berda, E. B., A brief user's guide to single-chain nanoparticles. *Polymer Chemistry* **2015,** *6* (2), 181-197.

49. Maiz, J.; Verde-Sesto, E.; Asenjo-Sanz, I.; Mangin-Thro, L.; Frick, B.; Pomposo, J. A.; Arbe, A.; Colmenero, J., Disentangling Component Dynamics in an All-Polymer Nanocomposite Based on Single-Chain Nanoparticles by Quasielastic Neutron Scattering. *Macromolecules* **2022,** *55* (6), 2320-2332.

50. Martin, H. J.; White, B. T.; Scanlon, C. J.; Saito, T.; Dadmun, M. D., Tunable synthetic control of soft polymeric nanoparticle morphology. *Soft Matter* **2017,** *13* (46), 8849-8857.

51. Martin, H. J.; White, B. T.; Yuan, G.; Saito, T.; Dadmun, M. D., Relative Size of the Polymer and Nanoparticle Controls Polymer Diffusion in All-Polymer Nanocomposites. *Macromolecules* **2019,** *52* (7), 2843-2852.

52. Miller, B.; Imel, A. E.; Holley, W.; Baskaran, D.; Mays, J. W.; Dadmun, M. D., The Role of Nanoparticle Rigidity on the Diffusion of Linear Polystyrene in a Polymer Nanocomposite. *Macromolecules* **2015,** *48* (22), 8369-8375.

53. Ormategui, N.; García, I.; Padro, D.; Cabañero, G.; Grande, H. J.; Loinaz, I., Synthesis of single chain thermoresponsive polymer nanoparticles. *Soft Matter* **2012,** *8* (3), 734-740.

54. Rubio-Cervilla, J.; Frisch, H.; Barner-Kowollik, C.; Pomposo, J. A., Synthesis of Single-Ring Nanoparticles Mimicking Natural Cyclotides by a Stepwise Folding-Activation-Collapse Process. *Macromolecular Rapid Communications* **2019,** *40* (1), 1800491.

55. Arbe, A.; Pomposo, J. A.; Moreno, A. J.; LoVerso, F.; González-Burgos, M.; Asenjo-Sanz, I.; Iturrospe, A.; Radulescu, A.; Ivanova, O.; Colmenero, J., Structure and dynamics of single-chain nano-particles in solution. *Polymer* **2016,** *105* (Supplement C), 532-544.

56. Blasco, E.; Tuten, B. T.; Frisch, H.; Lederer, A.; Barner-Kowollik, C., Characterizing single chain nanoparticles (SCNPs): a critical survey. *Polymer Chemistry* **2017,** *8* (38), 5845-5851.

57. Chen, T.; Zhao, H.-Y.; Shi, R.; Lin, W.-F.; Jia, X.-M.; Qian, H.-J.; Lu, Z.-Y.; Zhang, X.-X.; Li, Y.-K.; Sun, Z.-Y., An unexpected N-dependence in the viscosity reduction in all-polymer nanocomposite. *Nature Communications* **2019,** *10* (1), 5552.

58. Klonos, P. A.; Patelis, N.; Glynos, E.; Sakellariou, G.; Kyritsis, A., Molecular Dynamics in Polystyrene Single-Chain Nanoparticles. *Macromolecules* **2019,** *52* (23), 9334-9340.

59. Liao, S.; Wei, L.; Abriata, L. A.; Stellacci, F., Control and Characterization of the Compactness of Single-Chain Nanoparticles. *Macromolecules* **2021,** *54* (24), 11459-11467.

60. Tian, X.; Xue, R.; Yang, F.; Yin, L.; Luan, S.; Tang, H., Single-Chain Nanoparticle-Based Coatings with Improved Bactericidal Activity and Antifouling Properties. *Biomacromolecules* **2021,** *22* (10), 4306-4315.

61. Chen, R.; Berda, E. B., 100th Anniversary of Macromolecular Science Viewpoint: Re-examining Single-Chain Nanoparticles. *ACS Macro Letters* **2020,** *9* (12), 1836-1843.

62. Zimmerman, S. C.; Wendland, M. S.; Rakow, N. A.; Zharov, I.; Suslick, K. S., Synthetic hosts by monomolecular imprinting inside dendrimers. *Nature* **2002,** *418* (6896), 399-403.

63. Thota, B. N. S.; Urner, L. H.; Haag, R., Supramolecular Architectures of Dendritic Amphiphiles in Water. *Chemical Reviews* **2016,** *116* (4), 2079-2102.

64. Renterghem, L. M. V.; Lammens, M.; Dervaux, B.; Viville, P.; Lazzaroni, R.; Prez, F. E. D., Design and Use of Organic Nanoparticles Prepared from Star-Shaped

Polymers with Reactive End Groups. *Journal of the American Chemical Society* **2008,** *130* (32), 10802-10811.

65. Rodriguez, K. J.; Hanlon, A. M.; Lyon, C. K.; Cole, J. P.; Tuten, B. T.; Tooley, C. A.; Berda, E. B.; Pazicni, S., Porphyrin-Cored Polymer Nanoparticles: Macromolecular Models for Heme Iron Coordination. *Inorganic Chemistry* **2016,** *55* (19), 9493-9496.

66. Mackay, M. E.; Dao, T. T.; Tuteja, A.; Ho, D. L.; Van Horn, B.; Kim, H.-C.; Hawker, C. J., Nanoscale effects leading to non-Einstein-like decrease in viscosity. *Nature Materials* **2003,** *2*, 762.

67. Imel, A. E.; Rostom, S.; Holley, W.; Baskaran, D.; Mays, J. W.; Dadmun, M. D., The tracer diffusion coefficient of soft nanoparticles in a linear polymer matrix. *RSC Advances* **2017,** *7* (25), 15574-15581.

68. Shrestha, U. M.; Han, L.; Saito, T.; Schweizer, K. S.; Dadmun, M. D., Mechanism of Soft Nanoparticle Diffusion in Entangled Polymer Melts. *Macromolecules* **2020,** *53* (17), 7580-7589.

69. Chremos, A.; Douglas, J. F., Communication: When does a branched polymer become a particle? *The Journal of Chemical Physics* **2015,** *143* (11), 111104.

70. Tan, H.; Xu, D.; Wan, D.; Wang, Y.; Wang, L.; Zheng, J.; Liu, F.; Ma, L.; Tang, T., Melt viscosity behavior of C60 containing star polystyrene composites. *Soft Matter* **2013,** *9* (27), 6282-6290.

71. Schmidt, R. G.; Gordon, G. V.; Dreiss, C. A.; Cosgrove, T.; Krukonis, V. J.; Williams, K.; Wetmore, P. M., A Critical Size Ratio for Viscosity Reduction in

Poly(dimethylsiloxane)−Polysilicate Nanocomposites. *Macromolecules* **2010,** *43* (23), 10143-10151.

72. Eslami, R.; Ghaffarian, S. R.; Salehi, M.; Rafizadeh, M., Evaluation of non-Einstein rheology behavior of soft nanoparticles/epoxy nano-composites and their multifunctional effects on curing kinetics. *Polymer Testing* **2018,** *66*, 350-359.

73. Tuteja, A.; Duxbury, P. M.; Mackay, M. E., Multifunctional Nanocomposites with Reduced Viscosity. *Macromolecules* **2007,** *40* (26), 9427-9434.

74. Meng, Y.; Otaigbe, J. U., Mechanism of Unexpected Viscosity Decrease of Nylon 6 Melts by Low-Tg Inorganic Tin Fluorophosphate Glass during Processing. *Applied Rheology* **2011,** *21* (4).

75. Kim, S.-H.; Choi, K.; Choi, H. R.; Kim, T.; Suhr, J.; Kim, K. J.; Choi, H. J.; Nam, J.-D., Non-Einstein Viscosity Phenomenon of Acrylonitrile–Butadiene–Styrene Composites Containing Lignin–Polycaprolactone Particulates Highly Dispersed by High-Shear Stress. *ACS Omega* **2019,** *4* (6), 10036-10043.

76. Kalathi, J. T.; Grest, G. S.; Kumar, S. K., Universal Viscosity Behavior of Polymer Nanocomposites. *Physical Review Letters* **2012,** *109* (19), 198301.

77. Jain, S.; Goossens, J. G. P.; Peters, G. W. M.; van Duin, M.; Lemstra, P. J., Strong decrease in viscosity of nanoparticle-filled polymer melts through selective adsorption. *Soft Matter* **2008,** *4* (9), 1848-1854.

78. Tan, H.; Lin, Y.; Zheng, J.; Gong, J.; Qiu, J.; Xing, H.; Tang, T., Particle-size dependent melt viscosity behavior and the properties of three-arm star polystyrene–Fe3O4 composites. *Soft Matter* **2015,** *11* (20), 3986-3993.

79. Mangal, R.; Srivastava, S.; Archer, L. A., Phase stability and dynamics of entangled polymer–nanoparticle composites. *Nature Communications* **2015,** *6* (1), 7198.

80. Kim, D.; Srivastava, S.; Narayanan, S.; Archer, L. A., Polymer nanocomposites: polymer and particle dynamics. *Soft Matter* **2012,** *8* (42), 10813-10818.

81. Heydarnezhad, H. R.; Mohammadi, N.; Alegria, A., Non-Einstein Rheology in Segmented Polyurethane Nanocomposites. *Macromolecules* **2021,** *54* (6), 2783-2796.

82. Xu, C.; Ohno, K.; Ladmiral, V.; Composto, R. J., Dispersion of polymer-grafted magnetic nanoparticles in homopolymers and block copolymers. *Polymer* **2008,** *49* (16), 3568-3577.

83. Chevigny, C.; Dalmas, F.; Di Cola, E.; Gigmes, D.; Bertin, D.; Boué, F.; Jestin, J., Polymer-Grafted-Nanoparticles Nanocomposites: Dispersion, Grafted Chain Conformation, and Rheological Behavior. *Macromolecules* **2011,** *44* (1), 122-133.

84. Lange, F.; Judeinstein, P.; Franz, C.; Hartmann-Azanza, B.; Ok, S.; Steinhart, M.; Saalwächter, K., Large-Scale Diffusion of Entangled Polymers along Nanochannels. *ACS Macro Letters* **2015,** *4* (5), 561-565.

85. Emamy, H.; Kumar, S. K.; Starr, F. W., Structural Properties of Bound Layer in Polymer–Nanoparticle Composites. *Macromolecules* **2020,** *53* (18), 7845-7850.

86. Jimenez, A. M.; Zhao, D.; Misquitta, K.; Jestin, J.; Kumar, S. K., Exchange Lifetimes of the Bound Polymer Layer on Silica Nanoparticles. *ACS Macro Letters* **2019,** *8* (2), 166-171.

87. Jouault, N.; Moll, J. F.; Meng, D.; Windsor, K.; Ramcharan, S.; Kearney, C.; Kumar, S. K., Bound Polymer Layer in Nanocomposites. *ACS Macro Letters* **2013,** *2* (5), 371-374.

88. Leblanc, J. L., Rubber–filler interactions and rheological properties in filled compounds. *Progress in Polymer Science* **2002,** *27* (4), 627-687.

89. Cheng, S.; Holt, A. P.; Wang, H.; Fan, F.; Bocharova, V.; Martin, H.; Etampawala, T.; White, B. T.; Saito, T.; Kang, N.-G.; Dadmun, M. D.; Mays, J. W.; Sokolov, A. P., Unexpected Molecular Weight Effect in Polymer Nanocomposites. *Physical Review Letters* **2016,** *116* (3), 038302.

90. Holt, A. P.; Griffin, P. J.; Bocharova, V.; Agapov, A. L.; Imel, A. E.; Dadmun, M. D.; Sangoro, J. R.; Sokolov, A. P., Dynamics at the Polymer/Nanoparticle Interface in Poly(2-vinylpyridine)/Silica Nanocomposites. *Macromolecules* **2014,** *47* (5), 1837-1843.

91. Holt, A. P.; Sangoro, J. R.; Wang, Y.; Agapov, A. L.; Sokolov, A. P., Chain and Segmental Dynamics of Poly(2-vinylpyridine) Nanocomposites. *Macromolecules* **2013,** *46* (10), 4168-4173.

92. Zhang, W.; Emamy, H.; Pazmiño Betancourt, B. A.; Vargas-Lara, F.; Starr, F. W.; Douglas, J. F., The interfacial zone in thin polymer films and around nanoparticles in polymer nanocomposites. *The Journal of Chemical Physics* **2019,** *151* (12), 124705.

93. Rittigstein, P.; Priestley, R. D.; Broadbelt, L. J.; Torkelson, J. M., Model polymer nanocomposites provide an understanding of confinement effects in real nanocomposites. *Nature Materials* **2007,** *6* (4), 278-282.

94. Starr, F. W.; Douglas, J. F.; Meng, D.; Kumar, S. K., Bound Layers "Cloak" Nanoparticles in Strongly Interacting Polymer Nanocomposites. *ACS Nano* **2016,** *10* (12), 10960-10965.

95. Rittigstein, P.; Torkelson, J. M., Polymer–nanoparticle interfacial interactions in polymer nanocomposites: Confinement effects on glass transition temperature and suppression of physical aging. *Journal of Polymer Science Part B: Polymer Physics* **2006,** *44* (20), 2935-2943.

96. Moll, J.; Kumar, S. K., Glass Transitions in Highly Attractive Highly Filled Polymer Nanocomposites. *Macromolecules* **2012,** *45* (2), 1131-1135.

97. Harton, S. E.; Kumar, S. K.; Yang, H.; Koga, T.; Hicks, K.; Lee, H.; Mijovic, J.; Liu, M.; Vallery, R. S.; Gidley, D. W., Immobilized Polymer Layers on Spherical Nanoparticles. *Macromolecules* **2010,** *43* (7), 3415-3421.

98. Randazzo, K.; Bartkiewicz, M.; Graczykowski, B.; Cangialosi, D.; Fytas, G.; Zuo, B.; Priestley, R. D., Direct Visualization and Characterization of Interfacially Adsorbed Polymer atop Nanoparticles and within Nanocomposites. *Macromolecules* **2021,** *54* (21), 10224-10234.

99. Monnier, X.; Napolitano, S.; Cangialosi, D., Direct observation of desorption of a melt of long polymer chains. *Nature Communications* **2020,** *11* (1), 4354.

100. Gin, P.; Jiang, N.; Liang, C.; Taniguchi, T.; Akgun, B.; Satija, S. K.; Endoh, M. K.; Koga, T., Revealed Architectures of Adsorbed Polymer Chains at Solid-Polymer Melt Interfaces. *Physical Review Letters* **2012,** *109* (26), 265501.

101. Douglas, J. F.; Johnson, H. E.; Granick, S., A Simple Kinetic Model of Polymer Adsorption and Desorption. *Science* **1993,** *262* (5142), 2010-2012.

102. Frantz, P.; Granick, S., Kinetics of polymer adsorption and desorption. *Physical Review Letters* **1991,** *66* (7), 899-902.

103. Zuo, B.; Zhou, H.; Davis, M. J. B.; Wang, X.; Priestley, R. D., Effect of Local Chain Conformation in Adsorbed Nanolayers on Confined Polymer Molecular Mobility. *Physical Review Letters* **2019,** *122* (21), 217801.

104. Wolterink, J. K.; Stuart, M. A. C.; Barkema, G. T., Desorption of polymers: role of the stagnant layer. *Molecular Physics* **2006,** *104* (4), 639-645.

105. Douglas, J. F.; Schneider, H. M.; Frantz, P.; Lipman, R.; Granick, S., The origin and characterization of conformational heterogeneity in adsorbed polymer layers. *Journal of Physics: Condensed Matter* **1997,** *9* (37), 7699-7718.

106. Santore, M. M., Dynamics in adsorbed homopolymer layers: Understanding complexity from simple starting points. *Current Opinion in Colloid & Interface Science* **2005,** *10* (3), 176-183.

107. Josmin P. Jose, S. K. M., Sabu Thomas, Kuruvilla Joseph, Koichi Goda, Meyyarappallil Sadasivan Sreekala, Advances in Polymer Composites: Macro- and Microcomposites - State of the Art, New Challenges, and Opportunities. In *Polymer Composites: Volume 1*, Sabu Thomas, K. J.; Sant Kumar Malhotra, K. G., and Meyyarappallil Sadasivan Sreekala, Eds. Wiley-VCH: 2012.

108. Dahiya, H. S.; Kishore, N.; Mehra, R. M., Effect of percolation on electrical and dielectric properties of acrylonitrile butadiene styrene/graphite composite. *Journal of Applied Polymer Science* **2007,** *106* (3), 2101-2110.

109. Perween, M.; Parmar, D. B.; Bhadu, G. R.; Srivastava, D. N., Polymer–graphite composite: a versatile use and throw plastic chip electrode. *Analyst* **2014,** *139* (22), 5919-5926.

110. Quivy, A.; Deltour, R.; Jansen, A. G. M.; Wyder, P., Transport phenomena in polymer-graphite composite materials. *Physical Review B* **1989,** *39* (2), 1026-1030.

111. Basha, M.; Wagih, A.; Melaibari, A.; Lubineau, G.; Eltaher, M. A., On the impact damage resistance and tolerance improvement of hybrid CFRP/Kevlar sandwich composites. *Microporous and Mesoporous Materials* **2022,** *333*, 111732.

112. Wang, K.; Guo, M.; Zhao, D.; Zhang, Q.; Du, R.; Fu, Q.; Dong, X.; Han, C. C., Facilitating transcrystallization of polypropylene/glass fiber composites by imposed shear during injection molding. *Polymer* **2006,** *47* (25), 8374-8379.

113. Yilmaz, E., Compatibilization of polyvinyl chloride - polymethyl methacrylate polymer blends with maleic anhydride-styrene-methyl methacrylate terpolymer. *Journal of Applied Polymer Science* **2022,** *139* (10), 51745.

114. Eastwood, E. A.; Dadmun, M. D., Multiblock Copolymers in the Compatibilization of Polystyrene and Poly(methyl methacrylate) Blends: Role of Polymer Architecture. *Macromolecules* **2002,** *35* (13), 5069-5077.

115. Self, J. L.; Zervoudakis, A. J.; Peng, X.; Lenart, W. R.; Macosko, C. W.; Ellison, C. J., Linear, Graft, and Beyond: Multiblock Copolymers as Next-Generation Compatibilizers. *JACS Au* **2022,** *2* (2), 310-321.

116. Nomura, K.; Peng, X.; Kim, H.; Jin, K.; Kim, H. J.; Bratton, A. F.; Bond, C. R.; Broman, A. E.; Miller, K. M.; Ellison, C. J., Multiblock Copolymers for Recycling Polyethylene–Poly(ethylene terephthalate) Mixed Waste. *ACS Applied Materials & Interfaces* **2020,** *12* (8), 9726-9735.

117. Xu, J.; Eagan, J. M.; Kim, S.-S.; Pan, S.; Lee, B.; Klimovica, K.; Jin, K.; Lin, T.-W.; Howard, M. J.; Ellison, C. J.; LaPointe, A. M.; Coates, G. W.; Bates, F. S., Compatibilization of Isotactic Polypropylene (iPP) and High-Density Polyethylene (HDPE) with iPP–PE Multiblock Copolymers. *Macromolecules* **2018,** *51* (21), 8585-8596.

118. Viswanathan, S.; Dadmun, M. D., Optimizing Hydrogen-Bonding in Creating Miscible Liquid Crystalline Polymer Blends by Structural Modification of the Blend Components. *Macromolecules* **2003,** *36* (9), 3196-3205.

119. Eastwood, E.; Viswanathan, S.; O'Brien, C. P.; Kumar, D.; Dadmun, M. D., Methods to improve the properties of polymer mixtures: Optimizing intermolecular interactions and compatibilization. *Polymer* **2005,** *46* (12), 3957-3970.

120. Radmard, B.; Dadmun, M. D., The accessibility of functional groups to intermolecular hydrogen bonding in polymer blends containing a liquid crystalline polymer. *Polymer* **2001,** *42* (4), 1591-1600.

121. Rasheed, A.; Dadmun, M. D.; Britt, P. F., Polymer-nanofiber composites: Enhancing composite properties by nanofiber oxidation. *Journal of Polymer Science Part B: Polymer Physics* **2006,** *44* (21), 3053-3061.

122. Rasheed, A.; Dadmun, M. D.; Ivanov, I.; Britt, P. F.; Geohegan, D. B., Improving Dispersion of Single-Walled Carbon Nanotubes in a Polymer Matrix Using Specific Interactions. *Chemistry of Materials* **2006,** *18* (15), 3513-3522.

123. Henry, N.; Harper, D.; Dadmun, M., Optimizing Noncovalent Interactions Between Lignin and Synthetic Polymers to Develop Effective Compatibilizers. *Macromolecular Chemistry and Physics* **2012,** *213* (12), 1196-1205.

124. Vasileiou, A. A.; Kontopoulou, M.; Docoslis, A., A Noncovalent Compatibilization Approach to Improve the Filler Dispersion and Properties of Polyethylene/Graphene Composites. *ACS Applied Materials & Interfaces* **2014,** *6* (3), 1916-1925.

125. Loste, J.; Lopez-Cuesta, J.-M.; Billon, L.; Garay, H.; Save, M., Transparent polymer nanocomposites: An overview on their synthesis and advanced properties. *Progress in Polymer Science* **2019,** *89*, 133-158.

126. Yong, H. W.; Kakkar, A., Nanoengineering Branched Star Polymer-Based Formulations: Scope, Strategies, and Advances. *Macromolecular Bioscience* **2021,** *21* (8), 2100105.

127. Rostom, S.; White, B. T.; Yuan, G.; Saito, T.; Dadmun, M. D., Polymer Chain Diffusion in All-Polymer Nanocomposites: Confinement vs Chain Acceleration. *The Journal of Physical Chemistry C* **2020,** *124* (34), 18834-18839.

128. Elkhoury, K.; Russell, C. S.; Sanchez-Gonzalez, L.; Mostafavi, A.; Williams, T. J.; Kahn, C.; Peppas, N. A.; Arab-Tehrany, E.; Tamayol, A., Soft-Nanoparticle Functionalization of Natural Hydrogels for Tissue Engineering Applications. *Advanced Healthcare Materials* **2019,** *8* (18), 1900506.

129. Hanlon, A. M.; Chen, R.; Rodriguez, K. J.; Willis, C.; Dickinson, J. G.; Cashman, M.; Berda, E. B., Scalable Synthesis of Single-Chain Nanoparticles under Mild Conditions. *Macromolecules* **2017,** *50* (7), 2996-3003.

130. Zhang, J.; Gody, G.; Hartlieb, M.; Catrouillet, S.; Moffat, J.; Perrier, S., Synthesis of Sequence-Controlled Multiblock Single Chain Nanoparticles by a Stepwise Folding–Chain Extension–Folding Process. *Macromolecules* **2016,** *49* (23), 8933-8942.

131. Pomposo, J. A.; Perez-Baena, I.; Lo Verso, F.; Moreno, A. J.; Arbe, A.; Colmenero, J., How Far Are Single-Chain Polymer Nanoparticles in Solution from the Globular State? *ACS Macro Letters* **2014,** *3* (8), 767-772.

132. Wichaita, W.; Kim, Y.-G.; Tangboriboonrat, P.; Thérien-Aubin, H., Polymer-functionalized polymer nanoparticles and their behaviour in suspensions. *Polymer Chemistry* **2020,** *11* (12), 2119-2128.

133. Metzner, A. B., Rheology of Suspensions in Polymeric Liquids. *Journal of Rheology* **1985,** *29* (6), 739-775.

134. Meth, J. S.; Gam, S.; Choi, J.; Lin, C.-C.; Composto, R. J.; Winey, K. I., Excluded Volume Model for the Reduction of Polymer Diffusion into Nanocomposites. *The Journal of Physical Chemistry B* **2013,** *117* (49), 15675-15683.

135. Cui, W.; You, W.; Sun, Z.; Yu, W., Decoupled Polymer Dynamics in Weakly Attractive Poly(methyl methacrylate)/Silica Nanocomposites. *Macromolecules* **2021,** *54* (12), 5484-5497.

136. Bailey, E. J.; Riggleman, R. A.; Winey, K. I., Polymer Conformations and Diffusion through a Monolayer of Confining Nanoparticles. *Macromolecules* **2020,** *53* (19), 8171-8180.

137. Gam, S.; Meth, J. S.; Zane, S. G.; Chi, C.; Wood, B. A.; Winey, K. I.; Clarke, N.; Composto, R. J., Polymer diffusion in a polymer nanocomposite: effect of nanoparticle size and polydispersity. *Soft Matter* **2012,** *8* (24), 6512-6520.

138. Lin, C.-C.; Ohno, K.; Clarke, N.; Winey, K. I.; Composto, R. J., Macromolecular Diffusion through a Polymer Matrix with Polymer-Grafted Chained Nanoparticles. *Macromolecules* **2014,** *47* (15), 5357-5364.

139. Tung, W.-S.; Griffin, P. J.; Meth, J. S.; Clarke, N.; Composto, R. J.; Winey, K. I., Temperature-Dependent Suppression of Polymer Diffusion in Polymer Nanocomposites. *ACS Macro Letters* **2016,** *5* (6), 735-739.

140. Auffan, M.; Rose, J.; Bottero, J.-Y.; Lowry, G. V.; Jolivet, J.-P.; Wiesner, M. R., Towards a definition of inorganic nanoparticles from an environmental, health and safety perspective. *Nature Nanotechnology* **2009,** *4* (10), 634-641.

141. SasView. http://www.sasview.org/.

142. Receveur-Brechot, V.; Durand, D., How random are intrinsically disordered proteins? A small angle scattering perspective. *Curr Protein Pept Sci* **2012,** *13* (1), 55-75.

143. Burger, V. M.; Arenas, D. J.; Stultz, C. M., A Structure-free Method for Quantifying Conformational Flexibility in proteins. *Scientific Reports* **2016,** *6* (1), 29040.

144. Amitani, K.; Terao, K.; Nakamura, Y.; Norisuye, T., Small-Angle X-Ray Scattering from Polystyrene Polymacromonomers in Cyclohexane. *Polymer Journal* **2005,** *37* (4), 324-331.

145. Allegra, G.; Colombo, E.; Ganazzoli, F., Linear and regular star polymer in a good solvent. *Macromolecules* **1993,** *26* (2), 330-338.

146. Upadhya, R.; Murthy, N. S.; Hoop, C. L.; Kosuri, S.; Nanda, V.; Kohn, J.; Baum, J.; Gormley, A. J., PET-RAFT and SAXS: High Throughput Tools To Study Compactness and Flexibility of Single-Chain Polymer Nanoparticles. *Macromolecules* **2019,** *52* (21), 8295-8304.

147. Durand, D.; Vivès, C.; Cannella, D.; Pérez, J.; Pebay-Peyroula, E.; Vachette, P.; Fieschi, F., NADPH oxidase activator p67(phox) behaves in solution as a multidomain protein with semi-flexible linkers. *J Struct Biol* **2010,** *169* (1), 45-53.

148. Hammouda, B., A new Guinier-Porod model. *Journal of Applied Crystallography* **2010,** *43* (4), 716-719.

149. Beaucage, G., Small-Angle Scattering from Polymeric Mass Fractals of Arbitrary Mass-Fractal Dimension. *Journal of Applied Crystallography* **1996,** *29* (2), 134-146.

150. Nygaard, M.; Kragelund, B. B.; Papaleo, E.; Lindorff-Larsen, K., An Efficient Method for Estimating the Hydrodynamic Radius of Disordered Protein Conformations. *Biophys J* **2017,** *113* (3), 550-557.

151. Linegar, K. L.; Adeniran, A. E.; Kostko, A. F.; Anisimov, M. A., Hydrodynamic radius of polyethylene glycol in solution obtained by dynamic light scattering. *Colloid Journal* **2010,** *72*, 279-281.

152. Oono, Y.; Kohmoto, M., Renormalization group theory of transport properties of polymer solutions. I. Dilute solutions. *The Journal of Chemical Physics* **1983,** *78* (1), 520-528.

153. Kokufuta, E.; Ogawa, K.; Doi, R.; Kikuchi, R.; Farinato, R. S., Geometrical characteristics of polyelectrolyte nanogel particles and their polyelectrolyte complexes studied by dynamic and static light scattering. *J Phys Chem B* **2007,** *111* (29), 8634-40.

154. Ishizu, K.; Ono, T.; Uchida, S., Geometrical structure of star polymers in solution. *Macromolecular Chemistry and Physics* **1997,** *198* (10), 3255-3265.

155. Ishizu, K.; Sunahara, K.; Asai, S.-i., Synthesis and solution properties of gradient-modulus star copolymers. *Polymer* **1998,** *39* (4), 953-957.

156. Hossain, M. D. D.; Tran, L. T. B.; Park, J. M.; Lim, K. T., Facile synthesis of core-surface crosslinked nanoparticles by interblock RAFT polymerization. *Journal of Polymer Science Part A: Polymer Chemistry* **2010,** *48* (22), 4958-4964.

157. Liu, B.; Thayumanavan, S., Three-Component Sequential Reactions for Polymeric Nanoparticles with Tailorable Core and Surface Functionalities. *Chem* **2019,** *5* (12), 3166-3183.

158. Matsuno, J.; Kanamaru, T.; Arai, K.; Tanaka, R.; Lee, J. H.; Takahashi, R.; Sakurai, K.; Fujii, S., Synthesis and characterization of nanoemulsion-mediated core

crosslinked nanoparticles, and in vivo pharmacokinetics depending on the structural characteristics. *Journal of Controlled Release* **2020,** *324*, 405-412.

159. Shehata, N.; Nair, R.; Boualayan, R.; Kandas, I.; Masrani, A.; Elnabawy, E.; Omran, N.; Gamal, M.; Hassanin, A. H., Stretchable nanofibers of polyvinylidenefluoride (PVDF)/thermoplastic polyurethane (TPU) nanocomposite to support piezoelectric response via mechanical elasticity. *Scientific Reports* **2022,** *12* (1), 8335.

160. Pasichnyk, M.; Gaálová, J.; Minarik, P.; Václavíková, M.; Melnyk, I., Development of polyester filters with polymer nanocomposite active layer for effective dye filtration. *Scientific Reports* **2022,** *12* (1), 973.

161. Díez-Pascual, A. M.; Gómez-Fatou, M. A.; Ania, F.; Flores, A., Nanoindentation in polymer nanocomposites. *Progress in Materials Science* **2015,** *67*, 1-94.

162. Njuguna, J.; Pielichowski, K., Polymer Nanocomposites for Aerospace Applications: Properties. *Advanced Engineering Materials* **2003,** *5* (11), 769-778.

163. Li, Q.; Chen, L.; Gadinski, M. R.; Zhang, S.; Zhang, G.; Li, H. U.; Iagodkine, E.; Haque, A.; Chen, L.-Q.; Jackson, T. N.; Wang, Q., Flexible high-temperature dielectric materials from polymer nanocomposites. *Nature* **2015,** *523* (7562), 576-579.

164. Chen, J.; Huang, X.; Sun, B.; Jiang, P., Highly Thermally Conductive Yet Electrically Insulating Polymer/Boron Nitride Nanosheets Nanocomposite Films for Improved Thermal Management Capability. *ACS Nano* **2019,** *13* (1), 337-345.

165. Tuteja, A.; Mackay, M. E.; Hawker, C. J.; Van Horn, B.; Ho, D. L., Molecular architecture and rheological characterization of novel intramolecularly crosslinked

polystyrene nanoparticles. *Journal of Polymer Science Part B: Polymer Physics* **2006,** *44* (14), 1930-1947.

166. Azuah, R. T.; Kneller, L. R.; Qiu, Y.; Tregenna-Piggott, P. L.; Brown, C. M.; Copley, J. R.; Dimeo, R. M., DAVE: A Comprehensive Software Suite for the Reduction, Visualization, and Analysis of Low Energy Neutron Spectroscopic Data. *J Res Natl Inst Stand Technol* **2009,** *114* (6), 341-58.

167. Ganazzoli, F.; Raffaini, G.; Arrighi, V., The stretched-exponential approximation to the dynamic structure factor in non-entangled polymer melts. *Physical Chemistry Chemical Physics* **2002,** *4* (15), 3734-3742.

168. Sanchez-Sanchez, A.; Arbe, A.; Colmenero, J.; Pomposo, J. A., Metallo-Folded Single-Chain Nanoparticles with Catalytic Selectivity. *ACS Macro Letters* **2014,** *3* (5), 439-443.

169. Kwon, N. K.; Kim, H.; Han, I. K.; Shin, T. J.; Lee, H.-W.; Park, J.; Kim, S. Y., Enhanced Mechanical Properties of Polymer Nanocomposites Using Dopamine-Modified Polymers at Nanoparticle Surfaces in Very Low Molecular Weight Polymers. *ACS Macro Letters* **2018,** *7* (8), 962-967.

170. Santagiuliana, G.; Picot, O. T.; Crespo, M.; Porwal, H.; Zhang, H.; Li, Y.; Rubini, L.; Colonna, S.; Fina, A.; Barbieri, E.; Spoelstra, A. B.; Mirabello, G.; Patterson, J. P.; Botto, L.; Pugno, N. M.; Peijs, T.; Bilotti, E., Breaking the Nanoparticle Loading–Dispersion Dichotomy in Polymer Nanocomposites with the Art of Croissant-Making. *ACS Nano* **2018,** *12* (9), 9040-9050.

171. Liu, J.; Gao, Y.; Cao, D.; Zhang, L.; Guo, Z., Nanoparticle Dispersion and Aggregation in Polymer Nanocomposites: Insights from Molecular Dynamics Simulation. *Langmuir* **2011,** *27* (12), 7926-7933.

172. Koh, C.; Grest, G. S.; Kumar, S. K., Assembly of Polymer-Grafted Nanoparticles in Polymer Matrices. *ACS Nano* **2020,** *14* (10), 13491-13499.

173. Gong, S.; Chen, Q.; Moll, J. F.; Kumar, S. K.; Colby, R. H., Segmental Dynamics of Polymer Melts with Spherical Nanoparticles. *ACS Macro Letters* **2014,** *3* (8), 773-777.

174. Gooneie, A., Local Structural Fingerprints of Nanoparticle-Bound Polymer Layers. *The Journal of Physical Chemistry B* **2021,** *125* (3), 937-949.

175. Emamy, H.; Starr, F. W.; Kumar, S. K., Detecting bound polymer layers in attractive polymer–nanoparticle hybrids. *Nanoscale* **2021,** *13* (30), 12910-12915.

176. Kritikos, G.; Rissanou, A. N.; Harmandaris, V.; Karatasos, K., Bound Layer Polymer Behavior on Graphene and Graphene Oxide Nanosheets. *Macromolecules* **2020,** *53* (15), 6190-6203.

177. de Gennes, P. G., Polymers at an interface; a simplified view. *Advances in Colloid and Interface Science* **1987,** *27* (3), 189-209.

178. O'Shaughnessy, B.; Vavylonis, D., Irreversibility and Polymer Adsorption. *Physical Review Letters* **2003,** *90* (5), 056103.

179. Housmans, C.; Sferrazza, M.; Napolitano, S., Kinetics of Irreversible Chain Adsorption. *Macromolecules* **2014,** *47* (10), 3390-3393.

180. Jiang, N.; Shang, J.; Di, X.; Endoh, M. K.; Koga, T., Formation Mechanism of High-Density, Flattened Polymer Nanolayers Adsorbed on Planar Solids. *Macromolecules* **2014,** *47* (8), 2682-2689.

181. Napolitano, S., Irreversible adsorption of polymer melts and nanoconfinement effects. *Soft Matter* **2020,** *16* (23), 5348-5365.

182. Nieto Simavilla, D.; Panagopoulou, A.; Napolitano, S., Characterization of Adsorbed Polymer Layers: Preparation, Determination of the Adsorbed Amount and Investigation of the Kinetics of Irreversible Adsorption. *Macromolecular Chemistry and Physics* **2018,** *219* (3), 1700303.

183. O'Shaughnessy, B.; Vavylonis, D., Non-equilibrium in adsorbed polymer layers. *Journal of Physics: Condensed Matter* **2005,** *17* (2), R63-R99.

184. de Gennes, P. G., Conformations of Polymers Attached to an Interface. *Macromolecules* **1980,** *13* (5), 1069-1075.

185. O'Shaughnessy, B.; Vavylonis, D., Irreversible adsorption from dilute polymer solutions. *The European Physical Journal E* **2003,** *11* (3), 213-230.

186. Simavilla, D. N.; Huang, W.; Vandestrick, P.; Ryckaert, J.-P.; Sferrazza, M.; Napolitano, S., Mechanisms of Polymer Adsorption onto Solid Substrates. *ACS Macro Letters* **2017,** *6* (9), 975-979.

187. Johnson, H. E.; Douglas, J. F.; Granick, S., Topological influences on polymer adsorption and desorption dynamics. *Physical Review Letters* **1993,** *70* (21), 3267-3270.

188. Hershkovits, E.; Tannenbaum, A.; Tannenbaum, R., Polymer Adsorption on Curved Surfaces: A Geometric Approach. *J Phys Chem C Nanomater Interfaces* **2007,** *111* (33), 12369-12375.

189. Arlen, M. J.; Dadmun, M. D.; Hamilton, W. A., Using neutron reflectivity to determine the dynamic properties of a copolymer in a homopolymer matrix. *Journal of Polymer Science Part B: Polymer Physics* **2004,** *42* (17), 3235-3247.

190. Lazar, S. T.; Kolibaba, T. J.; Grunlan, J. C., Flame-retardant surface treatments. *Nature Reviews Materials* **2020,** *5* (4), 259-275.

191. Babrauskas, V.; Fuoco, R.; Blum, A., Chapter 3 - Flame Retardant Additives in Polymers: When do the Fire Safety Benefits Outweigh the Toxicity Risks? In *Polymer Green Flame Retardants*, Papaspyrides, C. D.; Kiliaris, P., Eds. Elsevier: Amsterdam, 2014; pp 87-118.

192. Nagasawa, Y.; Hotta, M.; Ozawa, K., Fast thermolysis/FT-IR studies of fire-retardant melamine-cyanurate and melamine-cyanurate containing polymer. *Journal of Analytical and Applied Pyrolysis* **1995,** *33*, 253-267.

193. Kiliaris, P.; Papaspyrides, C. D.; Pfaendner, R., Polyamide 6 Filled with Melamine Cyanurate and Layered Silicates: Evaluation of Flame Retardancy and Physical Properties. *Macromolecular Materials and Engineering* **2008,** *293* (9), 740-751.

194. Hou, W.; Fu, Y.; Zeng, C.; Liu, N.; Yin, C., Enhancement of flame retardancy and mechanical properties of polyamide 6 by incorporating melamine cyanurate combined with attapulgite. *Journal of Applied Polymer Science* **2020,** *137* (2), 47298.

195. Luo, D.; Duan, W.; Liu, Y.; Chen, N.; Wang, Q., Melamine cyanurate surface treated by nylon of low molecular weight to prepare flame-retardant polyamide 66 with high flowability. *Fire and Materials* **2019,** *43* (3), 323-331.

196. Perdigão, L. M. A.; Champness, N. R.; Beton, P. H., Surface self-assembly of the cyanuric acid–melamine hydrogen bonded network. *Chemical Communications* **2006,** (5), 538-540.

197. Liu, Y.; Wang, Q., Melamine cyanurate-microencapsulated red phosphorus flame retardant unreinforced and glass fiber reinforced polyamide 66. *Polymer Degradation and Stability* **2006,** *91* (12), 3103-3109.

198. Casu, A.; Camino, G.; De Giorgi, M.; Flath, D.; Morone, V.; Zenoni, R., Fire-retardant mechanistic aspects of melamine cyanurate in polyamide copolymer. *Polymer Degradation and Stability* **1997,** *58* (3), 297-302.

199. Huang, H.; Zhang, K.; Jiang, J.; Li, J.; Liu, Y., Highly dispersed melamine cyanurate flame-retardant epoxy resin composites. *Polymer International* **2017,** *66* (1), 85-91.

200. Mehra, N.; Jeske, M.; Yang, X.; Gu, J.; Kashfipour, M. A.; Li, Y.; Baughman, J. A.; Zhu, J., Hydrogen-Bond Driven Self-Assembly of Two-Dimensional Supramolecular Melamine-Cyanuric Acid Crystals and Its Self-Alignment in Polymer Composites for Enhanced Thermal Conduction. *ACS Applied Polymer Materials* **2019,** *1* (6), 1291-1300.

201. Chen, J.; Rong, L.; Fang, W.; Liu, J.; Liu, X., Highly efficient intumescent flame retardant coating for ABS: Preparation and application. *Journal of Applied Polymer Science* **2022,** *139* (13), 51860.

202. Braun, U.; Schartel, B., Flame Retardancy Mechanisms of Aluminium Phosphinate in Combination with Melamine Cyanurate in Glass-Fibre-Reinforced Poly(1,4-butylene terephthalate). *Macromolecular Materials and Engineering* **2008,** *293* (3), 206-217.

203. Gijsman, P.; Steenbakkers, R.; Fürst, C.; Kersjes, J., Differences in the flame retardant mechanism of melamine cyanurate in polyamide 6 and polyamide 66. *Polymer Degradation and Stability* **2002,** *78* (2), 219-224.

204. Xu, S.; Li, J.; Ye, Q.; Shen, L.; Lin, H., Flame-retardant ethylene vinyl acetate composite materials by combining additions of aluminum hydroxide and melamine cyanurate: Preparation and characteristic evaluations. *Journal of Colloid and Interface Science* **2021,** *589*, 525-531.

205. Kadanyo, S.; Gumbi, N. N.; Matindi, C. N.; Dlamini, D. S.; Hu, Y.; Cui, Z.; Wang, H.; Hu, M.; Li, J., Enhancing compatibility and hydrophilicity of polysulfone/poly (ethylene-co-vinyl alcohol) copolymer blend ultrafiltration membranes using polyethylene glycol as hydrophilic additive and compatibilizer. *Separation and Purification Technology* **2022,** *287*, 120523.

206. Ferrarezi, M. M. F.; de Oliveira Taipina, M.; Escobar da Silva, L. C.; Gonçalves, M. d. C., Poly(Ethylene Glycol) as a Compatibilizer for Poly(Lactic Acid)/Thermoplastic Starch Blends. *Journal of Polymers and the Environment* **2013,** *21* (1), 151-159.

207. Baghdadi, Y. N.; Sinno, J.; Bouhadir, K.; Harb, M.; Mustapha, S.; Patra, D.; Tehrani-Bagha, A. R., The mechanical and thermal properties of graphitic carbon nitride (g-C3N4)-based epoxy composites. *Journal of Applied Polymer Science* **2021,** *138* (45), 51324.

208. Yan, C.; Luo, Y.-J.; Zhang, W.-G.; Zhu, Z.-F.; Li, P.-Y.; Li, N.; Chen, Y.-F.; Jin, T., Preparation of a novel melamine foam structure and properties. *Journal of Applied Polymer Science* **2022,** *139* (16), 51992.

209. Lommerse, J. P. M.; Price, S. L.; Taylor, R., Hydrogen bonding of carbonyl, ether, and ester oxygen atoms with alkanol hydroxyl groups. *Journal of Computational Chemistry* **1997,** *18* (6), 757-774.

VITA

Jacob E. Fischer was born June 8, 1992 in Huntington, West Virginia where he graduated from Huntington High School in May 2010. Jacob attended Bethany College (Bethany, WV) where he played collegiate baseball for 1 year. Additionally, served as Student Government Association President, and conducted research in polymer chemistry for Dr. Lisa C. Reilly and Dr. Scott Brothers and graduated with a Bachelor of Science in Chemistry and Math in May 2014. Jacob then went on to earn a Master of Arts in Mathematics in May 2016 from Marshall University (Huntington, WV). While there Jacob conducted research in time scales calculus for Dr. Bonita Lawrence. The following August, Jacob continues his graduate school career at the University of Tennessee-Knoxville under advisement of Professor Mark D. Dadmun, PhD.